Petroleum Science 23 (2026) 2136–2174

Contents lists available at ScienceDirect

Petroleum Science

journal homepage: www.keaipublishing.com/en/journals/petroleum-science

Review Paper

Advances in intelligent defect recognition method for oil and gas pipeline weld X-ray image

Wei-Chao Qian [a,b,c], Shao-Hua Dong [a,b,c,*], Meng Sun [b,c], Zi-Cong Han [b,c], Lin Chen [b,c,**]

[a] College of Artificial Intelligence, China University of Petroleum (Beijing), Beijing, 102249, China
[b] College of Safety and Ocean Engineering, China University of Petroleum (Beijing), Beijing, 102249, China
[c] Key Laboratory of Oil and Gas Safety and Emergency Technology, Ministry of Emergency Management, China University of Petroleum (Beijing), Beijing, 102249, China

ARTICLE INFO

Article history:
Received 25 March 2025
Received in revised form
6 September 2025
Accepted 14 December 2025
Available online 17 December 2025

Edited by Teng Zhu

Keywords:
Weld defect recognition
Image preprocessing
Signal processing
Feature design
Deep learning

ABSTRACT

Long-distance pipelines are essential for transporting oil and gas, with the quality of welds directly affecting their safety and reliability. Weld defects can emerge during the welding process due to improper techniques or environmental factors, which can result in pipeline leakage or rupture that pose a public safety and environmental risk and can lead to significant economic losses. Therefore, effective weld defect detection is crucial to ensure the safe operation of long-distance pipelines. Although traditional X-ray inspection is commonly used to detect weld defects, it is inefficient and subjective due to its dependence on manual analysis. New developments in computer vision have significantly improved the efficiency and accuracy of automated technology for defect recognition in pipeline weld X-ray images. As a result, there is an urgent need for a comprehensive review to support the development of this field and provide valuable insights. This paper comprehensively evaluates the progress in the technology for the intelligent recognition of defects in pipeline weld X-ray images, focusing on preprocessing and defect detection techniques. This review explores three key directions for intelligent weld defect recognition: signal processing, feature design, and deep learning-based methods. Deep learning-based defect recognition techniques were examined in detail from five primary perspectives: dataset creation, image classification, semantic segmentation, object detection, and performance evaluation. Finally, the challenges and future development trends in the intelligent recognition of defects in pipeline weld X-ray images are discussed, emphasizing areas that require further research and innovative advancements.

1. Introduction

As major fossil fuels, oil and gas are vital for global survival and development (Li et al., 2024b). These resources support economic stability and ensure global energy security (Li et al., 2024b). Long-distance pipelines (Kiyingi et al., 2022) are extensively used for oil and gas transportation due to their high efficiency and low cost (Li et al., 2022; Lu et al., 2024; Miao and Zhao, 2024; Qiu et al., 2024; Wu et al., 2021; Xu et al., 2010; Zhang et al., 2024). By the end of 2022, the total mileage of long-distance oil and gas pipelines in China reached 180,000 km, with projections indicating an expansion to 240,000 km by 2025 (Yang et al., 2024b). Welding is critical during long-distance pipeline construction to ensure structural integrity and durability (Huang et al., 2019; Wang et al., 2022a; Zhang et al., 2022a). However, variations in the welding process and environmental conditions can cause defects, such as porosity, cracks, and incomplete fusion in the weld seams (Li et al., 2023a; Zhang et al., 2023b). The subsequent pipeline leakage can easily lead to safety risk and accidents, such as explosions, causing serious economic losses and environmental pollution (Wang et al., 2023). The rapid growth in oil and gas demand has promoted the development of pipeline transportation, necessitating the effective detection of pipeline weld defects (Zhu et al., 2023).

Non-destructive testing (NDT) techniques are widely used to detect welding defects due to their non-invasive nature and high

* Corresponding author.
** Corresponding author.
E-mail addresses: shdong@cup.edu.cn (S.-H. Dong), chenlin@cup.edu.cn (L. Chen).

https://doi.org/10.1016/j.petsci.2025.12.020

efficiency, and include ultrasonic, eddy current, infrared, magnetic leakage, and X-ray methods (Wang et al., 2022b; Zhang et al., 2023c). X-ray techniques are particularly notable for their ability to produce high-resolution images that clearly reveal detailed information about weld defects, making them an intuitive approach for defect identification (Abdelkader et al., 2021). Currently, X-ray film photography is a primary method for on-site weld inspection. This process involves passing X-rays through the weld to create a negative image on the X-ray film. After development, the internal structure and defects of the weld become visible. However, this method presents several challenges, such as film contamination and potential loss, while it largely relies on manual analysis, which is time-consuming and labor-intensive. Furthermore, misjudgments and missed defects due to subjective interpretation are common, which significantly increase the complexity of defect evaluation (Kumar et al., 2023). Beyond the challenges arising from subjective interpretation, the quality of pipeline weld X-ray images significantly impacts the efficacy of manual inspection (Gupta et al., 2023; Yan, 2024). In practical applications, pipeline weld X-ray images often exhibit low contrast and brightness due to multiple factors, including variability in the X-ray radiation source energy, variations in the transmission angle, limitations in digitization equipment accuracy, and environmental interference. Poor contrast renders the grayscale differential between defects and background regions insignificant, increasing the difficulty of detecting subtle faults. Low brightness results in image detail loss, compromising accurate defect boundary localization, while variations in pipeline diameter present another significant challenge for defect detection. Substantial differences are evident between the image characteristics, defect representation features, and background complexity of large- and small-diameter pipeline weld X-ray images (Lv, 2022). The weld X-ray images of large-diameter pipelines typically exhibit broader weld areas, more complex background structures, and more significant interference features while those of small-diameter pipelines show narrower weld regions and more pronounced edges. Weld defects in small-diameter pipelines are spatially concentrated yet smaller in size due to constraints on wall thickness and curvature, rendering them more susceptible to noise interference and imaging angle effects (Shi et al., 2023a; Yang et al., 2025). These diameter-dependent image characteristics necessitate the use of varying observational foci and evaluation criteria for different pipeline diameters, which may lead to inconsistent detection outcomes.

The rapid advancement of automation and artificial intelligence has increasingly promoted the adoption of sophisticated image processing and computer vision techniques for weld defect detection (Yang et al., 2023b, 2024a). Deep learning, which emulates the neural architecture of the human brain, exhibits remarkable capabilities in complex image analysis tasks (Li and Gao, 2019; Sun et al., 2024). Nevertheless, image quality degradation and variations in pipeline diameter present substantial challenges for automated detection systems, particularly these based on deep learning. Images with low contrast and poor brightness can significantly impair the feature extraction capabilities of deep learning models, while noise interference compromises model generalization. Furthermore, the distinct imaging characteristics between large and small-diameter pipelines introduce domain adaptation challenges since models trained on specific diameter ranges often exhibit limited transferability across different pipeline geometries. Despite these technical difficulties, these advanced methodologies can augment or potentially replace manual inspection processes, substantially reducing subjective variability while enhancing both detection accuracy and operational efficiency.

Defect recognition in X-ray images of pipeline welds commonly involves three key components: X-ray image collection, image preprocessing, and defect recognition (Hou et al., 2020). As shown in Fig. 1, this paper focuses on the methods used for pipeline weld X-ray image preprocessing and the subsequent defect recognition process. It systematically reviews the advancements in image processing and computer vision technologies used for weld X-ray image defect detection. First, the various methods used for pipeline weld X-ray image preprocessing are introduced, including noise reduction and image enhancement techniques. Second, the paper delves into the current research progress on three primary approaches for weld defect recognition: signal processing, feature design, and deep learning-based methods. Third, five key areas of deep learning-based detection techniques are discussed: dataset development, image classification, semantic segmentation, object detection, and performance evaluation. This review concludes by summarizing the current state of the related research and reviewing the potential future developments in this field.

2. Pipeline weld X-ray image preprocessing method

Radiation source variations, digitizing equipment limitations, and the inherent complexity of weld structures can cause noise, uneven gray values, and blurriness in weld X-ray images. Furthermore, the uneven gray values cause low contrast between weld defects and the surrounding background, resulting in unclear defect edges. Pipelines with different diameters exhibit distinct weld X-ray image characteristics. The weld X-ray images of large-diameter pipelines typically display complex noise distribution and higher background interference, while those of small-diameter pipelines demonstrate pronounced edges, with smaller faults that are more susceptible to noise interference. These challenges impede accurate weld defect evaluation, necessitating preprocessing to improve weld X-ray image quality.

2.1. Noise reduction method of pipeline weld X-ray image

Pipeline weld X-ray images mainly contain photoelectronic noise generated during the photoelectronic conversion process and electronic noise due to the random thermal motion of electronic devices. The noise can be categorized into Gaussian noise, salt-and-pepper noise, and a combination of the two. The mixed noise model is shown in Eq. (1):

$$N_{\mathrm{m}} = N_{\mathrm{g}} + N_{\mathrm{sp}} \tag{1}$$

where N_{m} denotes mixed noise, N_{g} signifies Gaussian noise, and N_{sp} represents salt-and-pepper noise.

The traditional methods used for noise reduction in weld X-ray images can be broadly classified into: spatial and frequency domain filtering. Spatial domain filtering methods, such as mean (Xu et al., 2005a), Gaussian (Ajmi et al., 2019), and median filtering (Kumar et al., 2018; Wang and Han, 2002; Xu et al., 2005b), are commonly used to reduce noise in weld X-ray images due to their simplicity and straightforward implementation. However, the size of the filter window significantly influences the efficacy of median and mean filtering. Additionally, mean and Gaussian filters tend to damage image details and cause edge blurring. While median filtering helps preserve edge clarity, it is less effective at reducing Gaussian noise. Contrarily, appropriately designed frequency domain filters can effectively remove noise while preserving edge and detail information. Wiener filtering (Xu et al., 2005a) is a popular frequency-domain method used to reduce noise in weld X-ray images. It reduces the minimum mean square error (MMSE) between the output and ideal signals by analyzing the statistical

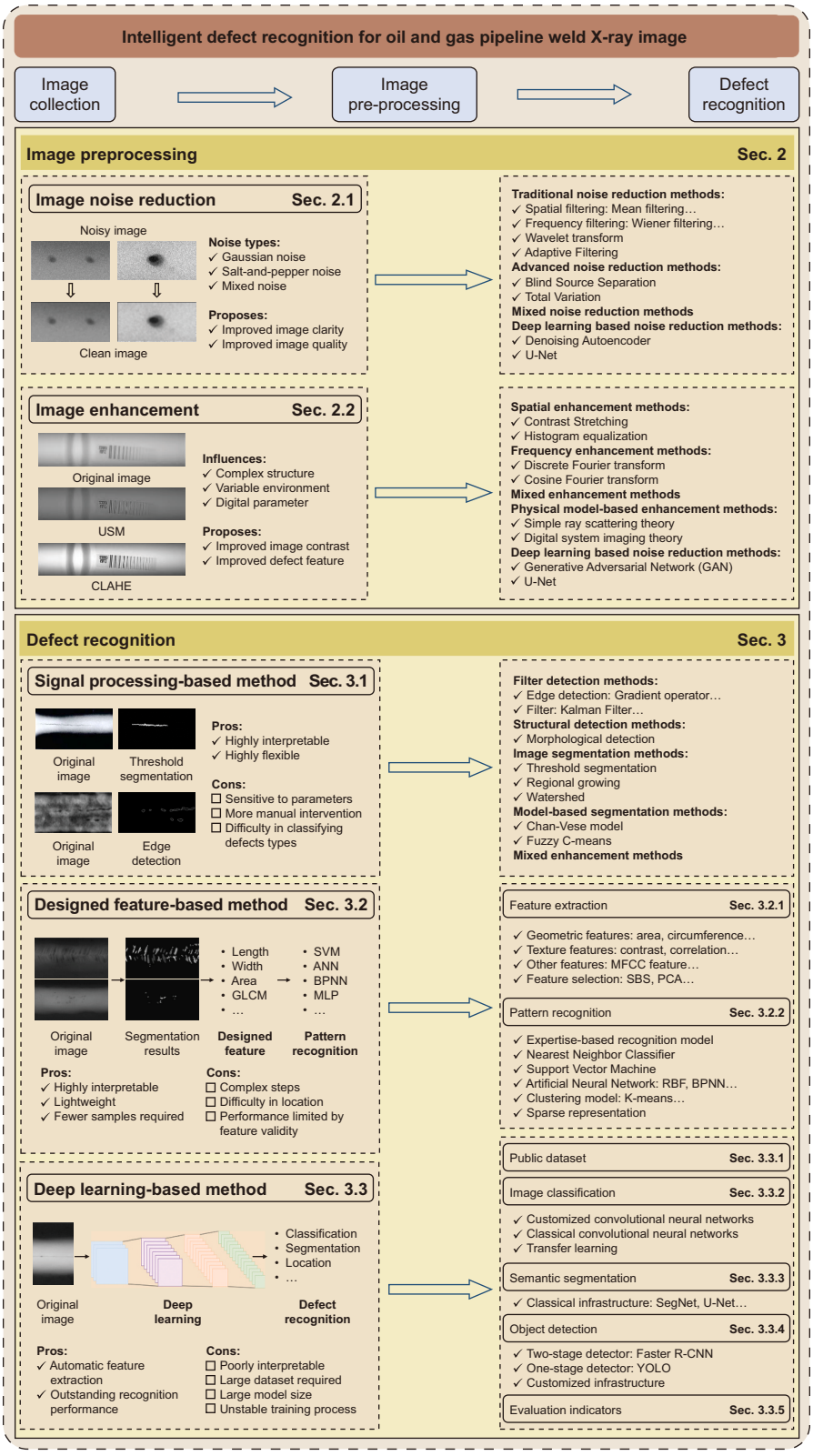

Fig. 1. A diagram of intelligent defect recognition in oil and gas pipeline weld X-ray images.

characteristics of both the signal and the noise. However, the efficacy of Wiener filtering depends heavily on the accuracy of the statistical signal and noise models. Model deviation from reality compromises the noise reduction performance. Furthermore, since Wiener filtering is based on the Gaussian noise model to optimally estimate the statistical features of noise, it performs poorly when dealing with non-Gaussian noise types. In addition to traditional spatial and frequency domain filtering techniques,

wavelet transform (Liu, 2007; Xu et al., 2005b; Yang and Wang, 2009) has gained popularity for weld X-ray image noise reduction due to its ability to perform multiscale analysis. However, the success of wavelet-based noise reduction largely depends on the proper selection of wavelet coefficients and thresholds. In summary, although traditional methods are extensively used to reduce noise in weld X-ray images, they present limitations. The subjective selection of filter parameters can impact the noise reduction efficacy and result in image detail loss. Additionally, these methods may not be sensitive to the mixed noise types often present in weld X-ray images, further limiting their applicability.

Various adaptive noise reduction methods based on traditional techniques have been applied to weld X-ray images to reduce the reliance on subjective parameters and optimize the noise reduction efficacy. These methods include adaptive Wiener filtering (Vilar et al., 2009a; Zapata et al., 2011), adaptive median filtering (Hwang and Haddad, 1995), and adaptive wavelet noise reduction (Li et al., 2011). Adaptive Wiener filtering reduces noise by calculating the mean and variance of local pixels and adjusting the degree of smoothing applied to each region based on the magnitude of the variance. Less smoothing is applied to regions with higher local variance to preserve more detailed information (Vilar et al., 2009a, b; Zapata et al., 2011). Gaussian low-pass filters are often used in conjunction with adaptive Wiener filtering to further optimize noise suppression (Vilar et al., 2009a, b; Zapata et al., 2011). Adaptive median filtering adjusts the window size based on whether the median of the original window exceeds a certain threshold, allowing for adaptive noise reduction (Hwang and Haddad, 1995). Since establishing an appropriate threshold becomes more complex as the noise density increases, the adaptive median filter may fail to effectively distinguish between noise and image details, resulting in blurring. To address this, a two-layer noise monitoring mechanism is introduced, which uses the maximum, minimum, and median pixel values in the window to optimize the adaptive median filtering threshold (Zhan et al., 2018). Additionally, weighting the mean and median pixel values in the active window helps remove noise while preserving detail information more effectively (Zhan et al., 2018). Adaptive wavelet noise reduction estimates the local noise variance of wavelet coefficients using the maximum variance method and dynamically adjusts the thresholds of these coefficients via Bayesian shrinkage. This process reduces noise while preserving image details, which enhances overall noise reduction performance (Li et al., 2011).

Several advanced methods have been introduced to optimize noise reduction in weld X-ray images and minimize the trade-off between noise suppression and detail preservation. These include non-local mean filtering (Buades et al., 2005), nonlinear diffusion filtering (Perona and Malik, 1990), bilateral filtering (Tomasi and Manduchi, 1998), blind signal separation noise reduction (Shen, 2020), and total variation noise reduction (Rudin et al., 1992). Non-local mean filtering enhances noise reduction performance by exploiting non-local self-similarity within the image. It uses similarity metrics to search for pixel blocks corresponding to the target pixel. Then the weighted average of these blocks is calculated to estimate the clean pixel values, which effectively reduces noise while preserving image details (Buades et al., 2005). Commonly used similarity metrics include the weighted Euclidean distance and Gaussian kernel (Lee et al., 2019). However, while non-local mean filtering excels at detail preservation, its performance is limited in low- and high-noise regions with low contrast. To address this, a relationship equation is established between the noise variance and gray value, enabling dynamic and adaptive adjustment of the noise variance (Cha et al., 2023). This allows for the prediction of the optimal parameter combination for the non-local mean algorithm. Consequently, the filter can improve noise reduction in high-noise regions while decreasing the filtering strength in low-noise regions, consequently preserving more details. Additionally, improved local noise reduction filtering (Shi et al., 2011) and neighborhood filtering (Shi et al., 2013), which are based on this noise variance estimation method, dynamically adjust the filtering parameters. This adaptive approach helps to avoid excessive smoothing, effectively balancing noise suppression and detail retention. Nonlinear diffusion filtering reduces noise by iteratively solving nonlinear partial differential equations. This method involves establishing an appropriate nonlinear diffusion coefficient, which is adjusted to suppress noise while preserving image details. Nonlinear diffusion filtering can be divided into nonlinear isotropic diffusion filtering and nonlinear anisotropic diffusion filtering according to the type of diffusion coefficient used (Weickert, 1998). Anisotropic diffusion filtering, which considers both local pixel intensity and gradient information, generally performs better than isotropic filtering in retaining detail while reducing noise (Faridafshin et al., 2021). To enhance the noise reduction performance of nonlinear anisotropic diffusion filtering, images are often decomposed into sub-bands representing features at different scales using wavelet transform. Anisotropic diffusion is then applied in the wavelet domain, which enhances the effective preservation of fine details (Boudani and Nacereddine, 2019). However, the performance of nonlinear anisotropic diffusion filtering may be limited in low-contrast regions due to its reliance on a fixed number of iterations or a standard termination criterion. This can result in an inability to effectively balance noise reduction and detail preservation. To address this issue, the grayscale probability is incorporated into the diffusion coefficients to improve noise reduction in low-contrast areas (Malarvel et al., 2017). Additionally, an entropy-based stopping criterion is introduced to prevent excessive smoothing that may lead to detail loss (Malarvel et al., 2017). Despite its efficacy, nonlinear anisotropic diffusion filtering requires significant computational resources since it calculates gradients in four directions for each iteration to determine the diffusion coefficient. A more efficient approach has been developed to reduce computational complexity. This method determines the diffusion coefficient according to the local pixel intensity distribution and only calculates the gradients in the horizontal and vertical directions, which significantly reduces computational cost (Michel-González et al., 2011). Bilateral filtering simultaneously considers spatial proximity and gray value similarity, using a Gaussian function to quantify these factors as weights, which are then used for weighted pixel averaging to effectively reduce noise while preserving image details (Tomasi and Manduchi, 1998). Although bilateral filtering can mitigate the trade-off between noise reduction and detail preservation, it struggles to accurately distinguish edges in images containing inhomogeneous gray values, resulting in edge blurring. Therefore, a grayscale compensation function is introduced to dynamically adjust the weights according to the similarity between the pixel grayscale levels (Lu and Huang, 2022). This improves the ability to distinguish between noise and edges, which protects edge details while still reducing noise. Canny edge detectors are also employed for edge detection. A cost function is used to select the most relevant pixels in the edge regions, which compensates for the detail loss that often occurs during traditional bilateral filtering and improves image clarity (Cha et al., 2023). Blind signal separation noise reduction isolates noise from the source signal by analyzing the statistical properties of the image and directly estimating the individual signal components. The methods commonly used to assess these statistical properties include independent

component analysis, principal component analysis (PCA) (Shen, 2020), and nonlinear principal component analysis (Shen et al., 2020). To enhance the efficacy of blind source separation for noise reduction and image detail preservation, the original signals are iteratively separated using deflation techniques (El-Tokhy and Mahmoud, 2015). This process involves extracting the desired source signals using methods such as peak maximization, quadratic gradient, and cyclic smoothing to optimize noise reduction and minimize detail loss. The total variation method reduces noise by iteratively minimizing an energy function that combines the data fidelity and regularization terms. The regularization term consists of the sum of the image gradient and the L_1 norm, where the L_1 norm is used to control the degree of regularization. Adjusting the L_1 norm helps preserve image details, particularly at the edges of weld X-ray images, while reducing noise. This approach prevents excessive smoothing, which can cause blurring of important edge structures (Cho and Lee, 2018; Faridafshin et al., 2021; Lee, 2019).

Although adaptive and advanced techniques can effectively optimize noise reduction and minimize detail loss, single noise reduction methods still face limitations in dealing with mixed noise. Therefore, hybrid noise reduction models have been developed by combining the strengths of multiple filters to enhance mixed noise reduction efficacy. Since median filtering is particularly effective at handling salt-and-pepper noise and wavelet transform excels at reducing Gaussian noise, these approaches are commonly combined to reduce mixed noise. However, median filtering and wavelet transform performance are highly sensitive to subjective parameters. Consequently, a mixed noise model (Shen et al., 2014), incorporating adaptive weighted median filtering (Zhan et al., 2018) and adaptive wavelet transform, is employed to improve the results. Computationally simple mean filtering is often combined with median filtering to further reduce mixed noise. A noise intensity estimation model is introduced to decrease the reliance on specific filtering window sizes and enhance noise reduction. This model adaptively adjusts the filtering window according to variations in noise intensity (Zhang et al., 2021d).

Convolutional neural networks (CNNs) (Li et al., 2005) are increasingly used to reduce noise in weld X-ray images due to the rapid development of deep learning. Compared to traditional methods, deep learning-based noise reduction models can automatically learn complex patterns (Luo et al., 2023). The parameters of these models are optimized using large datasets, resulting in superior noise reduction performance. In addition to classical CNNs, more advanced architectures such as U-Net (Kim et al., 2019) and denoising autoencoders (Farooq and Savaş, 2024) have been employed to reduce noise and predict cleaner weld X-ray images. However, conventional deep CNNs typically consider pixel-wise differences between the noisy and clean images, which can result in over-smoothing and vital detail loss. Therefore, generative adversarial networks (GANs) have been introduced to address this issue and improve the post-noise reduction image quality. GANs generate images with more natural textures by incorporating a more complex loss function that constrains the generator, effectively preventing over-smoothing (Sun et al., 2018b). Additionally, self-supervised learning leverages the images themselves to reduce noise and the reliance on paired training datasets, which significantly minimizes detail loss (Qian et al., 2024).

In summary, traditional filtering methods, such as spatial and frequency domain filtering, are limited by subjective parameters that can affect their noise reduction efficacy, often resulting in the loss of image detail. While adaptive filtering methods improve the balance between noise reduction and detail preservation by decreasing the reliance on subjective parameters, their performance is still constrained by factors such as noise type and parameter settings. Therefore, more advanced noise reduction techniques have been introduced, such as nonlocal mean filtering, nonlinear anisotropic diffusion, and blind signal separation. These methods enhance the balance between noise reduction and detail preservation by employing more sophisticated mathematical models and algorithms. Due to their unique formation process, weld X-ray images are often affected by mixed noise, which presents a challenge for single noise reduction methods. Consequently, noise reduction models have been proposed that combine multiple filters to optimize the efficacy in mixed noise scenarios. Unique noise characteristics must also be considered when denoising the X-ray images of pipelines with different diameters. Mixed noise issues are prominent in large-diameter pipeline weld X-ray images due to wide weld regions and complex backgrounds. Therefore, denoising methods must simultaneously address multiple noise types while preserving complex background features. Hybrid denoising models combined with appropriate edge-preserving techniques are more suitable for these applications. Narrow weld regions and smaller defects represent the primary challenges in small-diameter pipeline weld X-ray images, which require the precise retention of subtle features while suppressing noise. Edge-preserving methods such as nonlinear anisotropic diffusion and improved bilateral filtering are more applicable in these scenarios. In recent years, deep learning models have emerged as a powerful tool for reducing noise in weld X-ray images due to their considerable learning capabilities and adaptability. These models can effectively address various noise types and preserve image details while reducing noise. Despite the improved performance of deep learning-based noise reduction models, their applicability is limited by the constraints of available datasets. Additionally, since current deep learning models tend to focus on learning complex noise patterns from data, they often neglect the underlying principles of noise formation, which can substantially decrease their performance. Therefore, future research should focus on developing deep learning noise reduction models that can be trained with limited data using unsupervised or self-supervised methods, to overcome dataset limitations. Moreover, integrating physical- and data-guided approaches to create noise reduction models informed by physical principles can further enhance the performance of deep learning models.

2.2. Enhanced method of pipeline X-ray weld image

Pipeline weld X-ray images are digital representations of weld X-ray films, created using industrial negative digitizing and scanning equipment. However, various factors can substantially reduce X-ray images quality, including equipment limitations, environmental conditions, and improper digitizer operation, which can hinder defect assessment. Therefore, several image enhancement methods have been proposed to enhance the quality of X-ray images by improving their brightness, contrast, and detail. These techniques can be categorized into spatial-domain, frequency-domain, physical model-based, and deep learning-based enhancement methods.

Spatial domain enhancement methods employ the original image data. Pixel values are modified by utilizing either individual pixels or local relationships between pixels to improve image quality. Traditional spatial domain enhancement methods primarily include linear transformation (Luo et al., 2024), logarithmic transformation (Liu et al., 2021; Luo et al., 2024), contrast stretching (Thien et al., 2017; Njogu, 2016), and histogram

equalization (Li, 2016; Luo et al., 2024). Contrast stretching and histogram equalization are particularly effective. Contrast stretching improves overall contrast by mapping the gray values to a new range using a mapping function. However, simple contrast stretching can cause improper exposure and detail loss in images with uneven lighting. Consequently, local contrast stretching has been proposed, which considers the statistical properties of local regions and applies different mapping functions to various image areas for optimization (Liu, 2016). While local contrast stretching yields better results, it may introduce edge halos when a large luminance difference is evident between the two sides of an image edge. Fuzzy entropy is used to dynamically adjust the degree of local contrast stretching to further enhance its performance (Guo et al., 2023), which helps preserve edge information while improving image details. Since noise often shares high-frequency characteristics with image edges and textures, local contrast stretching can inadvertently amplify noise during the contrast enhancement process. Therefore, statistical features, such as mean and standard deviation, are used to segment the original image into foreground, boundary, and problematic regions (Mustafa et al., 2022). Local contrast stretching is then applied to the problematic regions, while global contrast stretching is used for the other areas to effectively reduce noise (Mustafa et al., 2022). Histogram equalization enhances image contrast by mapping pixel values to a new range, aiming for an approximately uniform pixel intensity distribution (Freeman, 1990). This approach is commonly used to enhance weld X-ray images due to its simplicity and straightforward implementation. However, it has certain limitations, including amplified noise, over-enhancement, fine detail loss, and unnatural results. These issues can be mitigated by the introduction of contrast limited adaptive histogram equalization (CLAHE) (Dang et al., 2015; Pisano et al., 1998), which limits over-enhancement and minimizes noise amplification by dividing the image into smaller regions, while using a predefined threshold to control the enhancement intensity. Sub-histogram equalization further refines the enhancement process by segmenting the image histogram according to the illumination thresholds, which increases control. It also corrects the cumulative distribution function (CDF), probability density function (PDF), and output function curve to improve the contrast while preserving the brightness for a more natural result (Zhao et al., 2020). Advanced methods such as bilateral filtering (Zhao, 2021; Zhao et al., 2020) and anisotropic diffusion filtering (Dang et al., 2015) are often applied after enhancement to decrease noise levels and enhance image quality. Since different weld defects exhibit distinct texture patterns in weld X-ray images, textural details are critical for accurate defect identification. Therefore, enhancement techniques focused on neighborhood-based information processing are proposed to improve image contrast and textural detail. These methods exploit the spatial correlation between neighboring pixels and include local pixel grouping (Movafeghi et al., 2015), variance (Chen, 2016; Li et al., 2024d), and deviation (Han et al., 2023). Local gradient field enhancement techniques employ pixel intensity gradients to enhance edges and other important features, consequently improving local contrast and reducing detail loss (Zhou et al., 2019). However, the sole use of this technique reduces visual quality since it disregards the global characteristics of the image. Therefore, the concept of minimum perceptual difference is used to divide the image into four luminance regions and adjust the gradient according to the luminance of each, which ensures that the enhancement is more consistent with human visual perception (Zhao, 2018). In addition to spatial domain enhancement methods, Jiang et al. (2017) proposed a pseudo-color enhancement approach based on color-space transformation. The hue-saturation-intensity (HSI) color space and pixel self-transformation techniques were employed to effectively improve the quality of low-grayscale, low-contrast pipeline weld X-ray images by adaptively adjusting the image intensity and hue parameters.

Although traditional spatial domain enhancement methods can effectively improve image quality, they are limited when dealing with textural details and noise, particularly due to the high-frequency characteristics of image edges and textures. One significant drawback is the potential loss of textural details. While optimizing traditional spatial domain enhancement techniques can improve performance, this often involves more complex algorithmic designs. Frequency-domain enhancement methods, such as discrete Fourier transform (DFT) and cosine Fourier transform (CFT), improve textural details by analyzing its frequency or wavelet domain features. However, CFT methods can introduce artifacts, especially in complex images such as weld X-rays (Movafeghi et al., 2023). Additionally, the low-frequency DFT resolution in low-resolution images can hinder detail recovery, which negatively affects image quality. Therefore, high-pass filters have been introduced (Rajab et al., 2007), which enhance the high-frequency DFT components, helping to highlight image details and improving the adaptability of the method to low-resolution images (Rajab et al., 2007). Unlike CFT and DFT, wavelet transform has been increasingly applied to enhance weld X-ray images due to its multiscale analysis capabilities and strong adaptive performance. Wavelet transforms employ thresholding, gain adjustment, or nonlinear transforms to enhance high-frequency information. To reduce the dependence on manually established wavelet thresholds, Rayleigh distribution is used for automatic threshold estimation to adaptively enhance the image details (Yahaghi et al., 2021).

Although both the individual spatial-domain and frequency-domain enhancement methods demonstrate strong performance, each focuses on specific areas. Spatial-domain enhancement methods primarily improve brightness and contrast, while frequency-domain techniques concentrate on enhancing textural details. Since properly designed frequency-domain methods can simultaneously enhance texture and reduce noise, hybrid methods have been proposed that integrate both to improve weld X-ray image quality. Common hybrid enhancement methods typically use spatial-domain techniques to enhance image brightness and contrast, after which frequency-domain strategies are employed to highlight specific details or reduce noise (Movafeghi et al., 2005; Sadah et al., 2013). The spatial-domain techniques used in these hybrid methods include histogram equalization (Sadah et al., 2013), power law transform (Sadah et al., 2013), and morphological transformations (Sadah et al., 2013). Commonly used frequency-domain methods include Gaussian low-pass filters (Sadah et al., 2013), Butterworth filters (Sadah et al., 2013), and wavelet transforms (Movafeghi et al., 2005). Moreover, a more sophisticated hybrid enhancement method has been proposed to reduce noise and enhance textural details due to their critical importance during weld defect analysis (Wang, 2015). This method first applies wavelet transform in the frequency domain to preserve details while reducing noise. Next, local histogram equalization is employed in the spatial domain to improve contrast. Finally, homomorphic filtering is applied in the frequency domain to optimize image brightness and contrast.

Although spatial-domain and frequency-domain enhancement methods can significantly improve image quality, these approaches primarily rely on the mathematical or statistical image processing properties without considering the underlying formation principles of the original or enhanced images. Consequently, these methods are less robust and may display poor enhancement efficacy when used for lower-quality or more complex images,

such as weld X-ray images, which often exhibit higher darkness levels. These limitations can be addressed by constructing a physical model that simulates the weld X-ray imaging process for more effective quality improvement. Physical models typically include approaches based on simple ray scattering, image signal processors, and Retinex theory. The simple ray scattering model is adapted from the atmospheric scattering model (Tang et al., 2024) for X-ray imaging, which suggests that an X-ray image consists of a combination of direct transmission and scattered X-rays. This model primarily describes the scattering phenomenon that occurs when X-rays pass through an object and how this affects image quality (Zhang, 2022; Zhang et al., 2021c). The image quality is enhanced by introducing dark channel prior constraints to estimate both the direct transmission function and scattering intensity (Kim et al., 2018). The simple ray scattering model is then used to calculate the image intensity (Kim et al., 2018). In addition, boundary constraints and context regularization are applied to ensure more accurate projection estimation and to enhance the preservation of key image features (Zhang, 2022; Zhang et al., 2021c). The image signal processor model is primarily used to construct mapping functions that describe the relationship between the blackness of solid X-ray film and the grayscales in digital images. These functions predict the corresponding grayscales at various black levels, ultimately optimizing image brightness. A human vision model, similar to the digital imaging system model, can also be used to enhance weld X-ray images (Chang et al., 2019). The image signal processor and human vision models are often combined for a more accurate mapping to further enhance efficacy (Mu et al., 2013). This combined model predicts grayscales more effectively, which ensures that the enhanced image aligns better with the visual characteristics of the human eye. The Retinex model is based on the reflectance imaging illumination model, which assumes that an image can be decomposed into light and reflectance components. The goal is to restore the illumination information of an object by recovering or estimating the surface reflectance, consequently enhancing the contrast and details of an image (Land, 1978). Retinex models are mainly categorized into single-scale, multiscale, and variable-frame models (Li, 2016). Single-scale Retinex models usually estimate the illumination component using a filter, which is subtracted from the original image to obtain the reflectance component. A fixed-scale Gaussian filter is typically used to estimate the illumination. However, since the single-scale Retinex model can exhibit bias due to the nature of the fixed-scale filter, it is often combined with other contrast enhancement and edge sharpness algorithms to extract key image information and further improve image quality (Mei et al., 2023).

The multiscale Retinex model uses Gaussian filters of varying scales to estimate the light component, which effectively reduces artifacts and distortions, particularly in images with uneven illumination. Although logarithmic transformation is often utilized for image stretching to simplify computation, this can yield pixel values that exceed the display range, resulting in textural detail loss and image ghosting. Consequently, alternative methods such as S functions (Chen, 2016; Zhao, 2021) or power-function-based composite functions (Zhou, 2020) are used for image stretching instead of logarithmic transformation to minimize this issue. Although the performance can be improved by enhancing the multiscale Retinex model, selecting appropriate scales and weight coefficients remains a significant challenge. Improper scale and weight selection can cause image distortion, excessive smoothing, and detail loss. Additionally, both the single and multiscale Retinex models tend to amplify noise, especially in low-light images. To address these challenges, the variable-frame Retinex model introduces additional constraints to estimate the illumination and reflectance components (Cheng et al., 2009). The variable-frame model aims to improve image detail preservation and noise reduction by optimizing these components over several iterations.

Deep learning-based methods show significant potential for enhancing pipeline weld X-ray images. Unlike traditional methods, these approaches automatically learn and extract complex features from images to enhance them using techniques such as GAN (Krichen, 2023) and U-Net (Ronneberger et al., 2015). Image classes are used to construct a conditional GAN, which guides the generator to produce images based on specific conditions, consequently improving image quality. U-Net utilizes an encoder-decoder architecture, where the encoder captures the image features, and the decoder reconstructs the image. Image, textural, and structural similarity loss values are often combined to guide the U-Net image recovery process in enhancing contrast and reducing detail loss (Yang et al., 2022a). Furthermore, Retinex-Net (Wei et al., 2018), a deep learning model based on Retinex theory, is frequently employed to enhance low-light images. Incorporating an attentional mechanism into Retinex-Net enhances brightness and contrast while minimizing noise amplification in X-ray images with significant dark regions (Qian et al., 2024).

In conclusion, although traditional spatial domain enhancement methods are easy to implement, they present certain limitations, such as detail loss, improper exposure, and noise amplification. While improved spatial domain methods can address some of these issues, they often increase algorithmic complexity. Additionally, although spatial domain techniques that process neighborhood information are increasingly used to enhance image quality, the choice of local neighborhoods still constrains their performance. Contrarily, while frequency domain enhancement methods focus on processing frequency or wavelet domain features to enhance textural details, these methods can introduce artifacts, especially in high-noise images. Therefore, hybrid methods that combine spatial and frequency domain techniques are used to enhance weld X-ray images that display minimal noise, clearer detail, and improved overall contrast. The image characteristics must also be considered when enhancing the weld X-ray images of pipelines with different diameters. Single global enhancement methods display limited efficacy for large-diameter pipeline weld X-ray images due to wide weld regions and uneven illumination issues. Hybrid enhancement techniques can better handle extensive grayscale variations. Specifically, methods that combine local histogram equalization and frequency domain filtering can improve overall contrast while preserving local details. The noise amplification and detail loss caused by excessive enhancement represent a significant challenge in small-diameter weld X-ray images. Contrast-limited adaptive histogram equalization methods combined with appropriate noise suppression strategies are more suitable. Despite their efficacy, hybrid methods are problematic since they involve multiple steps and parameter optimizations, making them less practical for more complex images. Regular spatial and frequency domain approaches lack resilience when dealing with complex images. Contrarily, physical model-based enhancement methods provide more stability by improving image quality according to imaging physics principles. However, their performance depends on the accuracy of the physical model and parameters. Unlike physical models, deep learning-based enhancement methods can automatically learn image features from large datasets for enhancement or restoration. These approaches are more flexible and robust, particularly in extreme cases, since they do not require manual input of complex physical models. However, the performance of deep learning methods relies heavily on the availability of high-quality training data, while their computational complexity and resource requirements tend to be higher than

traditional methods. Therefore, future research should focus on simplifying deep learning models while improving their efficacy with limited data. Reducing the reliance on large datasets and decreasing the computational complexity are essential to increase the practicality and efficiency of deep learning enhancement methods.

2.3. Evaluation metrics for pipeline weld X-ray image preprocessing

Both subjective analysis and objective quantitative indicators are essential to effectively evaluate the efficacy of image preprocessing methods. Subjective analysis relies on human visual judgment to assess the performance of an algorithm by evaluating the image directly after preprocessing. However, objective quantitative indices use mathematical formulas to numerically evaluate an image, allowing for a more direct, unbiased performance assessment. These objective indices help eliminate the subjectivity inherent in human judgment and can distinguish image quality differences that may not be visible to the human eye. Consequently, various objective quantitative metrics are introduced to more accurately assess the efficacy of the methods used for weld X-ray image preprocessing. These indicators include the mean (*Mean*), standard grayscale deviation (*Std*), contrast (*C*), signal-to-noise ratio (*SNR*), information entropy (*IE*), spatial frequency (*SF*), average gradient (*G*), peak signal-to-noise ratio (*PSNR*), and structural similarity index (*SSIM*).

Mean: This indicates image brightness. A high *Mean* value indicates a brighter image, as shown in Eq. (2):

$$Mean = \frac{\sum_{i=1}^{C}\sum_{j=1}^{H} f(i,j)}{C \times H} \tag{2}$$

where C and H indicate the image width and height, respectively, while $f(i,j)$ denotes the image gray value at (i,j).

Std: This uses the degree of dispersion between the gray value and the *Mean* to assess the contrast, as shown in Eq. (3). A larger value indicates a higher image contrast:

$$Std = \sqrt{\frac{1}{C \times H}\sum_{i=1}^{C}\sum_{j=1}^{H}(f(i,j) - Mean)^2} \tag{3}$$

where C and H indicate the image width and height, respectively, while $f(i,j)$ denotes the image gray value at (i,j) and *Mean* represents the image pixel mean.

C: This responds to the overall contrast of the image by calculating the weighted average of the squared differences in the grayscales between each pixel and its corresponding local neighborhood pixels, as shown in Eq. (4). A higher value indicates more distinct differences between light and dark with sharper details:

$$C = \sum_{\sigma}\sigma(i,j)^2 P_{\sigma}(i,j) \tag{4}$$

where $\sigma(i,j)$ denotes the grayscale difference between the center pixel and one in the local neighborhood. $P_{\sigma}(i,j)$ denotes the probability that the grayscale difference of a pixel in the local neighborhood is σ.

SNR: This measures the noise level by calculating the ratio of the effective signal strength to the noise signal strength, as shown in Eq. (5). A higher *SNR* indicates a more effective signal and improved performance of the noise reduction method:

$$SNR = 10 \times \log_{10}\left(\frac{P_{\text{signal}}}{P_{\text{noise}}}\right) \tag{5}$$

where P_{signal} is the power of the preprocessed image signal and P_{noise} is the noise power. In practice, the image power can be estimated by calculating the square sum of the image pixels.

IE: This is the quantitative metric of uncertainty in the grayscale distribution in an image, as shown in Eq. (6). A higher value indicates more uniform grayscale distribution in the image, yielding more details:

$$IE = -\sum_{i=1}^{C}\sum_{j=1}^{H} P(i,j)\log_2 P(i,j) \tag{6}$$

where C and H represent the image width and height, respectively, while $P(i,j)$ denotes the probability grayscale occurrence at (i,j).

SF: This is a physical measure of the textural detail in an image, as shown in Eq. (7) to Eq. (9). A higher *SF* indicates the emphasis of more details:

$$RF = \sqrt{\frac{1}{C \times H}\sum_{i=1}^{C}\sum_{j=1}^{H}(I(i,j) - I(i,j-1))^2} \tag{7}$$

$$CF = \sqrt{\frac{1}{C \times H}\sum_{i=1}^{C}\sum_{j=1}^{H}(I(i,j) - I(i-1,j))^2} \tag{8}$$

$$SF = \sqrt{RF^2 + CF^2} \tag{9}$$

where *RF* represents the row spatial frequency of the image, *CF* denotes the column spatial frequency of the image, C and H signify the image width and height, respectively, and $I(i,j)$ represents the image pixel value at (i,j).

G: This measures the intensity and clarity of the image details by calculating the pixel intensity transformation rate, as shown in Eq. (10). A higher *G* yields clearer image detail and better image quality:

$$G = \frac{1}{C \times H}\sum_{i=1}^{C}\sum_{j=1}^{H}\sqrt{\frac{\left(\frac{\partial I(i,j)}{\partial i}\right)^2 + \left(\frac{\partial I(i,j)}{\partial j}\right)^2}{2}} \tag{10}$$

where C and H denote the image width and height, respectively, $I(i,j)$ represents the image pixel value at (i,j), $\frac{\partial I(i,j)}{\partial i}$ denotes the image gradient in the horizontal direction, and $\frac{\partial I(i,j)}{\partial j}$ signifies the image gradient in the vertical direction.

PSNR: This measures the algorithm performance by comparing the difference between the original and preprocessed images, as shown in Eq. (11). A higher value indicates better preprocessed image quality and algorithm performance:

$$PSNR = 20 \times \log_{10}\left(\frac{MAX}{\sqrt{MSE}}\right) \tag{11}$$

where *MAX* denotes the maximum image pixel value and *MSE* represents the mean square error between the preprocessed and original images:

$$MSE = \frac{1}{C \times H}\sum_{i=0}^{C-1}\sum_{j=0}^{H-1}(I(i,j) - K(i,j))^2 \quad (12)$$

where C and H denote the image width and height, respectively, $I(i,j)$ represents the image pixel value (i,j), and $K(i,j)$ denotes the pixel value of the preprocessed image at (i,j).

SSIM: This combines brightness, contrast, and structural changes, representing a value between 0 and 1, as shown in Eq. (13). A value closer to 1 indicated a higher preprocessed image quality and algorithm performance:

$$SSIM(I,K) = \frac{(2\mu_I\mu_K + c_1)(2\sigma_{IK} + c_2)}{(\mu_I^2 + \mu_K^2 + c_1)(\sigma_I^2 + \sigma_K^2 + c_2)} \quad (13)$$

where I and K denote the original and preprocessed images, respectively, μ_I and μ_K represent the original and preprocessed image mean values, respectively, σ_{IK} denotes the covariance of the original and preprocessed images, σ_I and σ_K denote the variance of the original and preprocessed images, respectively, and c_1 and c_2 are smaller constants.

The characteristics and applicability of different evaluation metrics vary during pipeline weld X-ray image preprocessing. Although *Mean* can reflect the overall image brightness level, it cannot assess local detail quality. *Std* and *C* can indicate overall image contrast, but the noise interference may produce misjudgments. *SNR* and *PSNR* can accurately quantify the effect of denoising but tend to neglect detail loss. Although *SF* and *G* can present edge and textural information, these metrics are noise sensitive. *IE* can be employed to evaluate image detail richness but cannot distinguish between useful information and noise. *SSIM* comprehensively considers brightness, contrast, and structural changes but is more computationally complex than other metrics. Consequently, a multimetric approach is necessary to comprehensively evaluate image preprocessing performance. Traditional metrics fail to reflect quality differences in key regions such as the image quality indicator (IQI), weld, and defect areas, which vary in defect detection relevance. To better evaluate pipeline weld X-ray image quality, a comprehensive multiregion quality evaluation method was proposed based on tanalytical hierarchical process (Tian et al., 2025). This method was used to construct comprehensive quality indicators using the IQI count, sharpness, contrast, information entropy, and average grayscale, for quality assessment across different regions. Multiregion evaluation methods still present several drawbacks despite partially addressing regional differentiation assessment problems. Yahaghi et al. (2021) utilized dynamic wavelet transform to enhance welding radiographic image details and compared manual detection accuracy before and after enhancement. The results showed that the manual identification accuracy of crack defects improved by approximately 26% after image enhancement. Dang et al. (2015) significantly enhanced image quality using multistep enhancement methods, which improved information entropy improved by approximately 21.43% and defect segmentation accuracy by at least 41.37%. Since preprocessing aims to improve image quality to enhance defect detection, current evaluation metrics do not directly correlate with fault recognition performance. Additionally, existing evaluation systems primarily rely on fixed metric weights, restricting adaptation to the diverse requirements across different pipeline diameters, imaging conditions, and defect types. Therefore, future work should focus on developing defect detection task-oriented assessment frameworks and comprehensive adaptive-weight evaluation metrics. Machine learning or deep learning methods should be utilized in task-oriented frameworks to establish quantitative models between the image preprocessing metrics and key indicators such as defect detection accuracy and recall rates. Therefore, the evaluation results can be used to both assess preprocessing performance and guide detection performance improvement. Regarding adaptive-weight evaluation metrics, research should focus on developing automatic weight-adjustment algorithms using regional image features and application scenarios. These algorithms should allocate weights according to the different characteristics of the IQI, weld, and defect regions. They should also adapt to diverse application scenarios including different pipeline diameters, imaging conditions, and defect types to increase the valuation precision and practicality.

2.4. Brief summary

This section comparatively analyzes the methods used for pipeline weld X-ray image preprocessing to evaluate their performance and applicability. Table 1 lists the performance metrics and technical characteristics associated with the various denoising and image enhancement methods. Different preprocessing approaches exhibit notable variations in their technical principles and performance characteristics. Traditional spatial-domain and frequency-domain methods are widely applied and easy to implement. However, they often rely on subjective parameters, which can lead to image detail loss during denoising and may even amplify noise during enhancement. Contrarily, advanced filtering and hybrid methods improve the balance between denoising and detail preservation by employing more sophisticated mathematical models. These methods effectively address the mixed noise and non-uniform illumination issues commonly found in weld X-ray images. Although physics-based approaches yield more consistent enhancement results, their performance depends on model accuracy. While deep learning methods demonstrate superior performance in image denoising and quality enhancement due to their powerful learning capabilities, they require substantial high-quality training data and involve significant high computational complexity. Given the differences between the image characteristics of large-diameter and small-diameter pipelines, Table 2 summarizes the recommended methods for different pipeline types.

3. Defect recognition method for pipeline weld X-ray image

Methods for weld defect recognition in X-ray images are attracting considerable research and industry attention due to the rapid development in X-ray imaging and computer vision technologies. Ensuring pipeline weld quality in the oil and gas storage and transportation sectors is critical for ensuring safe operations. Traditional defect recognition methods rely on manual inspection, which is inefficient and prone to subjective bias. Contrarily, using computer vision technology to process digital X-ray images provides a fast, reliable approach for the intelligent detection of weld defects. Based on their technical principles, these methods can be categorized into three types according to their technical principles: signal processing-based, feature design-based, and deep learning-based defect recognition approaches.

3.1. Signal processing-based defect recognition method

Signal processing-based defect recognition methods identify defective areas in weld seams via digital signal processing, which typically involves: weld inspection and defect recognition. Regions likely to contain defects are extracted during the weld inspection phase, which reduces the impact of the background on recognition accuracy. Next, specialized methods are applied to accurately distinguish between defective and non-defective areas. Common

Table 1
A performance comparison of the representative preprocessing methods for pipeline weld X-ray images.

Method	Performance	Applicable scenario
Noise reduction method of pipeline weld X-ray image		
Adaptive median filtering + wavelet transform (Zhan et al., 2018)	*PSNR*: 32.860 *IE*: 6.8487	Mixed noise reduction
Neighborhood wavelet adaptive denoising (Li et al., 2011)	*PSNR*: 31.025 *SNR*: 39.816	Edge-preserving noise reduction
Nonlinear diffusion filtering (Malarvel et al., 2017)	*PSNR*: 36.960 *IE*: 4.0351	Edge-preserving noise reduction
Blind source separation denoising (Shen et al., 2020)	*PSNR*: 35.922 *SSIM*: 0.9254	Complex situation noise reduction
Total variable reduction (Faridafshin et al., 2021)	*PSNR*: 38.720	Variational optimization for noise reduction
GAN (Sun et al., 2018b)	*PSNR*: 32.950 *SSIM*: 0.8940	Complex pattern learning noise reduction
Self-supervised network (Qian et al., 2024)	*PSNR*: 36.444 *SSIM*: 0.9594	Self-supervised learning for noise reduction
Enhanced method of pipeline X-ray weld image		
Adaptive histogram equalization (Pisano et al., 1998)	*PSNR*: 12.495 *SSIM*: 0.4787	Contrast-limited enhancement
Multistep radiographic image enhancement (Dang et al., 2015)	*C*: 1790.7 *IE*: 7.50	Weld defect segmentation enhancement
Mixed enhancement (Wang, 2015)	*PSNR*:55.716	Edge detail enhancement
Simple diffusion model (Zhang et al., 2021c)	*SF*: 7.3031 *G*: 5.1718	Physical model enhancement
Retinex model (Chen, 2016)	*SNR*: 33.377 *IE*: 7.12	Light-reflection separation enhancement
Gradient field + local variance (Han et al., 2023)	*PSNR*: 15.717 *SSIM*: 0.8089	Detail retention enhancement
Self-paced learning with Retinex-Net (Qian et al., 2024)	*PSNR*: 28.261 *SSIM*: 0.9719	Deep learning enhancement

Table 2
The methods used to preprocess X-ray images of welds in pipelines with different diameters.

Pipeline type	Weld X-ray image characteristics	Noise reduction method	Enhanced method
Large-diameter pipelines	Wide weld regions, complex noise distribution, more background interference, and uneven illumination	Integrated multi-technique mixed denoising strategies and deep learning methods	Mixed enhancement techniques, multiscale Retinex models and deep learning methods
Small-diameter pipelines	Narrow weld regions, pronounced edge effects, and susceptible to noise interference and imaging angle influence	Edge-preserving denoising techniques and deep learning methods	Adaptive contrast enhancement and detail-preserving intelligent enhancement methods

signal processing-based methods include filter, structural detection, and image segmentation.

Edge detection methods employ image gradient filters to extract edges, lines, and isolated points, and include gradient operator Sobel (Sun, 2019; Sun and Yuan, 2006), Prewitt (Sun, 2019), Roberts (Sun, 2019), Laplace (Sun and Yuan, 2006), and Canny edge detection (Ajmi et al., 2018; Sun, 2019). Advanced filtering defect recognition techniques include Canny-Deriche filtering (Schwartz, 2003), Kalman filtering (Zou et al., 2015), anisotropic diffusion filtering (Malarvel et al., 2017), and wavelet transform (Li et al., 2020). However, since these filter-based methods lack sufficient flexibility due to the varying characteristics of different defect types, some studies have proposed filters with adjustable weights to better accommodate different weld defects (Radi et al., 2021, 2022). These filters enhance or suppress specific parts of the image, improving the distinction between the background, vertical defects, and horizontal defects.

Structural detection methods extract and model defect features according to spatial placement rules for defect identification (Vilnrotter et al., 1986). In recent years, morphological testing (Song et al., 1996) has been widely employed approach for structural inspection. This approach is based on mathematical morphology principles and uses specific operators to analyze weld defect characteristics. Basic morphological operators include dilation (Alaknanda et al., 2006), erosion (Alaknanda et al., 2006), opening operation (Srikanth, 2012), and closing operation (Faramarzi and Motamedi, 2011), which help enhance target features in weld X-ray images while reducing the impact of extraneous noise. Since morphological detection relies on predefined shape elements, it is particularly effective in identifying geometric features that are sensitive to the shapes and sizes of defects.

Image segmentation is a key computer vision technique that uses digital signal processing to identify and localize potential weld defects in weld X-ray images. These methods are categorized into threshold segmentation, region growing, and watershed transformation according to different technical principles.

Threshold segmentation distinguishes defects from the surrounding weld region by selecting an appropriate gray-level threshold (Shafeek et al., 2004a). Although Otsu's thresholding is widely used (Ben Mhamed et al., 2012; Hashim, 2017), it relies on the assumption that there is a significant gray-level difference between the foreground (defect) and the background. This can reduce its efficacy in segmenting defects with similar gray values as the background. Therefore, a histogram concavity-based global thresholding technique has been introduced to determine the threshold by analyzing the image histogram (Saravanan et al., 2007). This improves defect-background separation and thresholding segmentation versatility. Although both Otsu's and

histogram-based methods are commonly used, their ability to detect small weld seam defects is limited. To enhance detection accuracy, Otsu's global thresholding is first creates a binary image that highlights the weld region, after which Sauvola's local thresholding is applied to refine the weld boundaries (Thiruganam et al., 2010). However, since the efficacy of Sauvola's method relies heavily on parameter settings, improper tuning may cause over- or under-segmentation. Therefore, the integral image technique is employed to compute local thresholds, reducing dependence on parameter tuning (Mahmoudi and Regragui, 2009a, 2009b). These thresholding methods all rely on selecting suitable thresholds to segment the image into the defect and background regions. However, they present challenges when the defect gray value is not sufficiently lower than certain background regions, prompting the introduction of maximum fuzzy entropy to obtain a three-level thresholding method optimized using a genetic algorithm (Wang and Wong, 2005). This approach divides the image into three distinct levels to enhance region separation and defect detection accuracy. Additional advanced techniques have been proposed to further accommodate diverse inspection scenarios and defect types, including a multiscale segmentation method based on an energy model and iterative threshold optimization to improve segmentation accuracy (Ge and Zhang, 2009). Another approach involves a multiscale, multi-intensity segmentation strategy using parameter space compression, which enhances versatility and precision (Yan et al., 2020). Furthermore, the region growing method is a pixel-based approach that segments defects by merging neighboring pixels with similar features into a single region (Sato et al., 2000). This approach is often combined with threshold segmentation where the weld region is first divided using a thresholding technique, followed by further weld defect segregation via region growing (Zhang et al., 2019). Watershed transform is a region-based segmentation technique that separates defective background regions by simulating geographical features according to the gray-level distribution in the image (Beucher and Lantuéjoul, 1979). However, since these techniques often suffer from over-segmentation that can cause fragmented boundaries, multistage watershed techniques are frequently used to refine defect edges and optimize segmentation results (Alaknanda et al., 2009).

Despite their widespread use for weld defect recognition, traditional segmentation methods present significant limitations, particularly when dealing with weld X-ray images containing uneven grayscales, which reduces their performance. Researchers have increasingly relied on more sophisticated model-based segmentation techniques to address these challenges. These methods can generally be categorized into: the fuzzy C-means clustering model (FCM) and the Chan-Vese model. FCM improves segmentation by measuring the degree of association between the various categories and each pixel according to its membership function (Bezdek et al., 1984). This approach is particularly effective for handling images with uneven grayscales since it allows each pixel to represent multiple categories simultaneously, which increases edge definition accuracy, especially in complex images. Background subtraction is a typical preprocessing step when using the FCM for weld defect recognition, which enhances weld region segmentation and improves defect detection accuracy (Sundaram et al., 2014). Conversely, the Chan-Vese model is a level-set active-contour model that has demonstrated significant potential for processing images with gray-level inhomogeneity. It minimizes generalized energy functionality to determine the optimal segmentation boundary (Halim et al., 2013) but requires an initial defined contour. This can decrease the result accuracy if the initial contour differs significantly from the actual target contour, prompting the frequent use of rectangles of various sizes as initial contours for segmentation (Abd Halim et al., 2013). Additionally, to further improve algorithm automation and reduce human intervention, FCM is often employed to generate an initial contour, which is then refined using the Chan-Vese model (Abdelkader et al., 2021).

While filter detection, structure detection, and image segmentation are all effective for weld defect recognition, each method presents certain limitations. For example, a single approach may not be capable of recognizing all types of weld defects effectively. Research has shown that certain segmentation techniques excel at recognizing specific types of defects (Abdelkader et al., 2021). Edge-based segmentation is particularly effective for identifying slag entrapment, incomplete penetration, and transverse cracks, while region growing segmentation is more suitable for detecting root incomplete penetration, biting edges, and porosity. Watershed segmentation is highly effective for recognizing creeping-type porosities, unfused regions, slag entrapment, and slag lines. Consequently, studies have explored multimethod combinations for efficient, accurate defect recognition. For instance, threshold segmentation is often integrated with edge detection and morphological techniques. In this combined approach, edge detection is used to extract edge information from the threshold segmentation results (Al-Hameed et al., 2013; Alaknanda et al., 2006), while morphological operations are applied to remove isolated noise points and smooth the defect boundaries (Al-Hameed et al., 2013; Chi et al., 2019; Du et al., 2011; Wang et al., 2012). Additionally, researchers have proposed more complex recognition frameworks that leverage the strengths of various techniques. These methods may combine FCM for weld defect segmentation, edge detection for edge feature extraction, threshold segmentation for defect identification, and morphological operations for defect boundary refinement and minor defect detection (Yazid et al., 2011, 2012). These hybrid strategies aim to improve defect recognition, particularly in complex weld X-ray images.

In summary, different types of weld defects exhibit unique characteristics, which reduce the adaptability of filter detection methods, particularly those based on edge detection algorithms. While designing advanced filters with controllable weights can improve the accuracy of defect detection to some extent, determining the appropriate weights typically relies on expert knowledge or repeated trials. Contrarily, structured methods, such as morphological detection, can more effectively capture weld defect features and enhance their visibility via specific actions. However, the detection accuracy is still influenced by the shapes and sizes of the defects. Unlike morphological detection, image segmentation techniques can directly process weld X-ray images and achieve defect segmentation. Threshold segmentation typically uses global thresholding to initially define the weld region, while local thresholding provides more precise defect localization. Region growing algorithms are commonly combined with global thresholding as a complementary strategy to address the incomplete segmentation often caused by single-threshold methods. Integral image techniques have been introduced for adaptive local threshold calculation to further minimize the impact of the parameter settings on segmentation performance. Furthermore, more advanced multiscale and multi-intensity segmentation methods have been developed to address different detection contexts and defect types. The multistage watershed transform can also be used for weld defect segmentation. However, traditional segmentation methods may not produce satisfactory results since the quality of weld X-ray images are often inferior. In such cases, model-based segmentation methods demonstrate more effective application potential. Given the limitations of using a single technique, combining multiple methods into a

comprehensive recognition strategy offers potential for improving the overall accuracy of defect recognition. Signal processing-based defect recognition approaches are highly interpretable but primarily focus on detecting and localizing defects instead of identifying the precise defect type. This limitation requires resolution via more complex postprocessing techniques. Nevertheless, signal processing-based defect recognition methods play a fundamental role in intelligent weld fault detection. Their processing results enable precise fault type recognition by providing critical foundational information for feature design-based defect detection methods.

3.2. Feature design-based defect recognition method

Feature design-based defect recognition methods typically utilize defect candidate regions obtained via signal processing-based defect detection techniques as the foundation. These approaches accurately recognize different defect types via manually designed, extracted discriminative features and advanced pattern recognition methods. Feature design-based defect recognition approaches are more successful in precisely classifying defects than signal processing-based defect detection techniques. Their core principle lies in transforming defect regions detected during the signal processing stage into feature descriptors, such as geometric and textural features, and subsequently constructing corresponding pattern recognition models for defect type determination. This method primarily involves feature extraction and defect recognition model building.

3.2.1. Feature extraction

Weld defects typically appear in X-ray images as grayscale variations relative to the normal weld region. Early research focused on describing defects using simple one-dimensional grayscale curve features. Liao et al. (1999) extracted 25 grayscale features, including the symmetry index, median symmetry index, and goodness of fit, using curve fitting as input for the defect recognition model. Additionally, metrics such as the mean square error and peak intensity were introduced as grayscale features to improve defect recognition model accuracy and directly capture the associated grayscale variations (Liao, 2004; Liao et al., 2000).

Further research has subdivided weld defects into seven categories: cracks, lack of fusion, lack of penetration, linear defects, circular defects, root concavity, and root undercut (Institute, 2015). Lashkia (2001) simplified weld defect classification into three categories based on intuitive morphological weld defect characteristics: circular, longitudinal, and transversal defects. This classification emphasizes the importance of geometry in describing weld defect features such as size, location, and shape. Table 3 shows the calculation of the common shape and geometric features.

Weld X-ray images are susceptible to various factors, such as the position and distance of the radiation source, the shooting angle, and scale variations, frequently causing the same defect to display different geometric shapes. Therefore, basic geometric shapes are often insufficient to accurately describe defects. To improve characterization capability, researchers have proposed geometric shape attributes that are resistant to geometric transformations, most of which are based on geometric invariant moments such as Hu, Zernike, and Legendre moments (Chandrasekharan et al., 2004; Mekhalfa and Nacereddine, 2017; Nacereddine et al., 2000; Rale et al., 2009). Additionally, the geometric invariant properties of defects have been described by combining spatial moments with basic geometric shape parameters (Nacereddine and Tridi, 2005). Nacereddine et al. (2013) enhanced the ability of geometric features to assess defect compactness and rectangularity by integrating geometric invariants with Fourier descriptors, enabling better differentiation between cracks and lack of fusion.

Table 3
Shape and geometric features.

Feature name	Sign	Equation	Explanation
Area	S	$\sum_{x=1}^{n}\sum_{y=1}^{m} f(x,y)$	n: Length of outer rectange. m: Width of outer rectange. $f(x,y)$: Pixel values at (x,y) coordinates.
Perimeter	C	$n_2+\sqrt{2}n_1$	n_2: Pixel number in the horizontal and vertical directions. n_1: Pixel number in the diagonal direction.
Perimeter-to-area ratio	PSR	$\frac{C^2}{S}$	C: Defect perimeter. S: Defect area.
Centroid	(S_x,S_y)	$\left(\frac{1}{mn}\sum_{i=1}^{n}\sum_{j=1}^{m} a_i, \frac{1}{mn}\sum_{i=1}^{n}\sum_{j=1}^{m} b_i\right)$	n: Length of outer rectange. m: Width of outer rectange. (a_i,b_i): Pixel location coordinates
Major axis	L_1	$\sqrt{(x_1-x_2)^2+(y_1-y_2)^2}$	This represents the maximum distance between any two pixel points on the defect boundary.
Minor axis	L_2	$\sqrt{(x_2-x_3)^2+(y_2-y_3)^2}$	This represents the minimum distance between any two pixel points on the defect boundary.
Aspect ratio	LSR	$\frac{L_1}{L_2}$	L_1: Major axis. L_2: Minor axis.
Bounding box area	S_n	$L_1\times L_2$	L_1: Major axis. L_2: Minor axis.
Compactness	ε	$\frac{S}{S_n}$	S: Defect area. S_n: Outer rectangle area.
Circularity	R	$\frac{4\pi S}{C^2}$	C: Defect perimeter. S: Defect area.
Minor axis-to-defect area ratio	SSR	$\frac{L_2}{S}$	L_2: Minor axis. S: Defect area.
Symmetry	SYM	$\frac{S_2}{S_1}$	S_1: Front 1/4 area of the spindle. S_2: Rear 1/4 area of the spindle.
Apex acuteness	USP	$\frac{(S_1+S_2)}{S}$	S_1: Front 1/4 area of the spindle. S_2: Rear 1/4 area of the spindle. S: Defect area.
Heywood diameter	HD	$2\sqrt{\frac{S}{\pi}}$	S: Defect area.

Geometric features focus on attributes such as shape and location, making them suitable for identifying defects with clear geometric characteristics, including circular and linear defects. However, geometric features alone are insufficient for subtle defects such as cracks, lack of fusion, and inclusions, which are typically represented by small textural variations in weld X-ray images. Therefore, studies have incorporated textural features to enhance defect characterization. The simplest textural extraction method analyzes local and global histograms, combining these features according to specific rules for a more comprehensive textural description (Sun et al., 2018a). Researchers have also used wavelet transform to extract textural features, which further improves defect characterization by adding richer, finer information, building on its strength in multiscale signal analysis (Wu et al., 2019; Zhou et al., 2018). Dong et al. (2019) developed an improved local binary mode-completely localized three-valued (CLTP) textural feature description approach to enhance boundary definition and local detail. In recent years, the grayscale covariance matrix-based textural feature extraction method has gained popularity for weld defect analysis (Ali et al., 2015; Kumar et al., 2014a, 2014b). This technique highlights the spatial correlation between pixel grayscale values, offering richer textural information than histogram-based methods. Compared to wavelet-based techniques, the grayscale covariance matrix method calculates textural features from multiple perspectives to provide a more detailed description. Table 4 lists the specific methods for determining textural features based on grayscale covariance matrices.

$$p_{i,j} = \frac{G_{i,j}}{n} \tag{14}$$

$$\mu_r = \sum_{i=1}^{G} i \times \sum_{j=1}^{G} p_{i,j} \tag{15}$$

$$\mu_c = \sum_{j=1}^{G} j \times \sum_{i=1}^{G} p_{i,j} \tag{16}$$

$$\sigma_r = \sqrt{\sum_{i=1}^{G} (i-\mu_r)^2 \times \sum_{j=1}^{G} p_{i,j}} \tag{17}$$

$$\sigma_c = \sqrt{\sum_{j=1}^{G} (j-\mu_c)^2 \times \sum_{i=1}^{G} p_{i,j}} \tag{18}$$

where $G_{i,j}$ denotes the grayscale co-occurrence matrix with dimension $G \times G$, n represents the total number of pixel pairs in the matrix, μ_r and μ_c are the average grayscale values of the rows and columns, and σ_r and σ_c represent the standard grayscale value deviations for the rows and columns.

$$p_r(i) = \sum_{j=1}^{G} p_{i,j} \tag{19}$$

$$p_c(j) = \sum_{i=1}^{G} p_{i,j} \tag{20}$$

$$HX = -\sum_{i=1}^{G} p_r(i) \log_2 p_r(i) \tag{21}$$

$$HY = -\sum_{j=1}^{G} p_c(j) \log_2 p_c(j) \tag{22}$$

Table 4
Textural features.

Feature name	Sign	Equation
Contrast	C	$\sum_{n=0}^{G-1} n^2 \sum_{i=1}^{G} \sum_{j=1}^{G} (i-j)^2 p_{i,j}$
Correlation	$Corr$	$\sum_{i=1}^{G} \sum_{j=1}^{G} \frac{(i \times j) \times p_{i,j} - (\mu_r \times \mu_c)}{\sigma_r \times \sigma_c}$
Variance	V	$\sum_{i=1}^{G} \sum_{j=1}^{G} (i-\mu)^2 p_{i,j}$ $\mu = \sum_{i=1}^{G} \sum_{j=1}^{G} i \times p_{i,j}$
Inertia	I	$\sum_{i=1}^{G} \sum_{j=1}^{G} (i-j)^2 p_{i,j}$
Entropy	E	$-\sum_{i=1}^{G} \sum_{j=1}^{G} p_{i,j} \log_2 p_{i,j}$
Cluster shade	CS	$\sum_{i=1}^{G} \sum_{j=1}^{G} (i+j-\mu_r-\mu_c)^3 p_{i,j}$
Cluster prominence	CP	$\sum_{i=1}^{G} \sum_{j=1}^{G} (i+j-\mu_r-\mu_c)^4 p_{i,j}$
Inverse difference moment	IDM	$\sum_{i=1}^{G} \sum_{j=1}^{G} \frac{p_{i,j}}{1+(i-j)^2}$
Angular second moment	ASM	$\sum_{i=1}^{G} \sum_{j=1}^{G} \left(p_{i,j}\right)^2$
Sum average	SA	$\sum_{i=1}^{2G} i \times p_{r+c}(i)$ $p_{r+c}(k) = \sum_{i=1}^{G} \sum_{j=1}^{G} p_{i,j}$ $k = i+j = 0,1,2,\ldots,2G$
Sum variance	SV	$\sum_{i=1}^{2G} \left(i - \sum_{i=1}^{2G} i \times p_{r+c}(i)\right)^2 \times p_{r+c}(i)$
Sum entropy	SE	$-\sum_{i=2}^{2G} p_{r+c}(i) \log_2 p_{r+c}(i)$
Difference entropy	DE	$-\sum_{i=0}^{G-1} p_{r-c}(i) \log_2 p_{r-c}(i)$
Information measure of correlation 1	$IMC1$	$\frac{HXY - HXY1}{max(HX, HY)}$
Information measure of correlation 2	$IMC2$	$\sqrt{1 - \exp\left[-2 \times \frac{(HXY2 - HXY)}{max(HX,HY)}\right]}$

$$HXY = -\sum_{i=1}^{G}\sum_{j=1}^{G} p_{i,j}\log_2 p_{i,j} \tag{23}$$

$$HXY1 = -\sum_{i=1}^{G}\sum_{j=1}^{G} p_{i,j}\log_2\left(\frac{p_{i,j}}{p_r(i)}\right) \tag{24}$$

$$HXY2 = -\sum_{i=1}^{G}\sum_{j=1}^{G} p_{i,j}\log_2\left(\frac{p_{i,j}}{p_c(i)}\right) \tag{25}$$

where HX and HY denote marginal entropy, HXY represents combined entropy, and $HXY1$ and $HXY2$ signify conditional entropy.

The accuracy of feature description relies heavily on the quality of defect segmentation since the results of this process are used to determine the majority of geometric and textural characteristics. To enhance feature description generalization, studies have explored methods to extract attributes directly from defective images, bypassing the need for segmentation. Mel-frequency cepstral coefficients (MFCC), which have shown strong performance in audio signal processing (Civera et al., 2019), are now being applied to characterize weld defects. Unlike traditional geometric and textural features, MFCC reduces the reliance on segmentation and introduces frequency domain analysis, offering new insights into defect characterization. Moreover, combining MFCC with polynomial features improves feature description and the performance of the defect recognition model in noisy environments (Kasban et al., 2011; Zahran et al., 2013).

In summary, various features can be used to characterize weld defects. Although defect recognition models tend to perform better when more features are used, this increases both the feature vector dimensionality and computational cost, requiring feature selection or dimensionality reduction. Feature selection reduces dimensionality by identifying the most representative subset from the original feature set, with notable approaches including sequential forward selection (SFS) (Mery and Berti, 2003) and sequential backward selection (SBS) (Valavanis and Kosmopoulos, 2010). When constructing the optimal subset, SFS incrementally adds features while SBS removes them. Although both methods are intuitive, they are susceptible to local optima due to their unidirectional approach. Therefore, Garcia-Allende et al. (2009) proposed sequential forward floating selection (SFFS), which allowed the dynamic addition or removal of features during subset construction, increasing the possible feature combinations. Although SFFS reduces the risk of local optima compared to traditional SFS and SBS, it still presents substantial computational complexity, particularly in high-dimensional feature spaces. Liao et al. (2009) addressed this by introducing an ant colony optimization algorithm, which enhanced global search capability and supported parallel processing, allowing the effective identification of the optimal feature subset even in large spaces. Alternatively, dimensionality reduction retains key information while mapping the data from a high-dimensional space to a lower-dimensional one. PCA is a widely used linear technique that projects data into a new orthogonal feature space to reduce dimensionality while preserving essential information (Duan et al., 2019; Hassan et al., 2012; Nacereddine and Tridi, 2005; Vaithiyanathan et al., 2013; Vilar et al., 2008, 2009a, 2009b; Wang et al., 2016a, 2016b; Zhang and Shi, 2022). Studies have shown that using three principal components during PCA achieves a defect recognition accuracy of up to 85% (Li, 2019). However, this precision declines as the number of components increases, suggesting that extracting too many components can cause redundancy and decrease recognition performance (Li, 2019). PCA conventionally presupposes that the data or its components adhere to Gaussian distribution characteristics. However, in high-dimensional feature spaces, data frequently manifest more intricate non-Gaussian distribution attributes, implying that PCA may not guarantee independence among the extracted components. Conversely, independent component analysis (ICA) extracts statistically independent elements, which improves the accuracy of feature dimensionality reduction (Li, 2019; Li and Mu, 2019). PCA and ICA primarily focus on feature dimension reduction in linear problems and may fail to capture nonlinear data characteristics due to the complexity of weld defect patterns. To improve nonlinear information extraction from weld defect features, methods such as kernel principal component analysis (KPCA) and Laplacian mapping are applied to reduce feature dimensions. KPCA uses a kernel function to map data to a higher-dimensional space, where PCA transforms nonlinear relationships into linear ones, improving feature extraction efficiency (Zhang, 2017a, 2017b). Contrarily, Laplacian mapping is used to preserve local structures during dimensionality reduction, enhance feature independence, and reduce redundancy (Wang et al., 2017).

3.2.2. Defect recognition model

Defect recognition models are essential in feature-based defect detection methods. These models enable intelligent defect recognition by establishing mappings between weld defect features and types and are generally divided into two categories: those based on expert knowledge and those utilizing machine learning. Expert knowledge-based recognition models rely on the insights and experiences of experts for construction and may consider the features of different weld defect types, such as the aspect ratio, grayscale, contrast, entropy, and others. These features are often used to construct a recognition model as a tree classifier, using specific rules or conditions to determine defect types (Ba and Teng, 2001; Shafeek et al., 2004b; Sun, 2019). Fig. 2 shows the expert knowledge-based classification method with a tree classifier.

Expert knowledge-based recognition models offer high interpretability since each node corresponds to some form of expertise. However, their performance is often limited by the validity of the selected features and the accuracy of the decision rules. Conversely, machine learning-based recognition models offer greater flexibility since they use data to learn complex mapping relationships between defect features and types. These models are categorized into supervised and unsupervised recognition models. Supervised models require a dataset with known defect types for training and commonly include nearest neighbor classifiers, support vector machines (SVM), and artificial neural networks (ANN).

Nearest neighbor classifiers recognize weld defects by calculating the Cartesian distance between the feature vectors of test and training samples. The classifier determines the closest training samples and assigns the test sample to the class of the nearest neighbors (Sun et al., 2018a). However, traditional nearest-neighbor methods rely on a single nearest sample for classification, making the model susceptible to outliers or noise, which can reduce accuracy. K-nearest neighbor (KNN) improves performance by considering the K nearest neighbors instead of only one, which helps prevent overfitting and enhances robustness (Liao, 2009). However, KNN may still struggle with ambiguous classification boundaries between different weld defect types, leading to potential misclassifications. To better manage this uncertainty, fuzzy K-nearest neighbor (FKNN) introduces an affiliation function that calculates the degree to which a test sample belongs to each category, improving both the accuracy and reliability of defect recognition (Hassan et al., 2012; Wang and Liao, 2002).

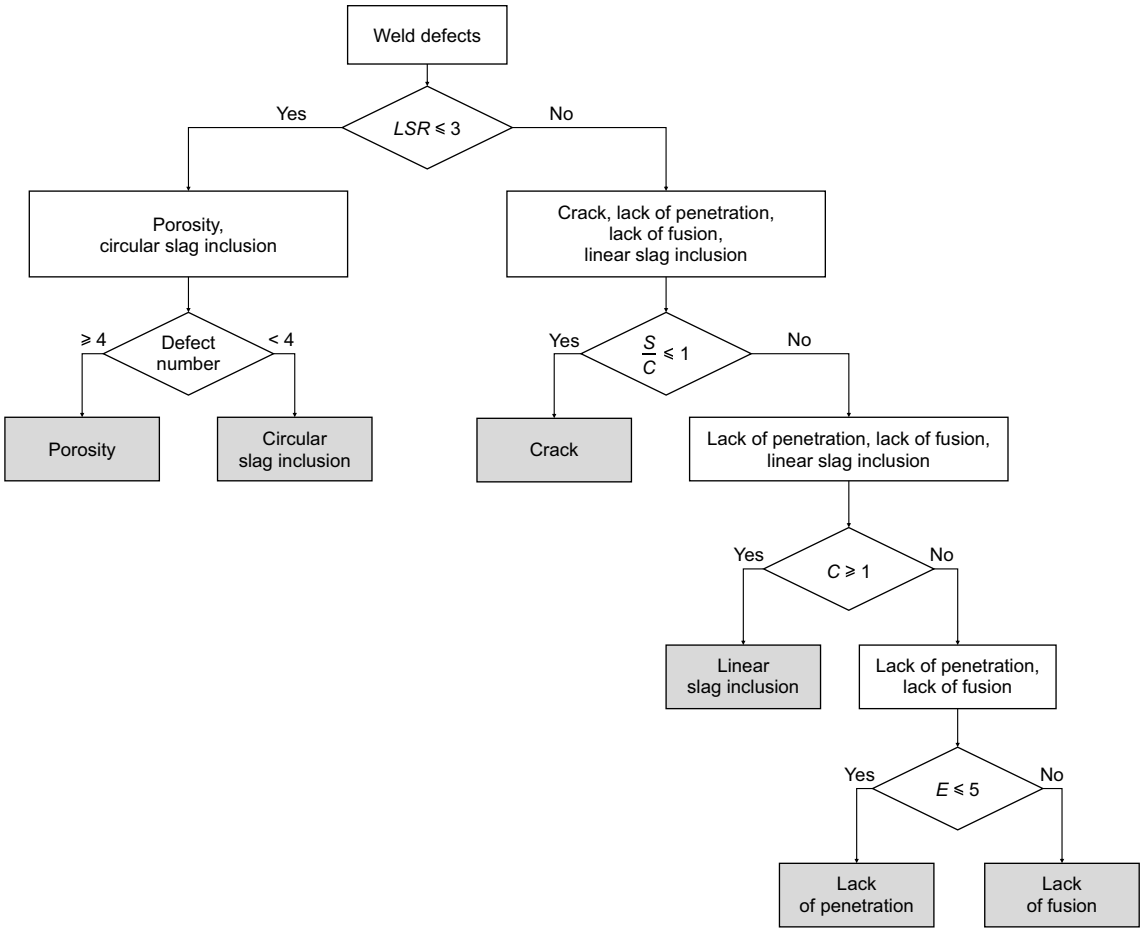

Fig. 2. Expert knowledge-based tree classifier.

Compared to nearest-neighbor classifiers, SVMs recognize weld defects by mapping feature vectors to a high-dimensional space and finding optimal hyperplanes that maximize the margin between different classes. The basic binary classification SVM is primarily used to distinguish between defects and non-defects (Ali et al., 2015; Shao et al., 2011) or to recognize circular versus linear defects (Li, 2019; Li and Mu, 2019; Wang et al., 2016b, 2017). However, weld defects are diverse, and simple binary classification SVMs cannot effectively recognize multiple defect types. Therefore, multiclass SVM models can be employed to transform a multiclass task into multiple binary classification tasks. Notable examples include the one-vs-one multiclass SVM (Ali et al., 2015;

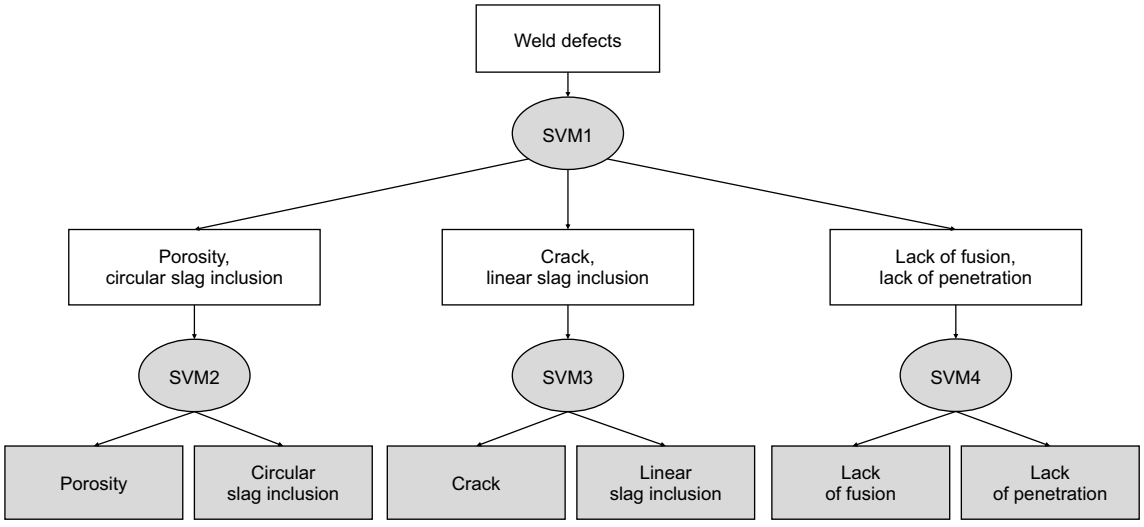

Fig. 3. The tree-structured multiclassification SVM model for weld defect recognition.

Faridafshin et al., 2018; Mekhalfa and Nacereddine, 2014) and the one-vs-rest multiclass SVM (Mekhalfa and Nacereddine, 2014; Xu et al., 2011). Although these multiclass SVMs can recognize multiple defects, the binary classifiers rise significantly, both linearly and quadratically, as the number of defect types increases, which elevates model complexity. Tree-structured multiclassification SVM models have been proposed to resolve this issue. These models reduce complexity by constructing multiple decision trees, each node differentiating between a smaller subset of classes (Dong et al., 2019; Fan, 2014). Studies have shown that the tree-structured multiclassification SVM model displays a respective improvement in recognition accuracy of 6% and 5% compared to other multiclass SVM approaches (Luo et al., 2010). Fig. 3 shows the tree-structured multiclassification SVM model for weld defect recognition.

Although multiclass SVMs can be effective for identifying weld defects, they often require multiple SVM models, which can complicate the implementation process and may affect prediction accuracy and efficiency. Contrarily, ANNs offer a more flexible, efficient solution. By simulating the learning process in the human brain, ANNs can automatically learn the complex relationships between inputs and outputs, making them capable of multiclass classification in a single model framework (Silva et al., 2001; Yahia et al., 2011). Common ANN-based defect recognition models include backpropagation (BP), radial basis function (RBF), and Bayesian neural networks. BP neural networks optimize and update the weights of each layer via error BP training, which minimizes the discrepancy between the predicted and actual results (Rumelhart et al., 1986). Researchers often use multilayer perceptron (MLP) models trained with BP neural networks to improve classification accuracy during weld defect recognition (Alghalandis and Alamdari, 2006; Boaretto and Centeno, 2017; Chandrasekharan et al., 2004; Silva et al., 2003, 2004; Kumar et al., 2014a, 2014b; Nacereddine et al., 2000; Nacereddine and Tridi, 2005; Valavanis and Kosmopoulos, 2010; Yin et al., 2008; Zahran et al., 2013; Zhang et al., 2003a, 2003c). One study developed an MLP model using error BP, which displayed significantly higher recognition accuracy than both the multiclass SVM and KNN models (Valavanis and Kosmopoulos, 2010). Moreover, incorporating additional regularization terms into the BP neural network loss function allows the model to focus on more generalizable features during the learning process while reducing the influence of specific patterns and noise (Vilar et al., 2008, 2009a, 2009b). This enhances the generalization capability of the defect recognition model, improving its overall performance. RBF neural networks are also essential during ANN-based weld defect recognition. These networks utilize the RBF to activate hidden layer nodes, which enhances their ability to capture spatial features (Qiao et al., 2016; Rale et al., 2009; Wei et al., 2019; Zhang, 2017b). Comparative studies have shown that RBF networks perform better than BP networks, improving accuracy by 0.72% (Zhang, 2017b). However, the relationship between features and defect types is complex since various factors can cause the same type of defect to exhibit different features depending on its location or orientation. Additionally, most features entered into the defect recognition model are obtained via various feature extraction techniques, which may result in overlapping between the attributes of multiple defect types and the introduction of uncertainty. Goumeidane et al. (2015) developed a Bayesian neural network-based weld defect recognition model in which probability distributions represented network weights to provide both the defect predictions and their uncertainty values. The results indicated that this approach achieved a 1.36% higher accuracy than the multiclass SVM. Fuzzy neural networks (FNNs) also address uncertainty by incorporating fuzzy logic. FNNs transform the features into fuzzy representations, the degree of which is quantified using an affiliation function to improve the ability of the model to handle uncertain feature descriptions. The affiliation function is often modeled using a π function (Tang et al., 2014; Zhang and Lin, 2023a, 2023b, 2004). Expert knowledge and relevant standards are used to create a fuzzy rule base, which is used to construct a hidden layer to improve the ability of the model to handle defect categories with unclear boundaries (Tang et al., 2014; Zhang and Lin, 2023a, 2003b, 2004). However, the computational cost of the FNN increases significantly when the rule base becomes more complex (Chady et al., 2017), which is addressed by integrating rough set theory and FNNs. Rough set theory helps streamline the decision rules, which reduces the FNN scale and enhances its efficiency without sacrificing accuracy. Chady et al. (2017) demonstrated that a weld defect recognition model based on rough set theory reduced the model size and improved accuracy. This optimized the model by extracting more concise decision rules, improving both the computational efficiency and recognition performance (Gao et al., 2006; Zhang et al., 2009). Researchers have begun exploring methods that combine manually designed domain features with more advanced deep learning models. These approaches improve weld fault recognition using the classification capacity and feature design interpretability of deep learning models. Gao et al. (2024) employed domain expertise to extract 14 key characteristics categorized as geometric, positional, or background region features, and utilized a transformer for feature encoding and defect type classification. Yang and Jiang (2021) proposed a method that combined unified deep neural networks with multilayer feature fusion using 11 defect features as input. This approach fused the features extracted from each hidden layer at the final hidden layer and outperformed support vector machines and conventional deep networks in detection accuracy.

Unlike supervised recognition models, unsupervised recognition models are designed to automatically uncover defect recognition patterns in datasets with unknown defect types. Weld defect identification approaches rely heavily on cluster analysis, with K-means and FCM clustering representing the primary techniques. Vaithiyanathan et al. (2013) proposed a framework based on K-means clustering, which effectively distinguished between burn-through, slag entrapment, and unfused defects. Additionally, FCM clustering methods have been developed to address the fuzzy nature of certain weld defects, such as porosity and oxide inclusions (Tridi et al., 2005; Wang et al., 2016a). These techniques significantly enhance the identification of subtle differences between defect types.

The precision of both supervised and unsupervised recognition models depends on quantifiable features and the accurate segmentation of defective regions. Eliminating the extraction process and directly evaluating the defects can improve model resilience and reduce its sensitivity to feature parameters. Sparse description-based defect recognition models offer an alternative approach to address this issue. For example, Xiao et al. (2024) developed a sparse description-based model for weld defect recognition, which specifically targeted circular, and linear defects, as well as noise in small-diameter pipes. This model yielded accuracy levels of 97.4% and 96.7% for circular and linear defects, respectively. A sparse representation model was constructed using training images, which were described using a complete dictionary matrix. Optimization algorithms were employed to obtain the sparse coefficients for each test sample, which were used to identify the weld defects. Specifically, defective and noisy regions were first extracted via suspected local image reconstruction (SDR) to obtain the training samples (Jia et al., 2024; Wang et al., 2018, 2021; Xiao et al., 2024). Fig. 4 shows the SDR definition. Various methods were proposed to resolve the

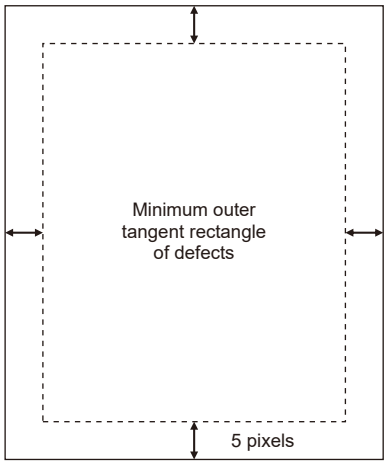

Fig. 4. SDR.

training sample dictionary matrix, including K-SVD (Xiao et al., 2024), orthogonal optimization (Jia et al., 2024), greedy algorithms (Wang et al., 2018), and compression-aware approaches (Li et al., 2013; Wang et al., 2021). Next, optimization algorithms such as orthogonal matching pursuit (Wang et al., 2021; Xiao et al., 2024) and 0-norm optimization (Jia et al., 2024) were employed to acquire the test sample sparse coefficients. Finally, the non-zero elements in the sparse coefficient vector were analyzed to facilitate effective weld defects recognition.

In summary, experience is the primary determinant of expert knowledge recognition models. Their accuracy is constrained by the efficacy of feature selection and expert knowledge. These models are also limited by the lack of a deterministic expert knowledge system that can comprehensively cover all weld defect types. Conversely, machine learning-based weld defect recognition models can automatically establish the underlying mapping between features and defect types, reducing the reliance on expertise. These models mainly include the nearest neighbor classifier, SVM, and ANN supervised methods and unsupervised clustering algorithms. Although the nearest neighbor classifier determines defect types by calculating the distance between samples, it is highly sensitive to outliers or noise, especially when these factors are near the query samples. SVM constructs a recognition model by maximizing the margin between classes, making it more resistant to noise and outliers. However, traditional SVM is a binary classifier and struggles with multiclass weld defect recognition. Although multiclass SVM can be constructed by combining multiple binary SVM models (one-vs-one, one-vs-all, or decision tree strategies), this increases complexity and computational cost. ANN-based models simplify this process by adjusting the number of output neurons, allowing multiclass defect recognition within the same framework. Furthermore, methods that combine manually designed features and advanced deep learning models show significant promise for preserving feature design interpretability while leveraging the powerful representation and classification capabilities of deep learning. These approaches are particularly effective in dealing with difficult-to-classify defect types. Unsupervised recognition models do not require labeled training datasets, instead attempting to identify patterns in the data itself. Additionally, fuzzy logic has been incorporated into both supervised and unsupervised models to better resolve uncertainties during defect recognition. These models rely on quantifiable feature parameters, the quality of which can influence model accuracy. Consequently, sparse description-based recognition models use a dictionary matrix to represent defect samples in the training set and recognize weld defects by solving sparse coefficients. However, this model involves two optimization steps: solving the dictionary matrix and determining sparse coefficients. Any errors in these steps can impact recognition accuracy. The complexity of defect recognition increases with the number of defect types as the sparse coefficient analysis becomes more intricate. In conclusion, while feature-based weld defect recognition models offer high interpretability and the ability to recognize multiple defect types, their efficacy depends on the quality of feature parameters or dictionary matrices. This ultimately impacts defect recognition accuracy.

3.3. Deep learning-based defect recognition method

Deep learning-based defect recognition methods automatically learn and extract complex features directly from radiographic weld images using powerful neural network architectures, enabling efficient weld defect recognition. This model eliminates the need for manually designed feature parameters, instead adaptively learning the patterns essential for distinguishing between different defect types. This addresses the limitations of traditional feature-based recognition methods. Deep learning-based defect recognition methods can be classified into three categories according to the type of output, including image classification, semantic segmentation, and object detection.

3.3.1. Public dataset

High-quality datasets are essential for deep learning-based defect recognition. A large volume of data is used for model training, enabling it to learn and extract the complex features and patterns necessary for accurate weld defect recognition. While most current models rely on datasets constructed by researchers, there are also publicly available weld defect datasets that offer valuable resources for model development and performance evaluation.

Totino et al. (2023) proposed the RIAWELC weld X-ray image dataset, containing 24,407 X-ray images acquired from real industrial production environments. The dataset included four types of weld defects: 7635 images of cracks (CR), 6320 images of porosity (PO), 4452 images of lack of penetration (LP), and 6000 no-defect reference images (ND). Fig. 5 shows some example images from the RIAWELC dataset. Additionally, Mery et al. (2015) developed the GDXray dataset, containing 19,407 X-ray images divided into five subsets: castings, welds, baggage, natural objects, and settings. The weld subset included 10 original weld X-ray images (W0001), along with detailed binary pixel-level annotations (W0002). Another part of the dataset, W0003, provided 68 weld X-ray images, some of which were annotated at the pixel level with the help of welding experts. Fig. 6 shows sample images from the GDXray dataset.

3.3.2. Image classification

Image classification-based methods train deep learning models using weld defect X-ray image-level labels to automate classification and recognition. CNNs (LeCun et al., 1989) are widely used for this process. A CNN typically consists of a convolutional, pooling, and classification layer (Fig. 7). The convolutional layer applies a series of convolutional kernels to automatically extract features from the input image, which are filtered and compressed by the pooling layer to reduce spatial dimensionality and retain important information. The classification layer, which is usually fully connected, converts the features processed via the convolutional and pooling layers into a one-dimensional feature vector, which is used to classify X-ray image defects.

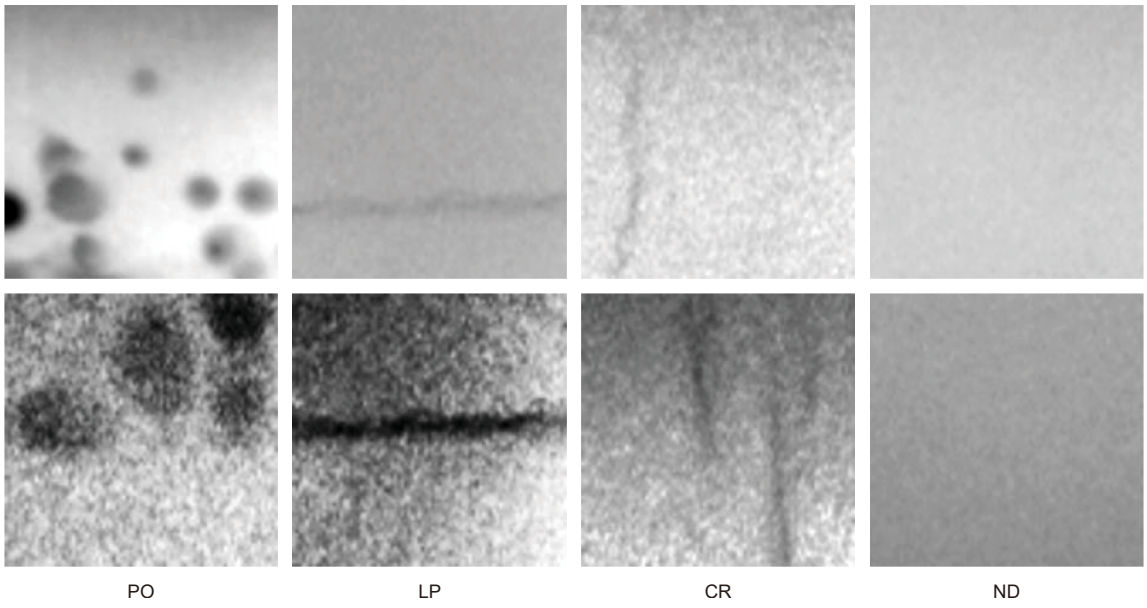

Fig. 5. Sample images from the RIAWELC dataset.

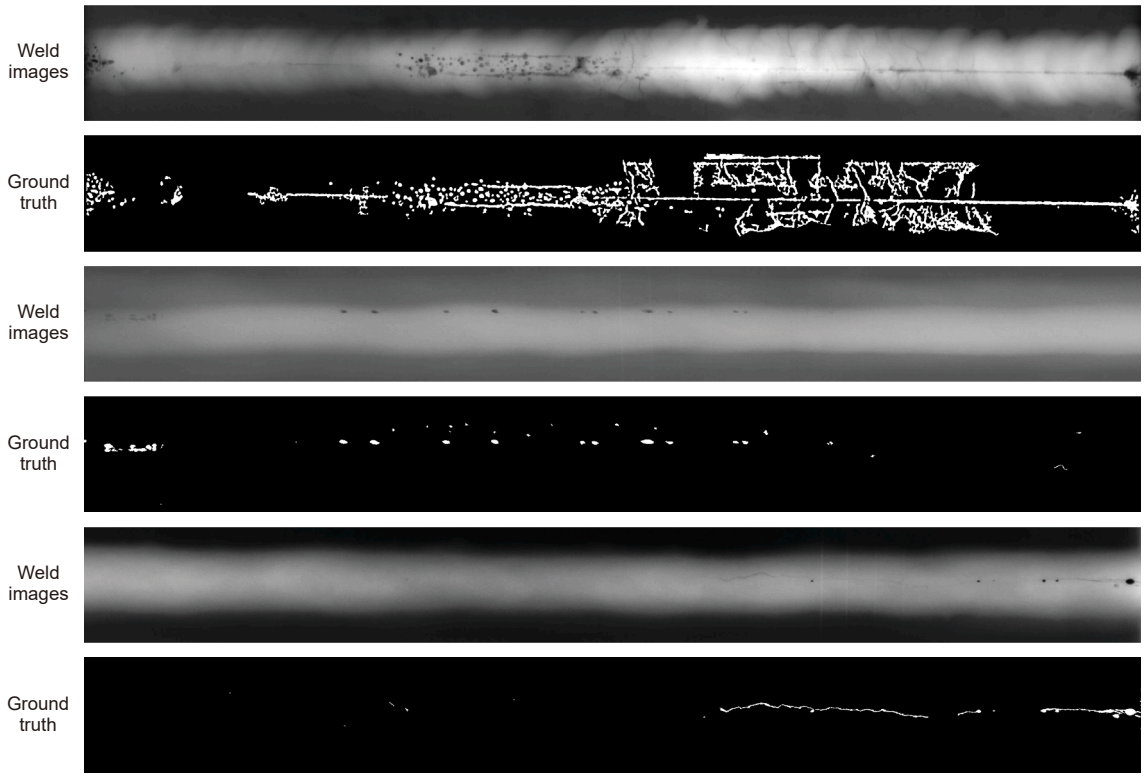

Fig. 6. Sample images from the GDXray dataset.

The foundational components of various custom CNNs are crucial for the efficient automated classification of weld defect X-ray images. These networks are optimized by adjusting hyper-parameters such as the number of layers, convolutional kernel sizes, and learning rates (Liu and Guo, 2018; Stephen et al., 2021; Zhang et al., 2021a). Stephen et al. (2021) proposed a nine-layer CNN specifically tailored to identify porosity, dense porosity, cracks, trapped tungsten, and defect-free images. The results showed that all the weld defects were correctly classified in the test set, except for the defect-free image, which was misclassified due to the absence of detectable edges. This outcome demonstrates the significant recognition potential of CNN-based models for weld defect classification. Activation functions, such as ReLU and Sigmoid, are commonly introduced to enhance the nonlinear expressiveness of CNNs. Studies have shown that CNNs using ReLU outperform those using Sigmoid in terms of classification accuracy

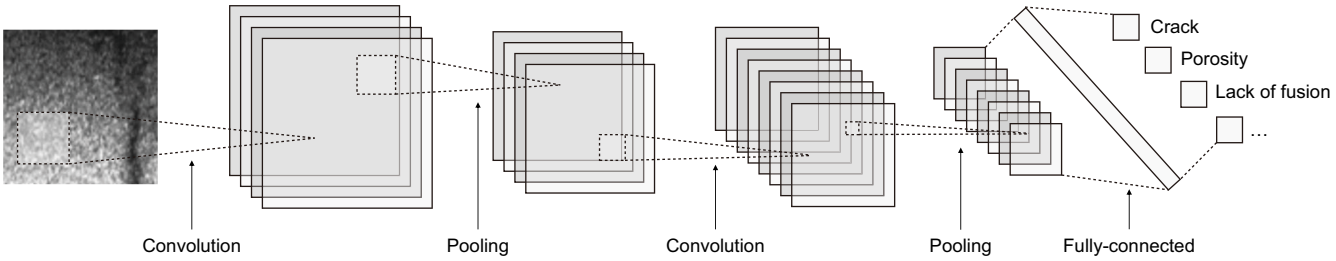

Fig. 7. A diagram of the CNN architecture.

(Li and Gao, 2019b). While ReLU improves performance, it may cause neuron inactivation for negative inputs, limiting the learning capacity of the model. Therefore, an ELU activation function has been proposed that combines the advantages of both Sigmoid and ReLU (Fan et al., 2020; Hu, 2020). Studies indicate that CNNs employing the ELU activation function exhibit superior feature extraction capabilities. A common approach for mitigating overfitting is the inclusion of a dropout layer after the fully connected layer. This randomly disables certain neurons, encouraging the model to learn more robust and generalized features (Say et al., 2023; Stephen and Lalu, 2021; Yang et al., 2019b). However, traditional dropout may remove valuable information, leading to the introduction of a random forest algorithm that selectively discards neurons based on feature importance (Jiang et al., 2020). Underfitting can also negatively affect model performance. To address both overfitting and underfitting, Chen et al. (2020) proposed a progressive CNN model, which dynamically increased the number of training samples by setting an accuracy threshold for the test samples. This model showed a 6.7% improvement in recognition accuracy compared to traditional CNNs. The pooling layer is critical for filtering and reducing feature dimensions. Although pooling techniques such as average and maximum pooling are commonly used, they may not always be effective for certain data, such as weld defects. Specifically, average pooling can dilute important features in regions with locally significant details, while maximum pooling may introduce noise in areas with smooth grayscale transitions. To address these challenges, alternative strategies such as adaptive pooling (Jiang et al., 2020) and variance pooling (Li and Xu, 2024) have been proposed for more efficient feature extraction and noise reduction. Hyperparameters, such as the number of network layers, convolutional kernel sizes, and learning rates, are vital for optimizing CNN performance and require careful consideration. Techniques, such as Bayesian optimization (Naddaf et al., 2020) in conjunction with the whale optimization algorithm (Li and Xu, 2024), are often employed to identify the optimal hyperparameter combination.

In addition to the basic CNN architecture, which consists of a simple stack of convolutional, pooling, and fully connected layers, more complex CNNs have been developed to enhance the accuracy and efficiency of weld defect classification. Shang et al. (2020) proposed replacing the fully connected layer with SVM to increase model performance in small sample datasets, leveraging the feature extraction strengths of CNNs while taking advantage of the robustness of SVMs in classification tasks, effectively reducing the risk of overfitting (Shang et al., 2020). Since weld defects typically manifest as subtle grayscale differences in radiographic images and occupy small areas, more advanced feature extraction techniques are necessary for improving classification accuracy, such as multiscale dense cross blocks, residual connections, dual-path cascade structures, and multiscale dilated convolutions. These methods enhance the ability of the model to detect small defective features while maintaining high classification efficacy, even in complex background conditions (Sonwane and Chiddarwar, 2024; Zhang and Wang, 2024). Additionally, capsule networks have been proposed as an alternative to traditional pooling and fully connected layers. Capsule networks can better preserve spatial hierarchies and fine-grained details, which improves the ability of the model to classify the same defects from different perspectives (Zhang and Wang, 2024).

Although these optimizations primarily focus on improving the CNN architecture, the quality of the dataset also crucially influences classification performance. Studies have shown that datasets without data augmentation can result in significant overfitting (Stephen and Lalu, 2021). Contrarily, data augmentation techniques can improve classification accuracy by as much as 15% (Stephen and Lalu, 2021). Common data augmentation methods such as random rotation, scaling, cropping, and flipping, increase training sample diversity, as well as the generalization capacity of the model (Say et al., 2023; Stephen and Lalu, 2021). However, real industry datasets often exhibit class imbalances and the underrepresentation of certain defect types. Using these imbalanced datasets for CNN training can cause the model to favor defect categories with more abundant samples, reducing the efficacy for less frequent categories. Hou et al. (2019) proposed a few-class oversampling technique for constructing a more balanced dataset, consequently improving the ability of the model to classify rare defect classes. Although oversampling techniques can reduce class imbalances, they primarily increase minority class quantities by copying or generating new samples, resulting in model overfitting. Therefore, Liu et al. (2023b) proposed a classification method based on basic class and cross-class hybrid feature learning. This approach combined a variable factor distance metric model and an image mixing mechanism model to effectively mitigate the impact of class imbalance on classification accuracy, and utilized progressive loss functions to mutually promote both. The results demonstrated that this method maintained a recognition accuracy above 86% even in highly imbalanced data conditions, exhibiting good robustness. Since defective regions typically occupy only a small portion of the image, the imbalance between the defect and background regions can reduce classification accuracy. While more complex feature extraction modules can help enhance feature representation, they also introduce additional computational overhead and model complexity. Consequently, SDR techniques are applied to augment datasets by increasing the defective area proportion. This encourages the model to focus on critical regions containing defects to improve classification accuracy (; Li and Gao, 2019, 2019b; Zhang et al., 2022b). Studies have shown that models trained on SDR datasets can yield classification accuracy values exceeding 98%, outperforming those trained on traditional datasets (Zhang et al., 2021b). Liu et al. (2024c) proposed DGICR-Net to address the challenge of extremely scarce labeled data samples. This method enhanced feature learning via a dual-graph interaction mechanism that leveraged inter-sample relational information. Consequently, it achieved 91.1%

classification accuracy with only 20% labeled samples, providing an effective solution for classifying weld defects when labeled data is limited.

The quality of pipeline weld X-ray images in datasets is also a key factor that limits defect classification model performance, particularly since low-contrast, low-brightness, and high-noise images severely degrade model classification accuracy (Qian et al., 2024). Images typically undergo various preprocessing procedures, such as histogram equalization and gamma correction, to enhance image quality before being entered into models to improve their performance. Guo et al. (2021) proposed a conditional generative adversarial network that effectively improved low-quality image contrast, while augmenting the training dataset and image quality. Although these effectively improve image quality and defect classification accuracy, they involve two independent processing steps. To further simplify the processing pipeline and improve classification performance, Liu et al. (2022a) proposed an end-to-end framework that directly integrated an adaptive image enhancement module into the front end of the classification network. This integrated design automatically optimized and adjusted the image enhancement parameters according to specific defect classification tasks, which maximized image quality and defect feature learning. The experimental results demonstrated that this end-to-end joint optimization strategy achieved 93.67% classification accuracy, approximately 7% higher than traditional ResNet methods.

In addition to customized CNNs, several standard CNN architectures have also been used for weld defect classification and recognition, including VGG, ResNet, AlexNet, and GoogLeNet. Wang (2022) compared VGG16, GoogLeNet, ResNet50, and AlexNet for weld defect classification, which showed excellent recognition efficacy and a classification precision value reaching 94.5% in real-world applications. Similarly, Gu et al. (2020) employed the DenseNet-121 model to detect five weld defect types, achieving a maximum accuracy level of 98.97%, which was approximately 5% higher than SVM. These studies demonstrate the efficacy of classic CNNs for weld defect classification and highlight their broad applicability in industrial scenarios. However, although DenseNet-121 exhibits high classification accuracy, its 121-layer architecture introduces significant computational complexity and overhead (Gu et al., 2020). Therefore, studies have focused on optimizing CNN models with lower complexity while maintaining or improving classification performance. One approach enhances feature acquisition by incorporating multiscale synthetic convolution and multiscale feature extraction blocks into VGG16 and ResNet50, respectively (Liu et al., 2024b; Zhang et al., 2021a). Additionally, deformable convolution and spatial pyramid pooling techniques have been applied to ResNet50 and AlexNet to improve the resilience of the model to geometrical defect variations (Huang, 2020; Liu et al., 2024b). Compared to DenseNet-121, MobileNet offers a smaller model size and lower computational requirements due to its use of depthwise separable convolution. Studies have further optimized MobileNet for weld defect classification using techniques such as null convolution, channel attention mechanisms, and residual structures (Chen et al., 2022; Pan et al., 2023). Depthwise separable convolution has been introduced into ResNet50 to reduce model size while maintaining or improving classification performance, providing a more efficient solution for weld defect recognition (Liu et al., 2024b).

Although classic CNNs have offer highly accurate weld defect classification, the use of large-scale datasets is often critical for optimal performance. However, the complexity and high costs associated with the actual welding production process make it challenging to construct large-scale weld defect datasets. Therefore, transfer learning has been introduced as an effective solution, which leverages pretrained models to reduce the dependence on large datasets, enabling more efficient weld defect classification. Pretrained models typically consist of CNNs trained on large, general-purpose datasets, with their parameters transferred to the weld defect classification task. This involves transferring most of the layer weights of the pretrained model and fine-tuning the final layers, or training newly added layers specifically for weld defect recognition. Studies have shown that transfer learning can improve the accuracy of CNN-based defect classification models by about 4% compared to traditional CNN models. Moreover, techniques such as gradient class activation mapping (Grad-CAM) indicate that transfer learning effectively help CNNs to focus on the defects themselves, which improves model performance (Wang and Yu, 2023). In the context of weld defect classification, common pretrained CNN models include VGG16 (Kumaresan et al., 2021, 2023), AlexNet (Hou et al., 2017), ResNet50 (Palma-Ramírez et al., 2024), SqueezeNet (Perri et al., 2023), MobileNet (Pan et al., 2020), and Xception (Guo et al., 2021). A typical approach in transfer learning involves freezing the feature extraction layers of the pretrained model, while adding a new classification layer for the weld defect task. This classification layer often consists of a fully connected layer or a simple MLP (Purnomo et al., 2024; Ting et al., 2024). Some studies have integrated artificial immune systems (AIS) in transfer learning frameworks as classifiers due to their strong online learning capabilities (Fioravanti et al., 2019). The results suggest that this approach can improve the F1 score by about 6% compared to using a fully connected layer as the classifier. However, directly using a pretrained model as a feature extractor for weld defect classification can be challenging due to significant differences between weld X-ray images and those in the generalized datasets used for pretraining. General datasets are typically obtained from the ImageNet database, which contains a large number of natural images covering different categories such as animals, plants, objects, and natural scenes (Deng et al., 2009). However, these natural images differ significantly from pipeline weld X-ray images due to inherent variation in imaging mechanisms, visual features, and target characteristics. First, X-ray imaging primarily employs material density differences and radiation transmission principles, resulting in grayscale images with no color information, low contrast, and blurred edges. This differs significantly from the high-contrast, color-rich natural images in ImageNet. These differences may cause inadequate extraction of the pipeline weld X-ray image characteristics by the pre-trained model feature extractors, which can bias the feature representations and affect recognition performance. Second, the weld defects in pipeline weld X-ray images are often represented as subtle grayscale variations or irregular geometric shapes, which differ fundamentally from the objects in ImageNet with clear contours, shapes, sizes, and textural features. This limits the transfer efficacy of the high-level semantic features obtained from natural images for weld defect recognition. Pipeline weld X-ray images often exhibit extremely small defect regions. This imbalanced defect-background distribution further increases the domain differences compared to the diverse scene distributions in ImageNet. Therefore, studies often freeze only the first few layers of the pretrained model or employ a lower learning rate to refine all the model weights (Chandra and Thakkallapally, 2021; Nazarov et al., 2021). Liu et al. (2023a) proposed a novel task transfer learning approach to enhance the interpretability and classification accuracy of weld defect models. This approach used an encoder trained on a weld X-ray image reconstruction task as the feature extraction component for the defect classification task. By simulating expert knowledge via this task transfer, the model more effectively learned the relevant weld defect features before connecting to a classifier for the final classification step.

Cheng et al. (2024) proposed a multimodal defect classification method that integrated domain expert knowledge with deep learning models, which transformed the defect detection standards and expert experience into textual descriptions. It provided a joint representation of the images and text via dual-encoder architecture and contrastive learning. This allowed the model to understand defect features based on expert knowledge, consequently improving its classification accuracy and interpretability. Compared to the previously mentioned methods, this multimodal recognition approach fully utilizes professional knowledge, reduces the dependence on a large number of annotated images, and increases the consistency of the classification results with expert cognition.

Image classification methods primarily rely on CNNs, which are designed to automatically recognize defect types in images. With the advances in computer vision, researchers have developed specialized CNN architectures for weld defect classification. Basic CNNs typically have relatively simple structures and consist of several convolutional, pooling, and classification layers. To enhance classification performance, the fundamental frameworks of these models are optimized, while additional enhancement techniques are explored for hyperparameter refinement to improve the results. Conversely, advanced CNN architecture significantly enhances feature extraction and classification accuracy by incorporating more complex components. Various data enhancement strategies have been developed to increase training sample quality and diversity, ultimately enhancing the generalization ability of the model. Numerous classical CNN models have proven effective for weld defect classification. Techniques such as deep separable convolution and channel attention mechanisms have been employed to further improve the performance of advanced CNN models, following a similar optimization strategy to that of customized CNNs. Transfer learning is a prominent approach in weld defect classification. By leveraging pretrained models, transfer learning reduces the dependency on large-scale proprietary datasets while maintaining, or even improving, classification accuracy. Recent research has explored multimodal methods that combine domain expert knowledge and image features. These approaches employ contrastive learning to combine images and textual knowledge, which improves classification accuracy and interpretability. Despite significant progress, image classification techniques still face certain challenges. Transfer learning and data augmentation can address issues related to small datasets, but some defect types still require sufficient labeled data to ensure model accuracy and resilience. Although knowledge-guided multimodal methods improve interpretability, fully bridging the gap between artificial intelligence decision-making and expert reasoning remains a significant challenge. Furthermore, while image classification methods can effectively identify the presence of defects, they typically cannot determine their precise locations in the image. Achieving accurate defect localization requires more sophisticated post-processing algorithms, representing a focal point for future improvement.

3.3.3. Semantic segmentation

Semantic segmentation-based methods train models using the pixel-level annotations of weld X-ray images, aiming to accurately classify and localize defects. Unlike image classification, which provides only an overall classification, semantic segmentation generates a prediction map of the same size as the input image. Each pixel in this map is assigned a class label to precisely identify defect locations and types. The semantic segmentation models commonly used for weld defect detection include SegNet, Fast-SCNN, DeepLab V3+, FPN (Feature Pyramid Networks), and U-Net, all of which have exhibited excellent performance in defect localization and detection.

SegNet is an encoder-decoder model designed specifically for semantic segmentation tasks (Badrinarayanan et al., 2017). Fig. 8 illustrates its detailed architecture. The decoder uses a multilayer convolutional and max-pooling structure similar to VGG16 to extract rich features from the input image. Unlike VGG16, SegNet also saves the position indices of the maximum values during max-pooling, which are then used to guide the nonlinear upsampling process in the decoder. This helps recover the feature map spatial structure and improves model performance. However, the multiple pooling operations of SegNet can result in crucial detail loss, especially for small targets such as weld defects in X-ray images, which may reduce defect detection accuracy. Therefore, an improved approach was proposed that reduced the number of max-pooling layers and incorporated atrous convolution (Chang and Wang, 2021). This technique extended the receptive field while increasing spatial information preservation, enhancing the multiscale contextual understanding and improving small defect detection accuracy. The ReLU activation function was replaced with ELU and SeLU to accelerate training, prevent neuron death, and improve generalization (Chang and Wang, 2021; Tokime et al., 2019).

Fast-SCNN is a lightweight model for real-time semantic segmentation, which significantly improves processing speed while maintaining segmentation accuracy (Poudel et al., 2019). As shown in Fig. 9, Fast-SCNN consists of a learning pyramid, a global feature extractor, a feature fusion module, and a classifier. The learning pyramid extracts base features from the input image and reduces the dimensionality of the feature map via downsampling. The global feature extractor captures multiscale contextual information using parallel atrous convolutions, which enhances the ability of the model to understand complex environments. Then, the feature fusion module integrates features from different paths to combine information, ensuring that the key details are preserved, after which the classifier is used for pixel-level categorization. The use of depthwise separable convolutions reduces the Fast-SCNN model size while retaining a high performance level. Zhao et al.

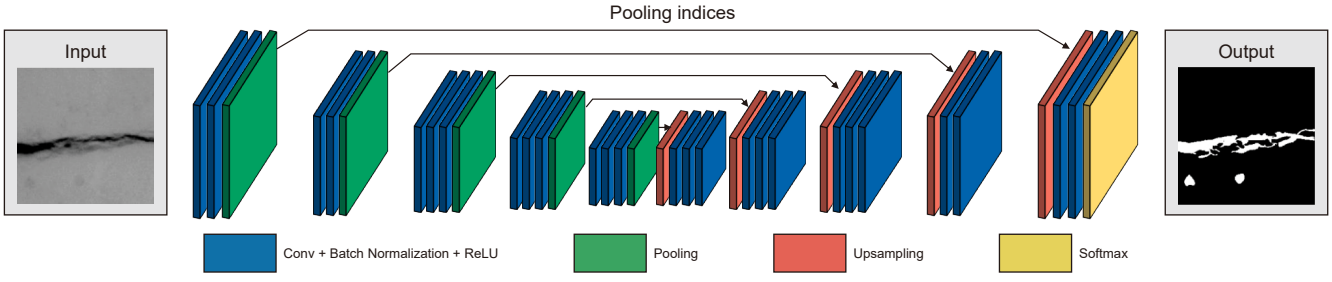

Fig. 8. A diagram of the SegNet architecture.

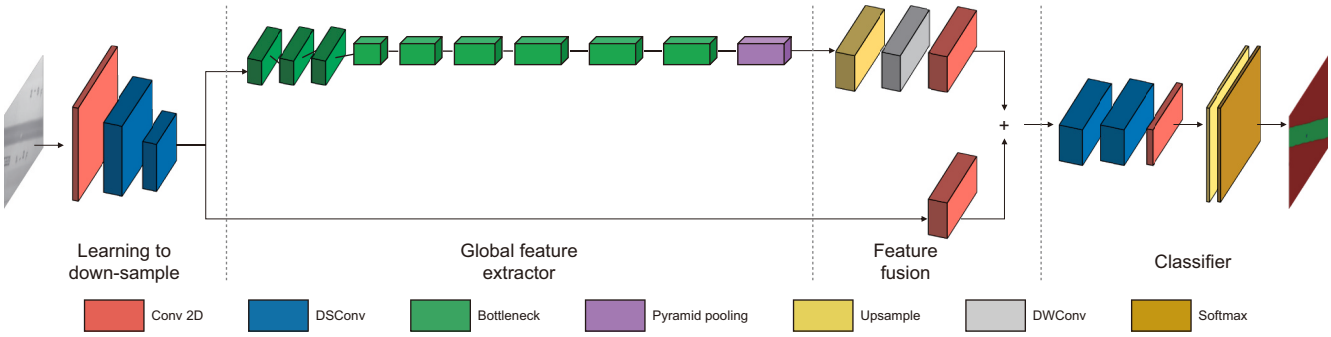

Fig. 9. A diagram of the Fast-SCNN architecture.

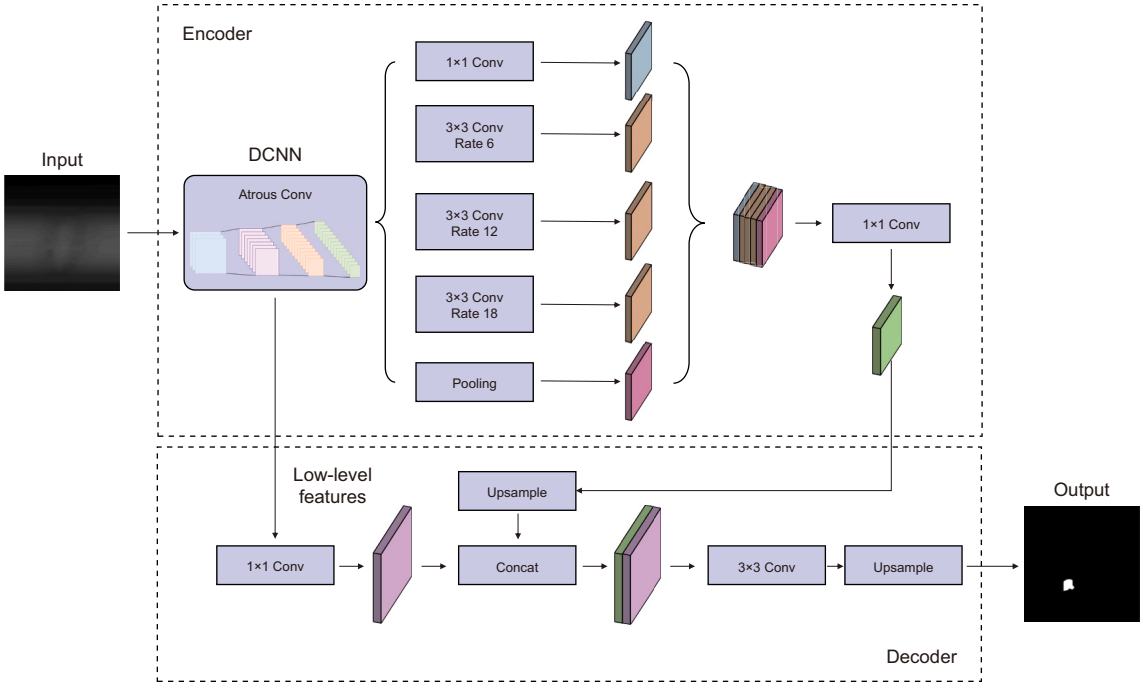

Fig. 10. A diagram of the DeepLab V3+ architecture.

(2021) validated the efficacy of Fast-SCNN for weld defect detection. The results showed that the model was capable of highly precise segmentation with an average processing time of only 12.3 ms, demonstrating its practicality for real-time weld inspection scenarios.

DeepLab V3+ (Chen et al., 2018) is an efficient semantic segmentation model, which consists of an encoder and a decoder (Fig. 10). The encoder extracts the basic input image features via a backbone network, augmented with a spatial pyramid pooling block that captures multiscale contextual information. The spatial pyramid pooling is implemented using atrous convolutions with varying expansion rates, allowing the model to adapt to targets of different sizes. The decoder further refines the segmentation, particularly for small targets and boundaries, by merging low-level detailed features with high-level abstract features, which optimizes the overall segmentation. DeepLab V3+ also employs depthwise separable convolutions, which reduce the computational complexity of the model while enhancing its learning capability. Gangadhara (2021) utilized a ResNet-101 backbone

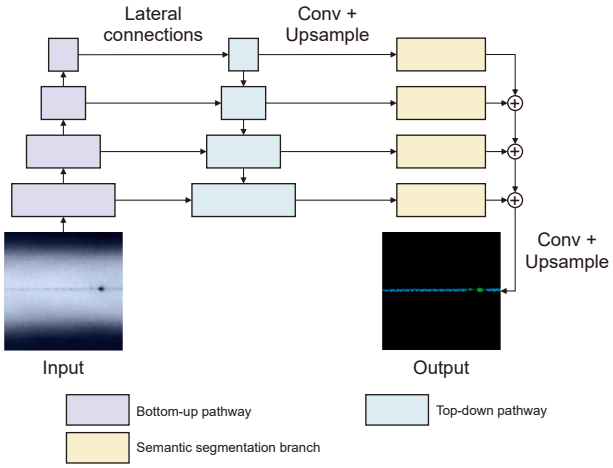

Fig. 11. A diagram of the FPN architecture.

pretrained on ImageNet for DeepLab V3+ in a solution for weld defect detection, which minimized the need for large datasets and improved performance. The model achieved an average detection accuracy of approximately 95.7% on the GDXray dataset.

The FPN is a foundational component for capturing multiscale features to improve object detection performance (Lin et al., 2017a), and consists of a bottom-up pathway, a top-down pathway, and lateral connections (Fig. 11). The bottom-up pathway typically comprises standard CNNs that extract multiscale features from the input image to generate a series of feature maps with varying abstraction levels. The top-down pathway restores the spatial resolution of these feature maps via upsampling, gradually passing high-level abstract features to lower levels. However, traditional CNNs often produce feature maps at a single scale, which can lead to inconsistent detection results, especially for objects of varying sizes. Therefore, the FPN introduces lateral connections, which combine low-level feature maps from the bottom-up pathway with upsampled high-level feature maps. This mechanism helps preserve spatial details while enhancing semantic information, which significantly improves detection performance. The FPN is not limited to object detection tasks but can also be used for semantic segmentation. In their study on weld defect segmentation, Xu et al. (2022) used ResNet-34 as the backbone for the bottom-up pathway and combined Dice and Focal loss to optimize the loss function. The results demonstrated that this model effectively improved segmentation efficacy due to the imbalance in pixel numbers between defective regions and the background.

U-Net is a symmetric encoder-decoder model used specifically for medical image segmentation (Ronneberger et al., 2015). Fig. 12 shows the U-Net architecture. The encoder gradually extracts high-level abstract features from the input image using a series of convolutional and pooling layers to capture deeper semantic information. The decoder reconstructs the feature maps via deconvolution, which are then merged with corresponding feature maps from the encoder using skip connections. Skip connections address the data loss caused by the convolution and pooling layers by passing low-level detail information to the decoder to improve segmentation performance. U-Net stands out from other models due to its symmetric structure and skip connection mechanism that can efficiently preserve fine-grained details such as weld defects, as well as its excellent performance on small-scale datasets. Therefore, U-Net is extensively used for semantic weld defect segmentation. However, the traditional U-Net model uses deconvolution for upsampling, which can introduce tessellated artifacts and often involves high computational costs due to a large number of parameters. Therefore, U-Net was optimized by combining nonlinear interpolative upsampling and 1D convolution to improve detection performance (Cai et al., 2024; Tyystjärvi et al., 2022). Conventional encoders typically use a two-layer convolutional structure for feature extraction. Although a deeper network can capture more complex semantic information, it also increases the risk of gradient vanishing, which impedes overall model performance. This standard convolutional approach also struggles to capture detailed features, particularly in challenging scenarios such as low-contrast or weak-textured weld images, which hinders detection. Therefore, residual structures and attention mechanisms have been incorporated into the encoder (Wang et al., 2024a; Yang et al., 2023a), enhancing the focus of the model on defect regions and mitigating gradient vanishing to improve defect detection in complex backgrounds. Li et al. (2025a) constructed encoders by combining residual U-shaped modules with multilayer perceptrons, which significantly enhanced multiscale feature extraction capability and reduced the number of encoder parameters. They also introduced a multiscale segmentation head based on dilated convolution attention mechanisms, which improved the capability of the model to segment defects of different sizes (Li et al., 2025a). Studies have also focused on improving the skip connections, introducing a high-low-level feature fusion block to enhance the ability of the model to recognize multiscale defects (Wang et al., 2024a). The results demonstrated an 8% improvement in segmentation accuracy compared to the original U-Net. Further improvements included combining the multiscale feature fusion block with an attention mechanism module to improve multiscale and contextual feature extraction capacity, which was particularly beneficial for small-defect detection (Yang et al., 2022c, 2023a). Furthermore, weighted loss functions or hybrid loss strategies combining binary cross-entropy and Dice loss have been introduced to address the pixel imbalance between weld defects and the background. These approaches help increase the defect

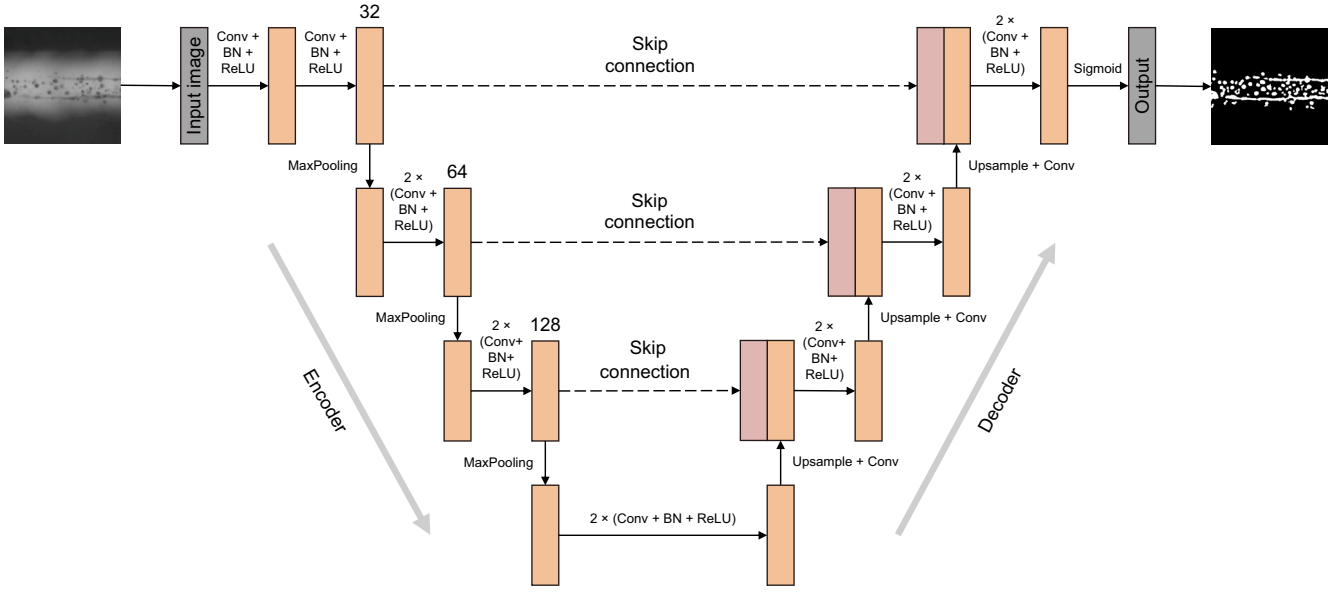

Fig. 12. A diagram of the U-Net architecture.

segmentation accuracy (Li et al., 2024c; Yang et al., 2022c, 2023a). Cui et al. (2025) developed the SDCT framework to improve the segmentation accuracy of micro-defects. This strategy employed a semantic discriminative encoder to enhance the representation of micro-defect features and incorporated a contrastive transformation mechanism to separate defect characteristics from background elements. This technique utilized a progressive iterative decoding approach to achieve precise micro-defect segmentation at the pixel-level. To improve the generalization ability of the model, Li et al. (2024c) proposed a multiscale, deeply supervised loss function, which facilitated feedback from different layers. An entropy-based uncertainty assessment method was introduced, which enabled the model to evaluate the reliability of its outputs, particularly when working with small or ambiguous datasets.

Differentiating between actual defects and the background features remains a significant challenge in X-ray weld defect detection, which can significantly affect segmentation accuracy. Similar issues exist in other non-destructive testing techniques. During pipeline magnetic flux leakage (MFL) detection, the close relationship between defect and weld signals also impacts detection precision. Therefore, Shen et al. (2024) proposed the CRNet, which employs sparse attention mechanisms and explores multiscale relationships to mitigate issues related to signal coupling, achieving a detection accuracy of 95.5%. Furthermore, multimodal semantic segmentation techniques have demonstrated promise for pipeline MFL defect detection. Shen et al. (2025a) developed the VLCIM, which facilitates precise pixel-level defect segmentation by fusing expert domain knowledge with visual features, attaining 86.7% mean intersection over union (*mIoU*) in the MFL-Seg dataset. This method integrates linguistic information into the visual encoder, progressively optimizing both visual and linguistic features, offering new multimodal fusion insights for X-ray weld defect segmentation.

Besides model architecture improvements, the quantity and quality of the training data also limit defect segmentation performance. Sufficient pixel-level annotation data allows models to learn richer defect feature representations, improving their segmentation capability and generalization performance for different defect types. Therefore, researchers typically employ basic methods such as horizontal flipping, vertical flipping, and random noise addition for data augmentation (Cai et al., 2024). However, traditional data augmentation methods produce samples with limited diversity, which makes it difficult to determine complex weld defect variations. Wang et al. (2025b) proposed a DA-DCGAN-based method to generate virtual defect images for model training, significantly improving segmentation accuracy by producing more realistic, diverse training samples. Although large-scale annotated data forms the foundation of high-performance models, image quality also directly affects defect segmentation performance. Low-contrast, high-noise pipeline weld X-ray images severely impact accurate defect boundary localization, which significantly reduces segmentation accuracy. Therefore, researchers typically use methods such as gamma correction and histogram equalization to improve image quality (Yang et al., 2021b). Some studies have developed more effective segmentation-specific image enhancing strategies. Xu et al. (2022) utilized linear color lookup tables to map high-resolution weld images from a 12-bit to an 8-bit depth, which improved the subsequent segmentation efficiency while preserving critical defect information and reducing data redundancy. Li et al. (2023a) proposed a high-resolution sample construction method that first precisely located weld regions using a random-walk Gaussian algorithm to reduce background interference. Then, a feature recombination strategy was designed for high-resolution images based on the weld aspect ratio characteristics. This approach effectively preserved weld information while preventing the information loss caused by traditional compression methods. The experiments demonstrated that this feature recombination processing method significantly improved defect segmentation model accuracy.

To summarize, several deep learning architectures are commonly used for weld defect semantic segmentation. SegNet, DeepLab V3+, Fast-SCNN, and U-Net all follow a typical encoder-decoder structure, while FPN features a specialized encoder-decoder design. It encodes features via a bottom-up backbone network while decoding occurs via a top-down path with lateral connections. However, the standard SegNet architecture relies on basic convolutional layers for feature extraction, which may cause information loss and negatively impact segmentation performance. Therefore, the encoder structure and activation functions have been enhanced to improve feature extraction efficiency and generalization capability. U-Net has attracted considerable attention due to its strong performance in various semantic segmentation tasks, prompting extensive research focusing on improving the encoder structure, skip connections, and loss functions, significantly enhancing segmentation accuracy. Despite the strong potential of semantic segmentation techniques for weld defect detection, a major challenge remains in obtaining high-precision defect pixel annotations, which continues to limit the development of these methods.

3.3.4. Object detection

Object detection-based recognition methods accurately localize and classify weld defects by primarily training models using bounding box annotations, which consist of rectangular boxes and corresponding category labels. While semantic segmentation can also be used for weld defect localization and classification, its output typically consists of a multiclass labeled map. Contrarily, the object detection approach provides a more intuitive result by directly labeling both the location and class of defects in the original X-ray image. Detection architectures are currently categorized into two-stage and one-stage detectors.

Two-stage detectors generate a set of candidate regions, followed by defect classification and bounding box regression to determine the final recognition results. Faster R-CNN is a typical example of this architecture (Fig. 13), consisting of two main components: the region proposal network (RPN) and the detector. The RPN generates candidate regions by sliding a window over the feature map to produce multiscale anchor points at each location, determining the likelihood of each anchor point being a target, as well as the bounding box adjustment parameters. The detector extracts features from these candidate regions, transforms them into fixed-size feature vectors using ROI pooling, and performs target classification and bounding box regression via fully connected layers. Lei et al. (2022) proposed a standard Faster R-CNN model to evaluate the related weld defect recognition efficacy, which accurately identified circular defects, lack of fusion, and linear defects. Guo et al. (2019) developed a Faster R-CNN that recognized seven defect types and no-defect cases, achieving a mean average precision (mAP) of 58.6%. Chen (2022) specifically proposed a Faster R-CNN model for defect recognition in radiographic small-diameter pipeline weld images, using VGG16 as the feature extraction network, which achieved an average accuracy of 85.91%. These studies highlight the strong potential of Faster R-CNN for weld defect detection. However, due to the diverse shapes and sizes of weld defects, as well as low-contrast and blurred boundaries, the standard Faster R-CNN may struggle with accurate recognition, prompting the integration of FPN and Faster R-CNN to enhance the detection of defects of varying sizes (Ji et al., 2023; Xu et al., 2023a). Additionally, a new channel and position attention

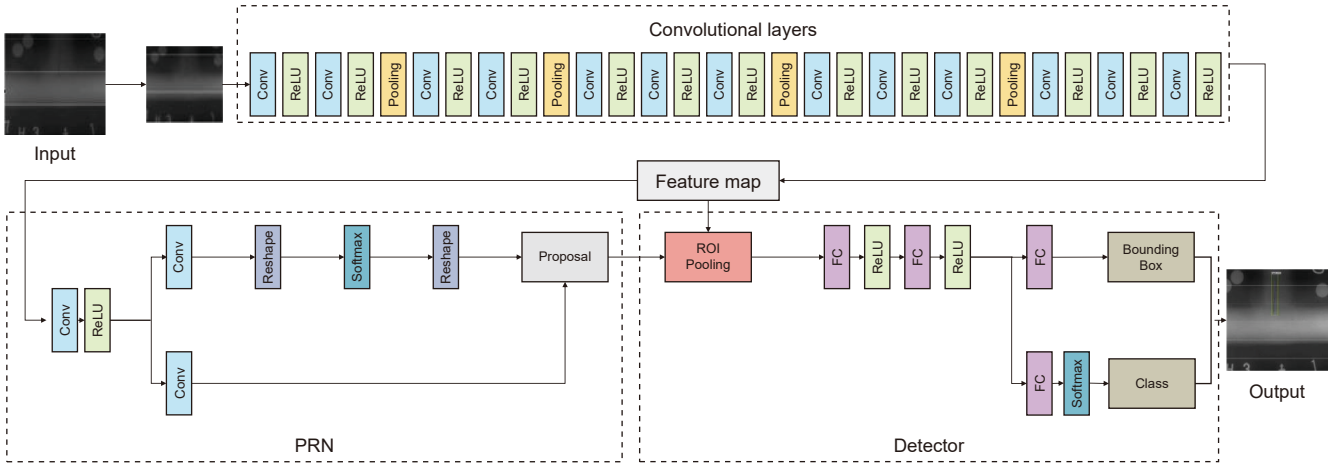

Fig. 13. A diagram of the Faster R-CNN architecture.

mechanism (SPAM) was introduced that allowed the model to focus on critical regions more precisely, which improved the average recognition accuracy for subtle defects by 4% (Ji et al., 2023). Oh et al. (2020) optimized the size and aspect ratio of the anchor frame by analyzing the weld defect dimensions. This improved the anchor frame to more effectively capture defects of different sizes and shapes, which enhanced detection performance. The standard Faster R-CNN framework sends candidate regions directly to the detector for classification and bounding-box regression, which can hinder performance due to inaccurate target localization. Therefore, Cai and Vasconcelos (2021) proposed Cascade R-CNN, which refined candidate regions via multiple cascaded bounding-box regression steps to improve localization accuracy. Similarly, Zhang et al. (2023a) developed a specialized weld defect recognition model based on Cascade R-CNN and introduced an adaptive threshold technique to improve defect segmentation, achieving an almost 90% recognition accuracy. To further enhance multiscale feature extraction, FPN was integrated into the Cascade R-CNN model. A feature batch elimination network was employed to randomly eliminate certain features, effectively reducing overfitting (Dai et al., 2025).

One-stage detectors directly predict defect class and location from the image without generating candidate regions. One-stage detectors are widely used in practical applications due to their simplicity and high efficiency. YOLOv3 (Redmon and Farhadi, 2018) and YOLOv5 (Zhu et al., 2021) are the most popular models for weld defect detection. Figs. 14 and 15 show the specific architecture of these models. YOLOv3 combines a new feature extraction network with residual blocks to increase the network depth while preventing gradient vanishing, consequently enhancing its feature extraction capability. It also incorporates a multiscale prediction block to improve detection accuracy for both large and small targets. Yang et al. (2019a) developed a weld defect detection model based on standard YOLOv3, achieving an average defect recognition accuracy of 91.02%, a 12% improvement over the standard Faster R-CNN. To accelerate model training, Yang et al. (2022b) reduced the size of the large-scale detection branch and introduced depth separable convolutions, reducing the weight of the model and its dependency on high-performance hardware (Yang et al., 2022b). Another study optimized YOLOv3 feature extraction by integrating Ghost convolution and cross-state local network (CSP) blocks to reduce model parameters and improve operational efficiency (Liu, 2021). YOLOv5 further optimizes the network structure, enhancing both detection accuracy and efficiency. It adopts a more efficient feature extraction design that reduces computational cost while maintaining extraction performance using the (CSP) technique. YOLOv5 also features an automatic anchor generation mechanism, which increases the ability of the model to detect targets of various sizes. Yang et al. (2021a) employed eight defect types to evaluate the recognition capability of YOLOv5, demonstrating excellent detection efficacy. To improve YOLOv5 feature extraction, both spatial and channel attention

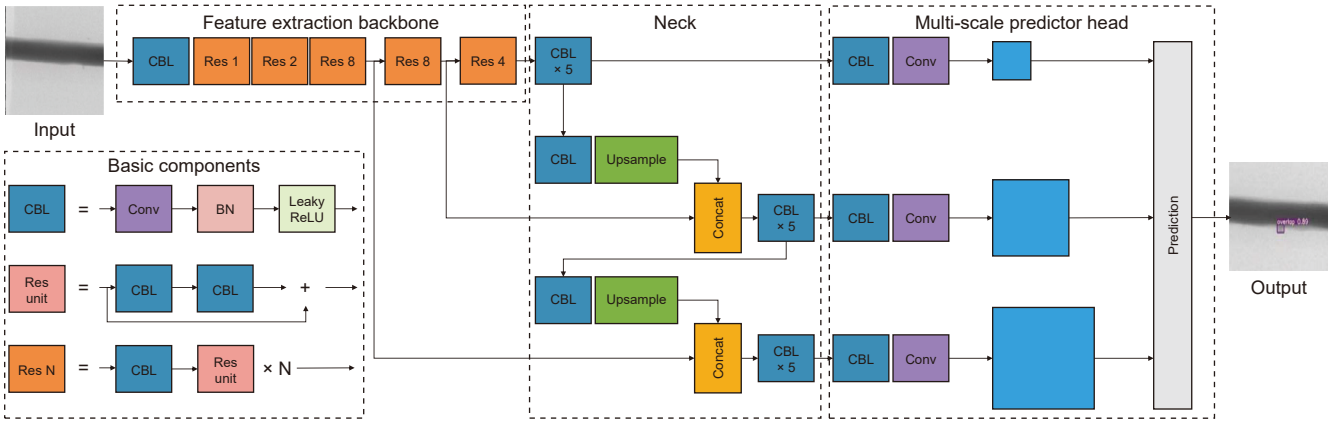

Fig. 14. A diagram of the YOLOv3 architecture.

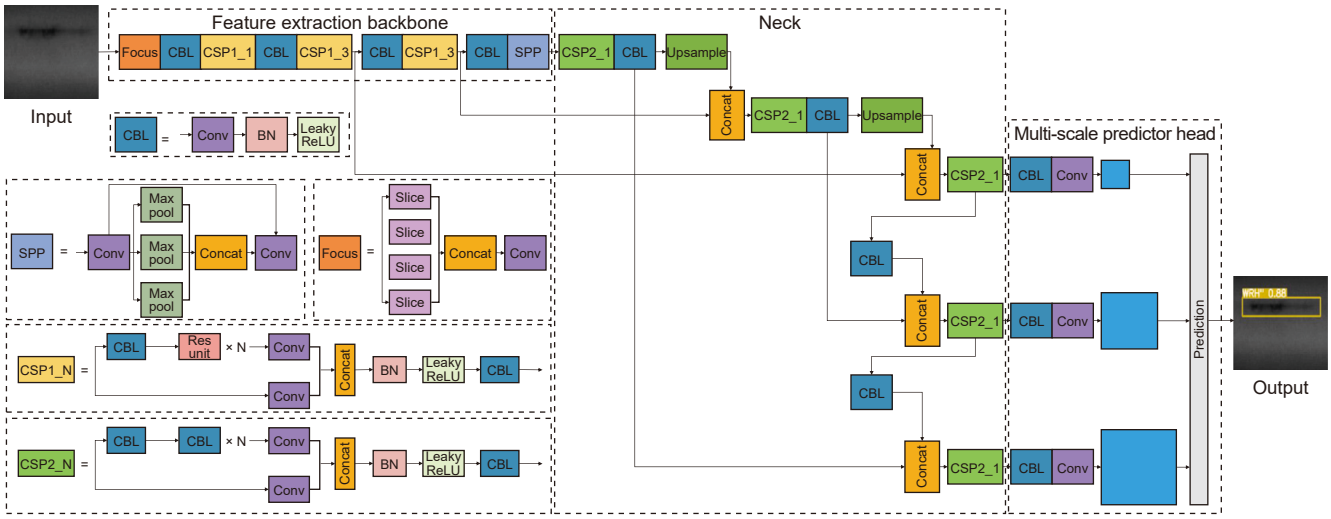

Fig. 15. A diagram of the YOLOv5 architecture.

mechanisms were added to minimize the impact of irrelevant features and enhance detection accuracy (Cheng et al., 2022; Xu et al., 2023b). Wang et al. (2025c) comprehensively analyzed the independent effects of channel and spatial attention mechanisms on weld defect detection in terms of feature extraction, salient pixel tracking, and feature clustering. The results indicated that spatial attention mechanisms significantly outperformed channel attention mechanisms, effectively improving feature information entropy, model focus on defect regions, and separation between defective and non-defective feature clustering. Since most weld defects are small, the detection accuracy for these defects is improved by removing the large-object detection layer and incorporating the GhostBottleneck module, along with DIoU and CIoU loss functions (Cheng et al., 2022). However, this optimization may reduce detection accuracy for large defects. Kwon et al. (2023) proposed a YOLOv5 twin-model approach for detecting both large and small defects, using multiscale feature maps to enhance recognition accuracy. In addition to YOLOv3 and YOLOv5, the RetinaNet one-stage detector (Lin et al., 2017b) has also been used for weld-defect detection. RetinaNet employs Focal loss to address the issue of imbalanced sample distribution in datasets. Experiments have shown that RetinaNet can maintain a high mAP of around 82% even in unbalanced samples (Wang et al., 2019). Based on the YOLO model, Jiang et al. (2025) proposed a weld defect detection method that integrated dynamic film reading knowledge from the non-destructive testing domain. This method simulated the dynamic manual film reading process via a logarithmic transformation-based multi-image decomposition approach. This technique employed channel attention mechanisms for multi-image feature fusion and the YOLO model for defect detection.

In addition to the research discussed above, several studies have developed customized models that exhibit excellent detection performance. To address the challenge of background noise from non-weld regions affecting defect recognition, Wang et al. (2024b) developed a comprehensive model capable of simultaneous weld region segmentation, defect classification, and localization. This model improved multiscale feature capturing by combining residual networks and FPNs, significantly enhancing the accuracy compared to classic models such as Faster R-CNN. Zuo et al. (2024d) proposed two feature extraction networks with different depths and widths for small-defect detection, using FPNs to fuse multiscale features. They also introduced an iterative detection mechanism to progressively enhance the model representation of tiny defects, improving detection accuracy by approximately 6% compared to YOLOv7 (Zuo et al., 2024d). Weld defects often exhibit significant shape and size differences. Zuo et al. (2024a) designed an anchor-free approach based on dynamic receptive fields and task alignment to improve the accuracy of complex defect detection. This method flexibly adjusted feature extraction ranges and decoupled localization and classification tasks to effectively address defect morphology and size diversity. A defect detection model was developed that improved complex deformation feature capturing by introducing spatial transformation attention and enhanced the prediction accuracy for multiscale defects via multilevel attention feature fusion (Zuo et al., 2024b). The results demonstrated that this method significantly improved detection accuracy, achieving a recall rate of 0.903 for large-scale cracks and 0.886 for small-scale cracks. Zhang et al. (2025) proposed DSF-YOLO to address the challenges posed by blurred boundaries and diverse defect shapes in weld X-ray images. This method incorporated a dynamic staged fusion feature extraction module and a dual multi-scale feature fusion module, which effectively combined global and local features via a dynamic fusion strategy within dual backbone networks. The results indicated that this model achieved 74.7% mAP50:95, surpassing the performance of YOLOv8-X, while reducing FLOPs by 75%. Recent studies have developed specific models for defect recognition in small-diameter pipeline weld X-ray images. Given the narrow weld regions and significant defect size variations in small-diameter pipelines, the proposed models employ full feature fusion networks that effectively enhance the capability to recognize defects with different scales and aspect ratios by merging deep semantic information and shallow shape features (Shi, 2021; Shi et al., 2023a). To address the specific requirements for detecting tiny defects in small-diameter pipelines, Bai (2023) designed AFFM-Net, which introduced a fusion attention mechanism based on shape and positional awareness. This was combined with a weighted feature pyramid network to more accurately capture defect morphology and spatial position information. Additionally, Yang et al. (2025) specifically targeted the characteristics of low-quality X-ray images of small-diameter pipelines, proposing a spatial-frequency feature fusion network based on multidimensional collaborative enhancement strategies. This

approach significantly improved defect recognition accuracy in complex imaging conditions via multidimensional, multiscale feature extraction, and spatial-frequency joint enhancement.

Similar to semantic segmentation methods, the quantity and quality of training images are also key factors that influence defect detection performance. Traditional methods such as horizontal flipping, vertical flipping, and random cropping are widely applied to increase training image diversity for data augmentation (Wang et al., 2019; Yang et al., 2021a). However, these traditional methods can only provide limited diversity and cannot effectively address situations of severe training data insufficiency. Li et al. (2024a) proposed a high-resolution X-ray welding defect data augmentation model based on real samples. The design included two data augmentation generation modes that simultaneously generated large quantities of defect images and annotations, which significantly improved training image diversity. Image quality significantly impacts object detection, especially when processing low-quality X-ray images. Research has shown that motion blur problems in images significantly reduce object detection performance (Kupyn et al., 2018). To address this issue, Yang et al. (2021a) proposed a deblurring method based on Hough transform that effectively improved defect detection accuracy. Although this method resolves motion blur problems, it still presents challenges with low contrast and insufficient dark detail that commonly exist in pipeline weld X-ray images. Wang et al. (2025b) constructed high-grayscale enhancement mapping functions for super 8-bit high-grayscale X-ray images, mapped 12-bit images to 16-bit high-resolution images, and designed a high-resolution pseudo-color enhancement strategy by combining HIS pixel self-transformation and RGB models to significantly enhance the dark details and contrast in images. Experiments show that models trained with processed images can achieve an average detection accuracy of 92.72%, displaying significantly improved detection efficacy for weak contrast and small-target defects. A general adaptive enhancement method based on spatial domain filtering was proposed that significantly improved image details. Deformable convolutions were introduced into the defect detection models, enabling flexible feature extraction from various complex faults (Zuo et al., 2023). Combining image enhancement with detection model optimization improved the detection accuracy by approximately 2.3% compared to the original image models. Zuo et al. (2024c) utilized a data calibration method based on window width and window level adjustment that eliminated the influence of invalid pixels, which significantly enhanced the dark details and image quality. This method achieved an actual recognition accuracy of 97.4% when combined with multiframework defect detection. Although these methods significantly enhance image quality and defect recognition, they mostly adopt separate processing approaches that increase the complexity of defect detection workflows. Therefore, Zuo et al. (2025a) used end-to-end intelligent weld defect detection system that tightly integrated adaptive image preprocessing with progressive feature extraction methods, which resulted in the collaborative optimization of low-brightness, low-contrast X-ray images to enhance defect detection. The results demonstrated that this end-to-end integrated approach significantly improved the detection accuracy compared to other methods.

Beyond model architecture optimization, researchers have begun exploring ways to improve model detection accuracy with limited annotation resources. As an effective technique for reducing annotation costs (Ren et al., 2021), active learning has gradually attracted attention for weld defect detection. Liu et al. (2022b) proposed a pipeline weld defect detection method based on active few-shot learning for the automatic screening of high-value samples from unlabeled data to facilitate expert annotation via uncertainty sampling strategies and effectively address annotated sample scarcity. To address more complex detection scenarios, Zuo et al. (2025b) proposed an active learning-based weld defect detection method for the intelligent selection of high-value samples from unlabeled data, which significantly improved fault recognition accuracy in unknown scenarios and increased the detection precision to 95.4% in real-world situations.

In summary, object detection-based methods offer significant advantages for weld defect recognition. Unlike semantic segmentation, object detection directly labels defect locations and types in the original image, providing more intuitive recognition results. Current weld defect detection architectures are mainly divided into two-stage and one-stage detectors. Two-stage detectors, such as Faster R-CNN, achieve high accuracy by first generating candidate regions, followed by classification and bounding box regression. However, they present high model complexity, slow detection speed, and a reliance on the quality of the candidate regions. One-stage detectors, such as YOLOv3 and YOLOv5, improve both detection speed and accuracy via direct defect classification and localization without generating candidate regions. To address the challenges posed by weld defects with low contrast, varying morphologies, and different sizes, techniques such as FPN and attention mechanisms have been introduced to enhance the multiscale detection capacity of the model. Additionally, research into customized models is advancing the field of intelligent weld defect detection. New domain knowledge fusion and active learning technologies offer new object detection-based defect recognition research avenues. Knowledge-guided detection methods improve recognition capability for specific defect types, while active learning strategies maintain or enhance detection performance while reducing annotation requirements, particularly excelling in few-shot and complex scenarios. Despite the success of object detection methods, further development is restricted by the lack of large-scale, high-quality, and accurately labeled datasets. Although active learning methods can effectively address dataset limitations, the selected high-value samples still require fine-grained annotation. While border-level annotation is cheaper than pixel-level annotation, it is still time-consuming and requires expertise, remaining a key obstacle in advancing this technology.

3.3.5. Evaluation indicators

Subjective and objective evaluations are commonly used to assess the performance of deep learning-based defect recognition methods. Subjective evaluation qualitatively analyzes the performance of a model by directly observing its test-set recognition results. Conversely, objective evaluation quantitatively measures the efficacy of a model according to predefined performance metrics. Classification is central to all methods, whether based on image categorization, semantic segmentation, or object detection. The confusion matrix serves as the foundation for calculating various evaluation metrics when evaluating classification performance (Table 5).

In Table 5, T_p denotes the number of samples whose true class is positive, with positive predicted results. F_n represents the number of samples whose true class is positive with negative predicted results. F_p signifies the number of samples whose true class is negative with positive predicted results. T_n denotes the number of samples whose true class is negative with negative predicted results. The specific meanings represented by T_p, F_n, F_p, and T_n in different tasks varies. Tables 6, 7, and 8 show the performance evaluation indicators in different tasks.

Table 5
The confusion matrix.

		Prediction	
		Positive	Negative
Reference	Positive	True positive (T_p)	False negative (F_n)
	Negative	False positive (F_p)	True negative (T_n)

Table 6
The performance evaluation indicators for the image classification methods.

Name	Equation	Explanation
Accuracy	$\frac{T_p + T_n}{T_p + F_p + F_n + T_n}$	T_p: The true class is the specific class, and the predicted class represents its sample numbers.
Precision	$\frac{T_p}{T_p + F_p}$	F_n: The true class is the specific class, and the predicted class represents other class sample numbers.
Recall	$\frac{T_p}{T_p + F_n}$	F_p: The true class is another class, and the predicted class represents specific class sample numbers.
F1 score	$2 \times \frac{Precision \times Recall}{Precision + Recall}$	T_n: The true class is another class, and the predicted class represents other class sample numbers.

Table 7
The performance evaluation indicators for the semantic segmentation methods.

Name	Equation	Explanation
Pixel accuracy	$\frac{T_p + T_n}{T_p + F_p + F_n + T_n}$	T_p: The true class is the specific class, and the predicted class represents its pixel numbers.
Precision	$\frac{T_p}{T_p + F_p}$	F_n: The true class is the specific class, and the predicted class represents other class pixel numbers.
Intersection over union	$\frac{T_p}{T_p + F_p + F_n}$	F_p: The true class is another class, and the predicted class represents the specific class pixel numbers.
Mean intersection over union (*mIoU*)	$\frac{1}{n}\sum_{i=1}^{n} IoU_i$	T_n: The true class is another class and the predicted class represents other class pixel numbers.
Dice	$\frac{2 \times T_p}{2 \times T_p + F_p + F_n}$	n: The total number of classes in the semantic segmentation task.

Table 8
The performance evaluation indicators for the object detection methods.

Name	Equation	Explanation
Average precision	$\int_0^1 P(r)\mathrm{d}r$	$P(r)$: Precision for recall r.
Mean average precision	$\frac{1}{n}\sum_{i=1}^{n} AP_i$	n: Total classes of the object detection task.
Intersection over union	$\frac{A \cap B}{A + B - (A \cap B)}$	AP: Average precision. A: Area of the projected bounding box. B: Area of the true bounding box.

3.4. Brief summary

This section compares representative algorithms from various categories to comprehensively evaluate the performance and applicable scenarios of different defect recognition methods. Table 9 presents the performance metrics, datasets, and applicable scenarios of the representative algorithms from three major categories: signal processing-, feature design-, and deep learning-based methods. In the computational efficiency/model size column, s denotes seconds per image, ms represents milliseconds per image, and M indicates model size. Different types of defect recognition methods exhibit distinct differences in detection performance and applicable scenarios. Specifically, although signal processing-based defect recognition methods are computationally simple, their performance is relatively limited. Feature design-based defect recognition methods demonstrate good detection efficacy in specific application scenarios, such as recognizing circular and linear defects in small-diameter pipelines. Deep learning-based methods exhibit superior recognition performance but require more significant data and computational resources.

Based on these comparisons, Table 10 provides an overview of the methods used for defect recognition in pipeline weld X-ray images, as well as an analysis of their strengths and weaknesses. Signal processing-based defect recognition methods simplify calculations by using direct mathematical operations. This involves simple pixel-level calculations without complex iterative processes or large matrix operations, which are easy to interpret, require minimal data, and maintain low computational costs. However, these methods primarily focus on detecting defects in the weld area without accurately identifying the defect types. Contrarily, feature design-based defect recognition methods manually design and extract features through image processing to facilitate richer defect descriptions. These features are used to construct pattern recognition models for precise defect type identification. The efficacy of these features directly impacts recognition performance. Moreover, most of the features are designed based on expert experience, which introduces subjectivity into the process. The efficiency of feature design-based methods primarily depends on the number and complexity of the extracted characteristics. Simple geometric features require

Table 9
The performance evaluation of the representative defect recognition methods.

Method	Performance	Computational efficiency/ model size	Dataset	Applicable scenario
Signal processing-based defect recognition method				
Vertical filter (Radi et al., 2022)	*Dice*: 0.9961	–	GDXray	Horizontal defect detection
Horizontal filter (Radi et al., 2021)	*Dice*: 1.0	–	GDXray	Vertical defect detection
Combining global and local thresholding (Thiruganam et al., 2010)	–	–	Self-built datasets	Defect detection in low computing resources
Feature design-based defect recognition method				
Shape geometric features + textural features + BP (Valavanis and Kosmopoulos, 2010)	*Accuracy*: 85.4%	–	Self-built datasets	Defect detection with few features
Shape geometric features + Bayesian network (Goumeidane et al., 2015)	*Accuracy*: 96.3%	–	Self-built datasets	Defect detection uncertainty quantification
Shape geometric features + fuzzy C-mean (Tridi et al., 2005)	*Accuracy*: 88.9%	–	Self-built datasets	Unsupervised defect detection
Sparse description (Xiao et al., 2024)	*Accuracy*: 97.2%	5.50 s	Self-built datasets	Circular and linear defect detection in small-diameter pipelines
Deep learning-based defect recognition method (image classification)				
Progressive CNN (Chen et al., 2020)	*Accuracy*: 98.7%	–	Self-built datasets	Lack of labeled defective samples
Hybrid feature learning based on base-class and cross-class (Liu et al., 2023b)	*Accuracy*: 92.1%	27.98 M	GDXray + Self-built datasets	Class imbalance defect detection
Consistent multiscale feature mapping (Liu et al., 2022a)	*Accuracy*: 93.7%	–	Self-built datasets	Low-quality weld radiographic defect detection
Comparative learning of defective prototypes for natural language supervision (Cheng et al., 2024)	*Accuracy*: 90.7%	–	Self-built datasets	Defect detection for interpretable decisions
Improved DG-MobileNet (Pan et al., 2023)	*Accuracy*: 98.62%	12.5 M	Self-built datasets	Highly efficient defect classification
Deep learning-based defect recognition method (semantic segmentation)				
Fast-SCNN (Zhao et al., 2021)	*mIoU*: 75.7%	12.3 ms	Self-built datasets	Highly efficient defect detection
VGG16-UNet (Sun et al., 2024)	*mIoU*: 82.8%	0.0373 s /94.95 M	Self-built datasets	
YOTT-DKNet (Li et al., 2024c)	*Dice*: 0.7181	0.836 M	GDXray	Detection uncertainty quantification
DA-DCGAN + U-Net (Wang et al., 2024a)	*mIoU*: 77.4%	0.15 s	GDXray	Lack of labeled defective samples
Multifeature enhanced fusion (Li et al., 2023a)	*Dice*: 0.7791	0.318 s	GDXray	High-resolution weld radiographic defect detection
Deep learning-based defect recognition method (object detection)				
STMA-Net (Zuo et al., 2024b)	*Precision*: 86.7% (Large crack) *Precision*: 81.0% (Small crack)	12.5 ms/16.5 M	GDXray + Self-built datasets	Complex shape and multiscale defect detection
High gray enhanced (Wang et al., 2025b)	*mAP*: 88.7%	1.765 s	Self-built datasets	High-resolution weld radiographic defect detection
Image quality enhancement and defect detection collaboration (Zuo et al., 2025a)	*Precision*: 85.3% (low light) *Precision*: 89.6% (foggy)	15.9 ms/23.4 M	Self-built datasets	Low-quality weld radiographic defect detection
Active learning (Zuo et al., 2025b)	*AP*: 94.5%	28.8 M	Self-built datasets	Defect detection for unknown scenarios
Active few-shot learning (Liu et al., 2022b)	*AP*: 89.7%	0.021s/15.2M	Self-built datasets	Lack of labeled defective samples
YOLO-Xweld (Yang et al., 2022b)	*mAP*: 99.8%	4.6 M	Self-built datasets	Environmental constraint detection

Table 9 (*continued*)

Method	Performance	Computational efficiency/ model size	Dataset	Applicable scenario
AFFM-Net (Bai, J., 2023)	*mAP*: 78.7%	102.85 M	Self-built datasets	Small-diameter pipeline defect detection
FFF-MD (Shi, 2021)	*mAP*: 82.1%	103.04 M		
Faster RCNN-VGG16 (Chen, 2022)	*mAP*: 85.9%	–		
MCSF-Net (Yang et al., 2025)	*mAP*: 78.7%	51 M		

Table 10
The strengths and weaknesses of the defect recognition methods for pipeline weld X-ray images.

Methods	Strengths	Weaknesses
Signal processing-based defect recognition method	• Highly interpretable. • Simple and inexpensive calculation.	• Defect type classification is challenging.
Feature design-based defect recognition method	• Characterize defects according to designed features to provide richer defect information. • Identify defect types using designed features.	• Designed features rely on expert knowledge. • Feature validity affects recognition performance.
Deep learning-based defect recognition method	• Features are automatically extracted instead of manually designed. • Excellent defect recognition performance for complex patterns.	• Training processes typically require large amounts of labeled data and powerful computational resources. • Poor interpretability.

minimal computational resources, while complex textural features involve intensive mathematical computations. Techniques for reducing dimensionality can help lower the feature vector dimensions to accelerate computational speed, while classifier selection also affects computational efficiency. For example, a simple KNN can be calculated rapidly, unlike a more complex multiclass SVM that requires more computational resources.

Unlike these two methods, deep learning-based defect recognition techniques are capable of automatic weld defect feature extraction and learning complex patterns and representations. These methods are superior in recognizing defects in intricate patterns, making them the most popular current approach for weld defect detection. Deep learning algorithms have demonstrated good adaptability in small-diameter pipeline weld defect recognition via reasonable model design. Various models have been proposed for the specific detection of small-diameter pipeline defects by optimizing the multiscale feature fusion and attention mechanisms. These models effectively addressed challenges such as narrow weld regions and minute defect sizes, confirming the flexibility and potential of deep learning methods to process the weld images of pipelines with different diameters. Furthermore, combining image quality optimization with detection methods is crucial for improving recognition performance. For low-quality X-ray images, appropriate image quality optimization techniques not only improve image quality but also significantly enhance defect detection accuracy. However, unlike methods that rely on direct pixel-level analysis and predefined feature extraction, the training of deep learning-based models requires a large volume of labeled data and significant computational resources due to their complex multilayer architectures and iterative parameter optimization processes. The accuracy and resilience of these models can only be improved through training on extensive labeled datasets. Additionally, the recognition results from deep learning methods are often difficult to interpret, which can hinder defect analysis. Furthermore, most current deep learning models still require optimization training for specific pipeline diameters and lack cross-diameter generalization capability, which limits model universality in practical industrial applications.

4. Challenges and prospects

Research aims to develop a model for pipeline weld X-ray image defect recognition that can assist or replace manual defect inspection and reduce the costs associated with traditional assessment techniques. As discussed in Section 3, deep learning-based defect recognition method outperforms other approaches and is the most efficient technique for intelligent weld defect recognition. This section discusses the challenges and prospects of deep learning-based defect recognition methods, focusing on aspects related to data, models, and applications (Fig. 16).

4.1. Data perspective

Since most deep learning-based methods are data-driven and depend on feature learning, the quality and quantity of data is crucial. However, several challenges arise in constructing suitable datasets. First, data collection is challenging, particularly when inspecting industrial weld X-ray images. The low specific defect occurrence rate makes it difficult to gather a sufficient number of images. Second, the collected data often requires extensive preprocessing. The complexity of actual industrial welding environments and the varying parameters of digital scanners increase the intricacy of the images. Pipeline diameter variations exacerbate image complexity. The weld X-ray images of large-diameter pipelines have complex backgrounds that require focused noise suppression, while those of small-diameter pipelines contain tiny defects that necessitate fine preservation of edge details during noise suppression. Therefore, effective preprocessing is essential to ensure adequate defect recognition algorithm performance. Additionally, data labeling presents a significant challenge. Most deep learning models require precise labels for training, which can be at the image level, pixel level, or in the form of bounding boxes. Generating these labels is time-consuming and labor-intensive, and relies heavily on specialized knowledge. Pipeline diameter variations also complicate annotation. Small-diameter pipeline weld defects demand higher annotation precision, while the weld X-ray images of large-diameter pipelines present complex backgrounds which may complicate accurate boundary definition.

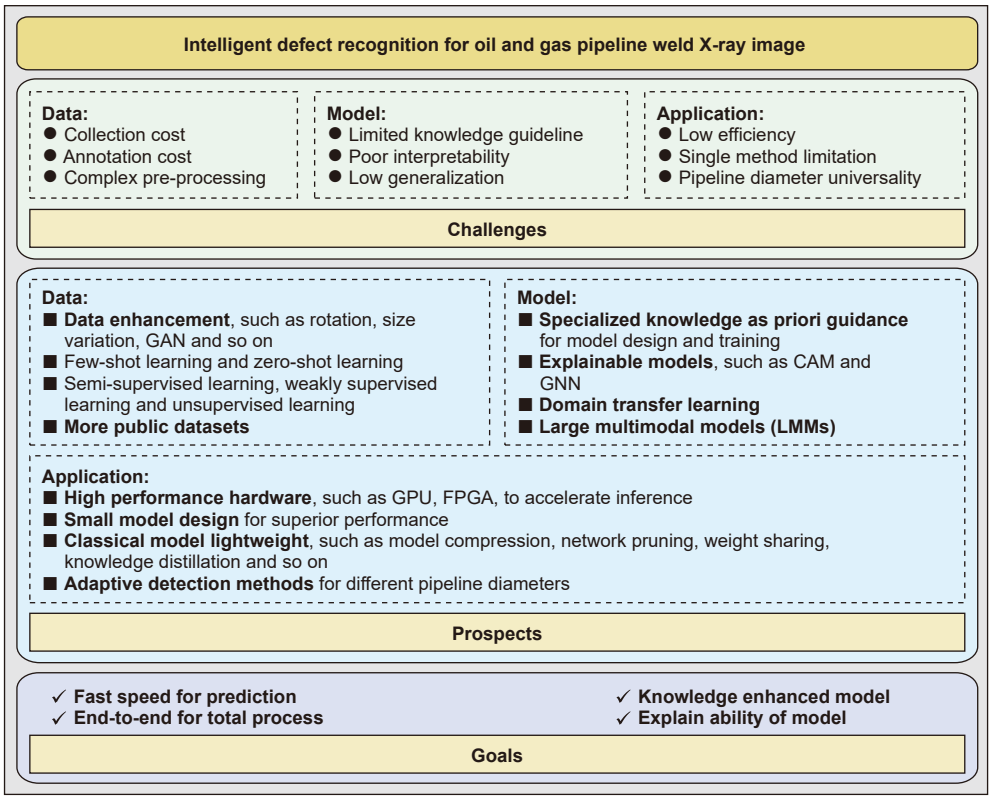

Fig. 16. The challenges and prospects of oil and gas pipeline weld X-ray image defect recognition.

Despite the challenges in collecting large-scale datasets, the issue of limited data can be partially mitigated using traditional augmentation techniques such as GANs. However, data diversity is crucial to ensure that the generated virtual samples yield the desired outcomes. Although deep learning methods outperform other approaches in weld X-ray image preprocessing, the size of the dataset remains a major obstacle for the development of these techniques. Few-shot learning (Shi et al., 2023b) and zero-shot learning (Li et al., 2025b) may offer viable solutions to address these challenges. Few-shot learning aims to train models with highly limited labeled data, while zero-shot learning focuses on recognizing defects absent during training. Extracting valuable information from unlabeled samples is essential to reduce the cost of labeled data. In this context, strategies such as semi-supervised (Wang et al., 2024c), weakly supervised (Li et al., 2023b), and unsupervised learning (Liu et al., 2024a) present promising alternatives. Semi-supervised learning enhances model performance with limited labeled data, weakly supervised learning achieves results with less expensive labels, and unsupervised learning focuses on defect detection without the need for labeled data. The FUDet proposed by Zhao et al. (2025) has shown exceptional promise for detecting MFL signals during unsupervised learning. This method relies solely on normal samples for training while achieving high-precision anomaly detection via modules designed for bidirectional discrimination, dynamic noise generation, and reconstruction classification. Essentially, it learns the distribution of anomalous features from normal data by merging feature discrimination with reconstruction techniques. This offers valuable insights for enhancing unsupervised learning in weld X-ray defect detection.

4.2. Model perspective

Deep learning models face several challenges in addition to data limitations. First, the lack of specialized knowledge is a significant issue. While deep learning methods can automatically extract features from large datasets, they often overlook the importance of domain-specific expertise, which complicates model training, hinders optimal performance, and reduces accuracy when addressing specific defects. Second, deep learning models suffer from poor interpretability. These models are often viewed as “black boxes”, with unclear decision-making processes that reduce their credibility and acceptance. Third, the generalization ability of these models is limited. Variations in weld X-ray image styles due to differences in pipeline diameter, imaging techniques, transmission angles, and scanning equipment can significantly impact model performance. The impact of pipeline diameter variations is particularly significant. The pipeline weld X-ray images of both large- and small-diameter pipelines exhibit obvious differences in weld region width and background complexity. Even when models perform exceptionally on training data from specific pipeline diameters, the detection efficacy may significantly decline when faced with images of pipelines with different diameters.

Incorporating specialized knowledge into deep learning models is essential to address these issues. This integration can optimize initial model parameters and guide the model to effectively capture relevant features, ensuring a more stable training process (Zhou et al., 2024). Knowledge graphs are gaining popularity for model enhancement due to their ability to fuse domain-specific knowledge. Techniques such as class activation mapping (CAM) can visualize the internal decision-making processes of a model to improve its interpretability (Shin et al., 2023). Leveraging the advanced inference capabilities of graph neural networks (GNNs) to predict defect types can further enhance interpretability (Apak and Farsadi, 2025). Lastly, domain adaptation techniques (Shang and Chen, 2024) can be used to transfer existing weld defect detection models to new scenarios, which addresses style variations and enhance model resilience to improve

generalization. The generalization capability for unknown defect types represents a critical challenge for deep learning models. Novel defect categories may emerge unexpectedly in industrial inspection settings, while conventional models often fail to effectively identify defect types obscured during training. To address this issue in pipeline MFL detection, Wang et al. (2025a) introduced the KTR-BUNN method. This approach used dual unbiased neural networks to identify and differentiate unknown defect types in target domains, effectively resolving detection challenges in varying operational conditions. Furthermore, Shen et al. (2025c) developed the EHD-Net. This method employs elastic knowledge transfer and distorted heterogeneous distillation learning, allowing for the rapid acquisition of new defect types while also mitigating the risk of forgetting previously learned categories. Both methods demonstrate superior generalization capabilities for unknown defect types in MFL datasets, providing valuable technical insights for intelligent X-ray weld defect detection when faced with new challenges. Additionally, large multimodal models (LMMs) represented by Generative Pre-Trained Transformer (GPT) offer new opportunities for intelligent weld defect recognition via their powerful multimodal understanding and reasoning capabilities. First, the multimodal capability of LMMs can be utilized to fuse textual knowledge such as weld defect detection grading standards, defect descriptions, and expert experience with pipeline weld radiographic images to construct knowledge-enhanced multimodal weld defect detection models. Therefore, advanced methods, such as Myriad (Li et al., 2023c), can be used to integrate mature intelligent weld defect detection algorithms into the LMM framework as visual experts, effectively combining algorithm accuracy and generalization via specially designed instruction frameworks and visual expert-guided encoders. Second, the powerful few-shot and zero-shot learning capabilities LMMs can effectively address data scarcity issues for rare defect types via meta-learning mechanisms, reducing the dependence on large amounts of annotated data. Furthermore, their strong generalization capability enables rapid adaptation across different pipeline diameters and welding process situations, significantly reducing data requirements and time costs for new scenario deployment. Finally, the instruction-following capability of LMMs enables them to generate corresponding analysis results according to different detection requirements, supporting diverse outputs ranging from simple defect determination to detailed causal assessment. In summary, utilizing LMMs to construct intelligent weld defect recognition models will drive their transformation from traditional single-model, single-scenario approaches to unified frameworks with multi-scenario adaptability.

4.3. Application perspective

The goal of pipeline weld X-ray image defect recognition is to apply it effectively in real-world weld inspections. While many deep learning-based defect recognition methods have demonstrated strong performance on test datasets, they still face several challenges in practical applications. A key issue is recognition inefficiency. These models often exhibit large sizes and high computational complexity, which reduce recognition speeds and efficacy in real-time or high-efficiency scenarios. Another challenge is multimethod integration. Relying on a single recognition approach typically only addresses defect detection, without meeting the broader needs of a comprehensive inspection process. Pipeline diameter adaptability is another important challenge in practical applications. Weld defect detection models for practical applications must be suitable for both small- and large-diameter pipelines. However, most current models still require training and optimization for specific diameter ranges, which limits system universality and practicality.

Several strategies can be employed to address these challenges and enhance the practical utility of defect recognition models. First, high-performance computing hardware can significantly improve model efficiency and reduce processing time. Second, model optimization techniques such as knowledge distillation (Tan et al., 2024), model compression (Zhong et al., 2024), and network pruning (Guan and Li, 2024) can reduce the model size and complexity, which accelerates processing and decreases computational requirements. Additionally, developing adaptive detection algorithms that combine pipeline diameter and defect recognition can automatically adjust detection strategies according to different pipeline diameters, improving their universality and accuracy. Finally, developing an integrated system that combines defect recognition with additional functionalities, such as defect grading and quantitative assessment, can better satisfy the diverse needs of real-world applications. Shen et al. (2025b) developed TOPC-Net, a multi-task learning framework aimed at enhancing pipeline MFL detection. It effectively merges defect detection with size quantification via an end-to-end optimization process. This integrated approach not only improves X-ray weld defect detection performance but also reduces computational costs. Such a system can rapidly detect and locate defects, assess their severity, and provide maintenance recommendations.

5. Conclusions

X-ray inspection is crucial for ensuring the weld quality in oil and gas pipelines and maintaining pipeline safety. Pipeline weld X-ray defect recognition methods aim to automatically identify weld defects, such as cracks, lack of penetration, and lack of fusion, using advanced image processing and computer vision algorithms. This improves detection efficiency and reduces errors from manual inspection, such as misjudgments or omissions. The defect recognition process consists of three main steps: X-ray image acquisition, image preprocessing, and defect identification. First, high-precision scanners digitize the original X-ray films, creating a dataset for further analysis. Next, image preprocessing enhances image quality and defect visibility by reducing noise reduction and enhancing contrast. While traditional preprocessing methods present various advantages, they often struggle with adaptability, especially in complex scenarios. Recently, deep learning-based preprocessing techniques have attracted considerable attention due to their ability to automatically learn optimal feature representations from large datasets, which significantly improved image quality and defect contrast. Weld defect recognition methods can be broadly categorized into signal processing-based, feature design-based, and deep learning-based techniques. Although traditional, signal processing techniques suffer from poor adaptability, lower accuracy, and a reliance on complex post-processing for detecting various defects. Feature design-based methods depend on manually created features and machine learning algorithms, with their performance largely determined by the feature design quality. Contrarily, deep learning methods automatically extract features in an end-to-end manner, addressing the limitations of manual feature design. Since defect detection involves both identifying defect types and accurate localization, deep learning methods, especially those based on semantic segmentation or object detection architectures, are more suitable for this task.

In summary, deep learning-based methods are superior for both weld X-ray image preprocessing and defect recognition. However, the need for large-scale, high-quality, and labeled datasets remains a significant limitation. The absence of domain-

specific expertise also makes deep learning models vulnerable to underperformance in complex scenarios. Other challenges include improving model generalization and scalability. Future research should focus on effectively integrating previous knowledge into deep learning models, constructing highly precise models using limited or low-quality data, and enhancing the generalization and interpretability. Multimodal models can enhance defect by integrating domain expertise, while active learning can mitigate the dependence on data quality. Employing incremental learning and domain adaptation can significantly improve the generalization capabilities of these models. These approaches pave the way for more robust and effective weld defect detection methods tailored for real-world applications.

CRediT authorship contribution statement

Wei-Chao Qian: Writing – original draft, Visualization, Methodology, Investigation, Formal analysis, Conceptualization. **Shao-Hua Dong:** Writing – review & editing, Supervision, Project administration. **Meng Sun:** Visualization, Investigation, Formal analysis. **Zi-Cong Han:** Visualization, Investigation, Formal analysis. **Lin Chen:** Writing – review & editing, Supervision, Project administration, Funding acquisition.

Declaration of competing interest

The authors declare no known competing financial interests or personal relationships that could have appeared to influence the work reported in this paper.

Acknowledgements

This work is supported by the Science Foundation of China University of Petroleum, Beijing (No. 2462023BJRC020) and the Strategic Cooperation Technology Projects of CNPC and CUPB (ZLZX2020-05).

References

Abd Halim, S., Ibrahim, A., Jayes, M.I., Manurung, Y.H.P., 2013. Weld defect features extraction on digital radiographic image using Chan-Vese model. In: 2013 IEEE 9th International Colloquium on Signal Processing and its Applications, pp. 67–72. https://doi.org/10.1109/CSPA.2013.6530016.

Abdelkader, R., Ramou, N., Khorchef, M., et al., 2021. Segmentation of X-ray image for welding defects detection using an improved Chan-Vese model. Mater. Today Proc. 42, 2963–2967. https://doi.org/10.1016/j.matpr.2020.12.806.

Ajmi, C., El Ferchichi, S., Laabidi, K., 2018. New procedure for weld defect detection based-Gabor filter. In: 2018 International Conference on Advanced Systems and Electric Technologies (IC_ASET), pp. 11–16. https://doi.org/10.1109/ASET.2018.8379826.

Ajmi, C., El Ferchichi, S., Zaafouri, A., Laabidi, K., 2019. Automatic detection of weld defects based on hough Transform. In: 2019 International Conference on Signal, Control and Communication (SCC, pp. 1–9. https://doi.org/10.1109/SCC47175.2019.9116162.

Al-Hameed, W., Mayali, Y., Picton, P., 2013. Segmentation of radiographic images of Weld defect. J. Global Res. Comput. Sci. 4 (7), 1–4. https://api.semanticscholar.org/CorpusID:270880.

Alaknanda, Anand, R.S., Kumar, P., 2006. Flaw detection in radiographic weld images using morphological approach. NDT E Int. 39 (1), 29–33. https://doi.org/10.1016/j.ndteint.2005.05.005.

Alaknanda, Anand, R.S., Kumar, P., 2009. Flaw detection in radiographic weldment images using morphological watershed segmentation technique. NDT E Int. 42 (1), 2–8. https://doi.org/10.1016/j.ndteint.2008.06.005.

Alghalandis, S.M., Alamdari, N., 2006. Welding defect pattern recognition in radiographic images of gas pipelines using adaptive feature extraction method and neural network classifier. In: 23rd World Gas Conference, pp. 1–13. https://api.semanticscholar.org/CorpusID:12278254.

Ali, K., Awan, M., Jalil, A., Mustansar, F., 2015. Localization and classification of welding defects using genetic algorithm based optimal feature set. In: 2015 International Conference on Information and Communication Technologies. ICICT), pp. 1–6. https://doi.org/10.1109/ICICT.2015.7469485.

Apak, S., Farsadi, M., 2025. Multi-branch spatial pyramid dynamic graph convolutional neural networks for solar defect detection. Comput. Electr. Eng. 121, 109872. https://doi.org/10.1016/j.compeleceng.2024.109872.

Ba, X.Y., Teng, Y.P., 2001. Study on the method of modeling identification of weld defect with computer. J. Anqing Normal Univer. (Nat. Sci. Ed.) 7 (4), 8–10. https://doi.org/10.3969/j.issn.1007-4260.2001.04.003 (in Chinese).

Badrinarayanan, V., Kendall, A., Cipolla, R., 2017. SegNet: A deep convolutional encoder-decoder architecture for image segmentation. IEEE Trans. Pattern Anal. Mach. Intell. 39 (12), 2481–2495. https://doi.org/10.1109/TPAMI.2016.2644615.

Bai, J.P., 2023. Research on detection method of small diameter pipe welding defect based on AFFM-net. Master thesis, Hebei University of Technology. https://doi.org/10.27105/d.cnki.ghbgu.2023.001263 (in Chinese).

Ben Mhamed, I., Abid, S., Fnaiech, F., 2012. Weld defect detection using a modified anisotropic diffusion model. EURASIP J. Appl. Signal Process. 46, 3–12. https://doi.org/10.1186/1687-6180-2012-46.

Beucher, S., Lantuéjoul, C., 1979. Use of watersheds in contour detection. In: International Workshop on Image Processing, real-time Edge and Motion Detection, pp. 17–21. https://api.semanticscholar.org/CorpusID:59652065.

Bezdek, J.C., Ehrlich, R., Full, W., 1984. FCM: The fuzzy c-means clustering algorithm. Comput. Geosci. 10 (2), 191–203. https://doi.org/10.1016/0098-3004(84)90020-7.

Boaretto, N., Centeno, T.M., 2017. Automated detection of welding defects in pipelines from radiographic images DWDI. NDT E Int. (86), 7–13. https://doi.org/10.1016/j.ndteint.2016.11.003.

Boudani, F.Z., Nacereddine, N., 2019. Diffusion in the wavelet domain for denoising radiographic images of welding defects. In: 2019 International Conference on Advanced Electrical Engineering (ICAEE), pp. 1–5. https://doi.org/10.1109/ICAEE47123.2019.9015093.

Buades, A., Coll, B., Morel, J.-M., 2005. A non-local algorithm for image denoising. In: 2005 IEEE Computer Society Conference on Computer Vision and Pattern Recognition (CVPR'05), pp. 60–65. https://doi.org/10.1109/CVPR.2005.38.

Cai, W., Shu, L.S., Geng, S.N., et al., 2024. Weld beads and defects automatic identification, localization, and size calculation based on a lightweight fully convolutional neural network. Opt Laser. Technol. 170, 110266. https://doi.org/10.1016/j.optlastec.2023.110266.

Cai, Z.W., Vasconcelos, N., 2021. Cascade R-CNN: High quality object detection and instance segmentation. IEEE Trans. Pattern Anal. Mach. Intell. 43 (5), 1483–1498. https://doi.org/10.1109/TPAMI.2019.2956516.

Cha, B.K., Lee, K.H., Lee, Y.J., Kim, K., 2023. Optimization method to predict optimal noise reduction parameters for the non-local means algorithm based on the scintillator thickness in radiography. Sensors 23 (24), 9803. https://doi.org/10.3390/s23249803.

Chady, T., Sikora, R., Misztal, L., et al., 2017. The application of rough sets theory to design of weld defect classifiers. J. Nondestruct. Eval. 36 (2), 40. https://doi.org/10.1007/s10921-017-0420-x.

Chandra, B., Thakkallapally, 2021. Defect classification from weld radiography images using VGG-19 based convolutional neural network. NDE 18 (1), 1–6. https://api.semanticscholar.org/CorpusID:236209298.

Chandrasekharan, R., Balasubramaniam, V., Jayakumar, T., et al., 2004. A novel tool for automated evaluation of radiographic weld images. In: 16th World Conference on NDT. https://api.semanticscholar.org/CorpusID:8443376.

Chang, Y.S., Gao, J.M., Jiang, H.Q., Wang, Z., 2019. A novel method of radiographic image enhancement based on phase symmetry. Insight - Non-Destr. Test. Cond. Monit. 61 (10), 577–583. https://doi.org/10.1784/insi.2019.61.10.577.

Chang, Y.S., Wang, W.K., 2021. A deep learning-based weld defect classification method using radiographic images with a cylindrical projection. IEEE Trans. Instrum. Meas. 70, 1–11. https://doi.org/10.1109/TIM.2021.3124053.

Chen, L., 2022. Intelligent recognition of small diameter pipe girth weld DR image defects based on deep learning. Chem. Equip. Technol. 43 (4), 30–35. https://doi.org/10.16759/j.cnki.issn.1007-7251.2022.08.008 (in Chinese).

Chen, L.C., Xie, D., Zhang, R., et al., 2020. Weld defects identification based on progressive convolution neural network. Comput. Eng. Design 41 (9), 2611–2615. https://doi.org/10.16208/j.issn1000-7024.2020.09.031 (in Chinese).

Chen, L.C., Zhu, Y.K., Papandreou, G., et al., 2018. Encoder-decoder with atrous separable convolution for semantic image segmentation. In: Computer Vision – ECCV 2018. Springer International Publishing, pp. 833–851. https://doi.org/10.1007/978-3-030-01234-2_49.

Chen, Y., 2016. Study on Algorithms for Industrial X-Ray Image Enhancing.. Doctor thesis (in Chinese), North University of China.

Chen, Y.F., Peng, H.S., Wang, J.T., Wang, H.W., 2022. Detection and recognition of weld defects based on lightweight convolutional neural network. Autom; Instrum. 37 (1), 49–54. https://doi.org/10.19557/j.cnki.1001-9944.2022.01.011 (in Chinese).

Cheng, H.Y., Jiang, H.Q., Yan, H.B., Zhang, W.J., 2024. Contrastive learning of defect prototypes under natural language supervision. Adv. Eng. Inform. 62, 102749. https://doi.org/10.1016/j.aei.2024.102749.

Cheng, S., Yang, H.G., Xu, X.Q., et al., 2022. Improved lightweight X-Ray aluminum alloy weld defects detection algorithm based on YOLOv5. Chin. J. Lasers 49 (21), 136–144. https://doi.org/10.3788/CJL202249.2104005 (in Chinese).

Cheng, Y.Y., Wang, Y., Hu, Y., 2009. Image enhancement algorithm based on Retinex for small-bore steel tube butt weld's X-ray imaging. WSEAS Trans. Math. arch. 8 (7), 279–288. https://dl.acm.org/doi/10.5555/1639385.1639387.

Chi, D.Z., Ma, Z.Q., Cheng, Y., et al., 2019. Defect detection method for a single lap joint based on X-ray image processing. Welding & Joining (08) 1–4+65. https://doi.org/10.12073/j.hi.20190514002 (in Chinese).
Cho, H.M., Lee, Y.J., 2018. Preliminary study of total variation noise reduction algorithm with high-energy industrial X-ray imaging system in nondestructive testing field. Results Phys. 2018 (10), 348–352. https://doi.org/10.1016/j.rinp.2018.06.036.
Civera, M., Ferraris, M., Ceravolo, R., et al., 2019. The Teager-Kaiser energy cepstral coefficients as an effective structural health monitoring tool. Appl. Sci. 9 (23), 5064. https://doi.org/10.3390/app9235064.
Cui, W.Q., Song, K.C., Zhang, Y., et al., 2025. Fine-grained tiny defect detection in spiral welds: A joint framework combining semantic discrimination and contrast transformation. IEEE Trans. Instrum. Meas. 74, 1–15. https://doi.org/10.1109/TIM.2025.3551901.
Dai, Z., Liu, X.J., Pan, Q., 2025. Defect recognition algorithm based on CCBFE-RCNN model for weld X-ray images. Trans. China Weld. Inst. 46 (1), 1–10. https://doi.org/10.12073/j.hjxb.20231104001 (in Chinese).
Dang, C.Y., Gao, J.M., Wang, Z., et al., 2015. Multi-step radiographic image enhancement conforming to weld defect segmentation. IET Image Process. 9 (11), 943–950. https://doi.org/10.1049/iet-ipr.2014.0716.
Deng, J., Dong, W., Socher, R., et al., 2009. ImageNet: a large-scale hierarchical image database. In: 2009 IEEE Conference on Computer Vision and Pattern Recognition, pp. 248–255. https://doi.org/10.1109/CVPR.2009.5206848.
Dong, S.H., Sun, X., Xie, S.Y., Wang, M.F., 2019. Automatic defect identification technology of digital image of pipeline weld. Nat. Gas. Ind. 39 (1), 113–117. https://doi.org/10.3787/j.issn.1000-0976.2019.01.013 (in Chinese).
Du, W.D., Wang, P., Wang, L.X., et al., 2011. Film weld defect recognition technology in pressure vessel based on expert system. Electro. Design Eng. 19 (21), 27–30. https://doi.org/10.14022/j.cnki.dzsjgc.2011.21.055 (in Chinese).
Duan, F., Yin, S.F., Song, P.P., et al., 2019. Automatic welding defect detection of X-Ray images by using Cascade AdaBoost with penalty term. IEEE Access 7, 125929–125938. https://doi.org/10.1109/ACCESS.2019.2927258.
El-Tokhy, M.S., Mahmoud, I.I., 2015. Classification of welding flaws in gamma radiography images based on multi-scale wavelet packet feature extraction using support vector machine. J. Nondestruct. Eval. 2015 (34), 34. https://doi.org/10.1007/s10921-015-0305-9.
Fan, D., Hu, A.D., Huang, J.K., et al., 2020. X-ray image defect recognition method for pipe weld based on improved convolutional neural network. Trans. China Weld. Inst. 41 (1), 7–11+97. https://doi.org/10.12073/j.hjxb.20190703002 (in Chinese).
Fan, L., 2014. Welding defect recognition technology based on image processing and machine learning. Ship Sci. Technol. 36 (12), 99–102. https://doi.org/10.3404/j.issn.1672-7649.2014.12.022 (in Chinese).
Faramarzi, F., Motamedi, W.M., 2011. Image processing for radiographic films of weld inspection. In: Proceedings of the International Conference on Image Processing, Computer Vision, and Pattern Recognition (IPCV). https://api.semanticscholar.org/CorpusID:4829669.
Faridafshin, J., Movafeghi, A., Faghihi, R., 2018. Multiclass detection of radiographic defects in welded joints using two-stage image enhancement and support vector machine. In: 12th European Conference on Non-destructive Testing (ECNDT 2018). https://www.ndt.net/?id=22720.
Faridafshin, M., Mirzaei, F., Movafeghi, A., Faghihi, R., 2021. Comparing non-linear diffusion and total variation noise reduction in radiography images of welds. In: 6th Iranian International NDT Conference. https://www.ndt.net/?id=26018.
Farooq, Y., Savaş, S., 2024. Noise removal from the image using convolutional neural networks-based denoising auto encoder. J. Emerg. Comput. Technol. 3 (1), 21–28. https://doi.org/10.57020/ject.1390428.
Fioravanti, C.C.B., Centeno, T.M., Delgado, M.R.D.B.D.S., 2019. A deep artificial immune system to detect weld Defects in DWDI radiographic images of petroleum pipes. IEEE Access 7, 180947–180964. https://doi.org/10.1109/ACCESS.2019.2959810.
Freeman, H., 1990. Machine Vision for Three-Dimensional Scenes. Academic Press, Inc.
Gangadhara, B., 2021. Defect detection using DeepLab V3+ on industrial radiography of machines. Int J Multidisciplinary Eng Curr Res 6 (6), 29–46.
Gao, D., Zhang, C.M., Li, G.Q., Zhang, X.G., 2006. Defect recognition of welding image based on rough-fuzzy network. J. East China Univ. Sci. Technol. 32 (9), 1126–1129. https://doi.org/10.14135/j.cnki.1006-3080.2006.09.023 (in Chinese).
Gao, F.C., Cheng, H.Y., Tian, Y., et al., 2024. A method for identifying girth weld defect based on fusion of domain features in transformer model. China Pet. Mach. 52 (8), 7–14. https://doi.org/10.16082/j.cnki.issn.1001-4578.2024.08.002 (in Chinese).
García-Allende, P.B., Mirapeix, J., Conde, O.M., et al., 2009. Spectral processing technique based on feature selection and artificial neural networks for arc-welding quality monitoring. NDT E Int. 42 (1), 56–63. https://doi.org/10.1016/j.ndteint.2008.07.004.
Ge, L.L., Zhang, Y.J., 2009. Hierarchical segmentation approach to detection of defects on welding radiographic images. In: 2009 4th IEEE Conference on Industrial Electronics and Applications, pp. 2089–2094. https://doi.org/10.1109/ICIEA.2009.5138570.
Goumeidane, A.B., Bouzaieni, A., Nacereddine, N., Tabbone, S., 2015. Bayesian networks-based defects classes discrimination in weld radiographic images. In: Computer Analysis of Images and Patterns. Springer International Publishing, pp. 554–565. https://doi.org/10.1007/978-3-319-23117-4_48.
Gu, J., Wang, Q.W., Zhang, M., Wang, J.J., 2020. Weld defect detection and recognition based on DenseNet network. Transducer Microsys. Technol. 39 (9), 129–131. https://doi.org/10.13873/j.1000-9787(2020)09-0129-03 (in Chinese).
Guan, B., Li, J.J., 2024. Lightweight detection network for bridge defects based on model pruning and knowledge distillation. Structures 62, 106276. https://doi.org/10.1016/j.istruc.2024.106276.
Guo, N., Gui, Z.G., Liu, Y., Kang, J.Q., 2023. Local contrast stretch enhancement Algorithm for X-Ray images based on fuzzy entropy. J. Test Meas. Technol. 37 (1), 29–36. https://doi.org/10.3969/j.issn.1671-7449.2023.01.006 (in Chinese).
Guo, R.Y., Liu, H., Xie, G., Zhang, Y.M., 2021. Weld defect detection from imbalanced radiographic images based on contrast enhancement conditional generative adversarial network and transfer learning. IEEE Sens. J. 21 (9), 10844–10853. https://doi.org/10.1109/JSEN.2021.3059860.
Guo, W.M., Liu, K., Qu, H.F., 2019. Welding defect detection of X-Ray images based on faster R-CNN model. J. Beijing Univ. Posts Telecommun. 42 (6), 20–28. https://doi.org/10.13190/j.jbupt.2019-097 (in Chinese).
Gupta, R., Anand, V., Gupta, S., Koundal, D., 2023. Deep learning model for defect analysis in industry using casting images. Expert Syst. Appl. 232, 120758. https://doi.org/10.1016/j.eswa.2023.120758.
Halim, S.A., Ibrahim, A., Manurung, Y.H., 2013. PDE-based model for weld defect detection on digital radiographic image. In: IEEE Workshop on Signal Processing Systems, pp. 146–151. https://doi.org/10.12720/IJSPS.1.2.146-151.
Han, M.R., Chen, P., Pan, J.X., 2023. X-ray image enhancement for complex workpieces based on gradient field and local deviation. J. Comput. Appl. 43 (S2), 182–185. https://doi.org/10.11772/j.issn.1001-9081.2023040492 (in Chinese).
Hashim, S.A.B.M., 2017. Segmenting weld bead digital image for weld defect detection using Otsu's method. In: 4th National Conference on Research and Education.
Hassan, J., Awan, A.M., Jalil, A., 2012. Welding defect detection and classification using geometric features. In: 2012 10th International Conference on Frontiers of Information Technology, pp. 139–144. https://doi.org/10.1109/FIT.2012.33.
Hou, W.H., Wei, Y., Guo, J., et al., 2017. Automatic detection of welding defects using deep neural network. J. Phys. Conf. 933 (1), 012006. https://doi.org/10.1088/1742-6596/933/1/012006.
Hou, W.H., Wei, Y., Jin, Y., Zhu, C.A., 2019. Deep features based on a DCNN model for classifying imbalanced weld flaw types. Measurement 131, 482–489. https://doi.org/10.1016/j.measurement.2018.09.011.
Hou, W.H., Zhang, D.S., Wei, Y., et al., 2020. Review on computer aided weld defect detection from radiography images. Appl. Sci. 10 (5), 1878. https://doi.org/10.3390/app10051878.
Hu, A.D., 2020. Research on Weld X-ray Image Defects Recognition Based on Deep Learning.. Master thesis, Lanzhou University of Technology. https://doi.org/10.27206/d.cnki.ggsgu.2020.000304 (in Chinese).
Huang, L., 2020. Design and implementation of weld defect detection system based on convolutional neural network. Master thesis, Beijing University of Posts and Telecommunications. https://doiorg/10.26969/d.cnki.gbydu.2020.000796 (in Chinese).
Huang, W.H., Zheng, H.L., Li, M.F., 2019. Development history and prospect of oil & gas storage and transportation industry in China. Oil Gas Storage Transp. 38 (1), 1–11. https://doi.org/10.6047/j.issn.1000-8241.2019.01.001 (in Chinese).
Hwang, H., Haddad, R.A., 1995. Adaptive median filters: New algorithms and results. IEEE Trans. Image Process. 4 (4), 499–502. https://doi.org/10.1109/83.370679.
Institute, C.S.E.I.R., 2015. Nondestructive Testing of Pressure equipments-part 2: Radiographic Testing. Xinhua Publishing House, Beijing (in Chinese).
Ji, C., Wang, H.B., Li, H.H., 2023. Defects detection in weld joints based on visual attention and deep learning. NDT E Int. 133, 102764. https://doi.org/10.1016/j.ndteint.2022.102764.
Jia, S.H., Li, Y.P., Gao, W.X., et al., 2024. Research on automatic identification method for pipeline girth weld defects based on X-ray images and sparse representation. Oil Gas Storage Transp. 43 (9), 1048–1055+1079. https://doi.org/10.6047/j.issn.1000-8241.2024.09.010 (in Chinese).
Jiang, H.Q., He, S., Gao, J.M., et al., 2020. An improved convolutional neural network for Weld defect recognition. J. Mech. Eng. 56 (8), 235–242. https://doi.org/10.3901/jme.2020.08.235 (in Chinese).
Jiang, H.Q., Zhang, M.J., Cheng, H.Y., et al., 2025. Fusion of dynamic film evaluation knowledge AI model for weld Defect detection. J. Mech. Eng. 61 (6), 24–32. https://doi.org/10.3901/JME.2025.06.024 (in Chinese).
Jiang, H.Q., Zhao, Y.L., Gao, J.M., Gao, Z.Y., 2017. Adaptive pseudo-color enhancement method of weld radiographic images based on HSI color space and self-transformation of pixels. Rev. Sci. Instrum. 88 (6), 065106. https://doi.org/10.1063/1.4985007.
Kasban, H., Zahran, O., Arafa, H., et al., 2011. Welding defect detection from radiography images with a cepstral approach. NDT E Int. 44 (2), 226–231. https://doi.org/10.1016/j.ndteint.2010.10.005.
Kim, K.S., Kang, S.Y., Kim, W.S., et al., 2018. Improvement of radiographic visibility using an image restoration method based on a simple radiographic scattering model for x-ray nondestructive testing. NDT E Int. (98), 117–122. https://doi.org/10.1016/j.ndteint.2018.05.008, 2018.
Kim, K.S., Kim, W.S., Kang, S.Y., et al., 2019. Model-based noise reduction in scatter correction using a deep convolutional neural network for radiography. J. Kor. Phys. Soc. 75 (2), 160–166. https://doi.org/10.3938/jkps.75.160.

Kiyingi, W., Guo, J.X., Xiong, R.Y., et al., 2022. Crude oil wax: A review on formation, experimentation, prediction, and remediation techniques. Pet. Sci. 19 (5), 2343–2357. https://doi.org/10.1016/j.petsci.2022.08.008.
Krichen, M., 2023. Generative adversarial networks. In: 2023 14th International Conference on Computing Communication and Networking Technologies (ICCCNT), pp. 1–7. https://doi.org/10.1109/ICCCNT56998.2023.10306417.
Kumar, D.D., Fang, C., Zheng, Y., Gao, Y.Q., 2023. Semi-supervised transfer learning-based automatic weld defect detection and visual inspection. Eng. Struct. 2023 (292), 116580. https://doi.org/10.1016/j.engstruct.2023.116580.
Kumar, J., Anand, R.S., Srivastava, S.P., 2014a. Flaws classification using ANN for radiographic weld images. In: 2014 International Conference on Signal Processing and Integrated Networks (SPIN), pp. 145–150. https://doi.org/10.1109/SPIN.2014.6776938.
Kumar, J., Anand, R.S., Srivastava, S.P., 2014b. Multi - class welding flaws classification using texture feature for radiographic images. In: 2014 International Conference on Advances in Electrical Engineering (ICAEE), pp. 1–4. https://doi.org/10.1109/ICAEE.2014.6838443.
Kumar, J., Srivastava, S.P., Anand, R.S., et al., 2018. GLCM and ANN based approach for classification of radiographics weld images. In: 2018 IEEE 13th International Conference on Industrial and Information Systems (ICIIS), pp. 168–172. https://doi.org/10.1109/ICIINFS.2018.8721421.
Kumaresan, S., Aultrin, K.S.J., Kumar, S.S., Anand, M.D., 2021. Transfer learning with CNN for classification of weld defect. IEEE Access 9, 95097–95108. https://doi.org/10.1109/ACCESS.2021.3093487.
Kumaresan, S., Aultrin, K.S.J., Kumar, S.S., Anand, M.D., 2023. Deep learning-based weld defect classification using VGG16 transfer learning adaptive fine-tuning. Int. J. Interact. Des. Manuf. 17 (6), 2999–3010. https://doi.org/10.1007/s12008-023-01327-3.
Kupyn, O., Budzan, V., Mykhailych, M., et al., 2018. DeblurGAN: blind motion deblurring using conditional adversarial networks. In: 2018 IEEE/CVF Conference on Computer Vision and Pattern Recognition, pp. 8183–8192. https://doi.org/10.1109/cvpr.2018.00854.
Kwon, J.E., Park, J.H., Kim, J.H., et al., 2023. Context and scale-aware YOLO for welding defect detection. NDT E Int. 139, 102919. https://doi.org/10.1016/j.ndteint.2023.102919.
Land, E.H., 1978. The retinex theory of color vision. Sci. Am. 237 (6), 108–128. https://doi.org/10.1038/scientificamerican1277-108.
Lashkia, V., 2001. Defect detection in X-ray images using fuzzy reasoning. Image Vis Comput. 19 (5), 261–269. https://doi.org/10.1016/S0262-8856(00)00075-5.
LeCun, Y., Boser, B., Denker, J.S., et al., 1989. Backpropagation applied to handwritten zip code recognition. Neural Comput. 1 (4), 541–551. https://doi.org/10.1162/neco.1989.1.4.541.
Lee, S.W., Cho, H.M., Lee, Y.J., 2019. High-energy industrial 2D X-ray imaging system with effective nonlocal means denoising for nondestructive testing. Nucl. Instrum. Methods Phys. Res. Sect. A Accel. Spectrom. Detect. Assoc. Equip. 925, 212–216. https://doi.org/10.1016/j.nima.2019.01.060.
Lee, Y., 2019. Feasibility study for application of total-variation-based noise-removal algorithm with 450-kVp high-energy industrial computed-tomography imaging system for non-destructive testing. Exp. Tech. 43 (2), 117–123. https://doi.org/10.1007/s40799-018-0276-8.
Lei, Z.Q., Zhang, F., Lin, S., Wang, F.X., 2022. Research on intelligent image recognition technology of pipeline girth weld inspection. Pipeline Techni. Equip. 2022 (3), 36–40. https://doi.org/10.3969/j.issn.1004-9614.2022.03.009 (in Chinese).
Li, B., Fan, L., Gao, Z.H., et al., 2020. Research on X-ray weld image defect recognition method based on wavelet transform. Autom; Instrum. 2020 (3), 63–67. https://doi.org/10.14016/j.cnki.1001-9227.2020.03.063 (in Chinese).
Li, C.H., Xu, Z.S., 2024. Study on defect identification method of pipeline weld based on integrated machine learning. Autom. Petro-Chem. Ind. 60 (1), 72–76. https://doi.org/10.3969/j.issn.1007-7324.2024.01.016 (in Chinese).
Li, L.L., Ren, J., Wang, P., et al., 2023a. Defect detection method for high-resolution weld based on wandering Gaussian and multi-feature enhancement fusion. Mech. Syst. Signal Process. 199, 110484. https://doi.org/10.1016/j.ymssp.2023.110484.
Li, L.L., Wang, P., Li, Y., et al., 2025a. High-resolution weld defect detection with RSU-MLP and dynamic kernel supervision. Measurement 242, 116208. https://doi.org/10.1016/j.measurement.2024.116208.
Li, L.L., Wang, P., Ren, J., et al., 2024a. Synthetic data augmentation for high-resolution X-ray welding defect detection and classification based on a small number of real samples. Eng. Appl. Artif. Intell. 133, 108379. https://doi.org/10.1016/j.engappai.2024.108379.
Li, M.Y., Chen, N., Suo, X.Y., et al., 2023b. An efficient defect detection method for nuclear-fuel rod grooves through weakly supervised learning. Measurement 222, 113708. https://doi.org/10.1016/j.measurement.2023.113708.
Li, N., Song, Y.R., Wang, Y., Ge, C.B., 2024b. Evolution, resilience and causes of global petroleum gas trade networks: 1995–2020. Pet. Sci. 21 (5), 3656–3674. https://doi.org/10.1016/j.petsci.2024.05.021.
Li, Q.G., Gao, W.X., 2019. Recognition of X-ray weld defects based on deep learning. J. Xi'an Shiyou University(Nat. Sci. Ed.) 34 (4), 74–81. https://doi.org/10.3969/j.issn.1002-025X.2013.02.015 (in Chinese).
Li, S., 2016. Research of industrial X-Ray image enhancement algorithm based on retinex. Inform. Technol. Inform. 2016 (3), 82–84. https://doi.org/10.3969/j.issn.1672-9528.2016.03.020 (in Chinese).
Li, S.L., Wang, M.Q., Li, G.Y., et al., 2011. Application of locally adaptive wavelet DomainDenosing to X-Ray image processing. Nucl. Electron. Detect. Technol. 31 (4), 455–458. https://doi.org/10.3969/j.issn.0258-0934.2011.04.021 (in Chinese).
Li, X.Y., Li, L.L., Wang, P., et al., 2024c. You only train twice: A lighter and faster method for industrial weld defect detection based on dynamic kernel network. Measurement 231, 114642. https://doi.org/10.1016/j.measurement.2024.114642.
Li, Y., Gao, W.X., Tang, N., Cui, Y.N., 2013. Detection for weld defects in spiral welded pipe by X-ray based on compressed sensing. Welding Technol. 42 (2), 51–55+76. https://doi.org/10.13846/j.cnki.cn12-1070/tg.2013.02.003 (in Chinese).
Li, Y.H., Han, M.R., Li, K., et al., 2024d. X-Ray image enhancement framework based on improved local adaptive contrast field for complex workpieces. IEEE Trans. Nucl. Sci. 71 (5), 1225–1232. https://doi.org/10.1109/TNS.2024.3389106.
Li, Y.P., Gao, W.X., 2019b. Research on X-ray welding image defect detection based on convolution neural network. J. Phys. Conf. 1237 (3), 032005. https://doi.org/10.1088/1742-6596/1237/3/032005.
Li, Y.Q., Lu, J.M., Wang, L., et al., 2005. Removing noise from radiological image using multineural network filter. In: 2005 IEEE International Conference on Industrial Technology, pp. 1365–1370. https://doi.org/10.1109/ICIT.2005.1600848.
Li, Y.T., He, X.N., Shuai, J., 2022. Risk analysis and maintenance decision making of natural gas pipelines with external corrosion based on Bayesian network. Pet. Sci. 19 (3), 1250–1261. https://doi.org/10.1016/j.petsci.2021.09.016.
Li, Y.Z., Wang, H.L., Yuan, S.H., et al., 2023c. Myriad: Large multimodal model by applying vision experts for industrial anomaly detection. arXiv. https://doi.org/10.48550/arXiv.2310.19070.
Li, Z., 2019. Research on X-ray weld defect detection and recognition algorithm based on independent analysis. Xi'an Shiyou University. Master thesis (in Chinese).
Li, Z., Mu, X.Y., 2019. X-Ray weld defect recognition based on ICA. Modern Comput. (13), 59–61+66. https://doi.org/10.3969/j.issn.1007-1423.2019.13.012 (in Chinese).
Li, Z.F., Song, S.H., Liu, X.J., et al., 2025b. A zero-shot quantitative evaluation model for subsurface defects size based on ultrasonic nondestructive testing. Measurement 241, 115738. https://doi.org/10.1016/j.measurement.2024.115738.
Liao, T.W., 2009. Improving the accuracy of computer-aided radiographic weld inspection by feature selection. NDT E Int. 42 (4), 229–239. https://doi.org/10.1016/j.ndteint.2008.11.002.
Liao, T.W., 2004. Fuzzy reasoning based automatic inspection of radiographic welds: weld recognition. J. Intell. Manuf. 15 (1), 69–85. http://dpi.org/10.1023/B:JIMS.0000010076.56537.07.
Liao, T.W., Li, D.M., Li, Y.M., 1999. Detection of welding flaws from radiographic images with fuzzy clustering methods. Fuzzy Set Syst. 108 (2), 145–158. https://doi.org/10.1016/S0165-0114(97)00307-2.
Liao, T.W., Li, D.M., Li, Y.M., 2000. Extraction of welds from radiographic images using fuzzy classifiers. Inf. Sci. 126 (1), 21–40. https://doi.org/10.1016/S0020-0255(00)00016-5.
Lin, T.Y., Dollár, P., Girshick, R., et al., 2017a. Feature pyramid networks for object detection. In: 2017 IEEE Conference on Computer Vision and Pattern Recognition (CVPR), pp. 936–944. https://doi.org/10.1109/CVPR.2017.106.
Lin, T.Y., Goyal, P., Girshick, R., et al., 2017b. Focal loss for dense object detection. In: 2017 IEEE International Conference on Computer Vision (ICCV), pp. 2999–3007. https://doi.org/10.1109/ICCV.2017.324.
Liu, H., Guo, R.Y., 2018. Detection and identification of SAWH pipe weld defects based on X-ray image and CNN. Chin. J. Sci. Instrum. 39 (4), 247–256. https://doi.org/10.19650/j.cnki.cjsi.J1702865 (in Chinese).
Liu, H.L., 2016. Adaptive local contrast enhancement based tone mapping for high dynamic range images. Master thesis (in Chinese), Southwestern University of Finance and Economics.
Liu, J.H., Liu, X.Y., Qu, F.M., et al., 2022a. A defect recognition method for low-quality weld image based on consistent multiscale feature mapping. IEEE Trans. Instrum. Meas. 71, 1–11. https://doi.org/10.1109/TIM.2022.3171609.
Liu, J.H., Zhao, Z., Fu, M.R., et al., 2022b. Active small sample learning based the pipe weld defect detection method. Chin. J. Sci. Instrum. 43 (11), 252–261. https://doi.org/10.19650/j.cnki.cjsi.J2209872 (in Chinese).
Liu, M.Y., 2021. Research on defect recognition and localization for X-ray welding images based on convolutional neural network. Master thesis. Huazhong University of Science & Technology. https://doi.org/10.27157/d.cnki.ghzku.2021.000501 (in Chinese.
Liu, P., 2007. An enhancement technology for X-Ray images based on wavelet transform. J. North Univ. China (Natural Sci. Ed.) (6), 552–555. https://doi.org/10.3969/j.issn.1673-3193.2007.06.017 (in Chinese).
Liu, Q., Xiao, R.Q., Xu, Y.Q., et al., 2024a. A defect classification algorithm for gas tungsten arc welding process based on unsupervised learning and few-shot learning strategy. J. Manuf. Process. 131, 1219–1229. https://doi.org/10.1016/j.jmapro.2024.09.084.
Liu, T.Y., Zheng, H.B., Zheng, P., et al., 2023a. An expert knowledge-empowered CNN approach for welding radiographic image recognition. Adv. Eng. Inform. 56, 101963. https://doi.org/10.1016/j.aei.2023.101963.
Liu, X.J., Cao, L.J., Liu, H., et al., 2024b. Research on weld defect recognition technology based on improved VGG-16 network structure. Aero. Manuf. Technol. 02, 55–59. https://doi.org/10.20177/j.cnki.htzzjs.2024.02.022 (in Chinese).
Liu, X.Y., Liu, J.H., Wang, Z., et al., 2023b. Basic-class and cross-class hybrid feature learning for class-imbalanced weld defect recognition. IEEE Trans. Ind. Inf. 19 (9), 9436–9446. https://doi.org/10.1109/TII.2022.3228702.

Liu, X.Y., Liu, J.H., Zhang, H.Q., et al., 2024c. DGICR-Net: Dual-Graph interactive consistency reasoning network for Weld defect recognition with limited labeled samples. IEEE Trans. Instrum. Meas. 73, 1–12. https://doi.org/10.1109/TIM.2024.3372220.
Liu, Y., Zhang, P.C., Gui, Z.G., 2021. An enhancement framework based on gradient domain tone mapping and fuzzy logical for X-ray image of complex workpiece. NDT E Int. 121, 102455. https://doi.org/10.1016/j.ndteint.2021.102455.
Lu, P., Huang, Q.J., 2022. Robotic weld image enhancement based on improved bilateral filtering and CLAHE algorithm. Electronics 11 (21), 3629. https://doi.org/10.3390/electronics11213629.
Lu, X.A., Jiang, L.L., Zhang, J.S., Wang, M.G., 2024. Securing offshore resources development: A mathematical investigation into gas leakage in long-distance flexible pipes. Pet. Sci. 21 (4), 2734–2744. https://doi.org/10.1016/j.petsci.2024.01.020.
Luo, A.M., Shen, C.H., Yi, B., Li, K., 2010. Method of multi-classification by improved binary based on SVM for welding defects recongnition. Trans. China Weld. Inst. 31 (7), 51–54+115. https://hjxb.hwi.com.cn/hjxb/en/article/id/20100713 (in Chinese).
Luo, G., Xiao, L.Z., Luo, S.H., et al., 2023. A study on multi-exponential inversion of nuclear magnetic resonance relaxation data using deep learning. J. Magn. Reson. 346, 107358. https://doi.org/10.1016/j.jmr.2022.107358.
Luo, Y., Zhang, Y.F., Jiang, J.S., 2024. Image preprocessing technology for defects on radiographic testing flim. Nondestruct. Test. 46 (2), 22–28. https://doi.org/10.11973/wsjc202402005 (in Chinese).
Lv, H.Y., 2022. Research on quality improvement method based on X-ray pipe weld images. Master thesis (in Chinese). Northeastern University. https://doi.org/10.27007/d.cnki.gdbeu.2022.001299.
Mahmoudi, A., Regragui, F., 2009a. Fast segmentation method for defects detection in radiographic images of welds. In: 2009 IEEE/ACS International Conference on Computer Systems and Applications, pp. 857–860. https://doi.org/10.1109/AICCSA.2009.5069430.
Mahmoudi, A., Regragui, F., 2009b. Welding defect detection by segmentation of radiographic images. In: 2009 WRI World Congress on Computer Science and Information Engineering, pp. 111–115. https://doi.org/10.1109/CSIE.2009.501.
Malarvel, M., Sethumadhavan, G., Bhagi, P.C.R., et al., 2017. Anisotropic diffusion based denoising on X-radiography images to detect weld defects. Digit. Signal Process. 68, 112–126. https://doi.org/10.1016/j.dsp.2017.05.014.
Mei, J.Q., Chen, W.Y., Jia, F., 2023. Quality improvement algorithm for X-ray non-destructive testing image. JTianjin Univer Technol. Edu. 33 (1), 44–49. https://doi.org/10.19573/j.issn2095-0926.202301008 (in Chinese).
Mekhalia, F., Nacereddine, N., 2014. Multiclass classification of weld defects in radiographic images based on support vector machines. In: 2014 Tenth International Conference on Signal-Image Technology and Internet-based Systems, pp. 1–6. https://doi.org/10.1109/SITIS.2014.72.
Mekhalia, F., Nacereddine, N., 2017. Gentle adaboost algorithm for weld defect classification. In: 2017 Signal Processing: Algorithms, Architectures, Arrangements, and Applications, pp. 301–306. https://doi.org/10.23919/SPA.2017.8166883.
Mery, D., Berti, M.A., 2003. Automatic detection of welding defects using texture features. Insight-Non-Destructive Test. Cond. Monit. 45 (10), 676–681. https://doi.org/10.1784/insi.45.10.676.52952.
Mery, D., Riffo, V., Zscherpel, U., et al., 2015. GDXray: The database of X-ray images for nondestructive testing. J. Nondestruct. Eval. 34 (4), 42. https://doi.org/10.1007/s10921-015-0315-7.
Miao, X.Y., Zhao, H., 2024. Dynamic plugging regulating strategy of pipeline robot based on reinforcement learning. Pet. Sci. 21 (1), 597–608. https://doi.org/10.1016/j.petsci.2023.08.016.
Michel-González, E., Cho, M.H., Lee, S.Y., 2011. Geometric nonlinear diffusion filter and its application to X-ray imaging. Biomed. Eng. Online 10 (1), 47. https://doi.org/10.1186/1475-925X-10-47.
Movafeghi, A., Kargarnovin, M.H., Soltanian-Zadeh, H., et al., 2005. Flaw detection improvement of digitised radiographs by morphological transformations. Insight-Non-Destructive Test. Cond. Monit. 47 (10), 625–630. https://doi.org/10.1784/insi.2005.47.10.625.
Movafeghi, A., Yahaghi, E., Mohammadzadeh, N., 2015. Defect detection improvement of digitised radiographs by principal component analysis with local pixel grouping. J. Nondestruct. Eval. 34 (2), 17. https://doi.org/10.1007/s10921-015-0290-z.
Movafeghi, A., Yahaghi, E., Yar Mohammadi, A., Ghafele-Bashi, S.M.H., 2023. Fourier transforms for recognition of weld defects in industrial radiography. J. Nondestructive Test. Technol. 3 (11), 13–22. https://doi.org/10.30494/JNDT.2022.367717.1105.
Mu, W.L., Gao, J.M., Jiang, H.Q., et al., 2013. A method of radiographic image quality enhancement. In: 2013 Fifth International Conference on Measuring Technology and Mechatronics Automation, pp. 29–32. https://doi.org/10.1109/ICMTMA.2013.19.
Mustafa, W.A., Yazid, H., Alkhayyat, A., et al., 2022. Contrast correction using hybrid statistical enhancement on weld defect images. Comput. Mater. Continua (CMC) 71 (3), 5327–5342. https://doi.org/10.32604/cmc.2022.023492.
Nacereddine, N., Drai, R., Benchaala, A., 2000. Weld defect extraction and classification in radiographic testing based artificial neural networks. In: Proceedings of 15th World Conference on Non Destructive Testing, pp. 15–21.
Nacereddine, N., Tridi, M., 2005. Computer-aided shape analysis and classification of weld defects in industrial radiography based invariant attributes and neural networks. In: ISPA 2005 Proceedings of the 4th International Symposium on Image and Signal Processing and Analysis, pp. 88–93. https://doi.org/10.1109/ISPA.2005.195389, 2005.
Nacereddine, N., Ziou, D., Hamami, L., 2013. Fusion-based shape descriptor for weld defect radiographic image retrieval. Int. J. Adv. Manuf. Technol. 68 (9), 2815–2832. https://doi.org/10.1007/s00170-013-4857-5.
Naddaf, M., Naddaf-Sh, S., Zargarzadeh, H., et al., 2020. Next-Generation of weld quality assessment using deep learning and digital radiography. In: Artificial Intelligence in Manufacturing, AAAI Spring Symposium Series.
Nazarov, R.M., Gizatullin, Z.M., Konstantinov, E.S., 2021. Classification of defects in welds using a convolution neural network. In: 2021 IEEE Conference of Russian Young Researchers in Electrical and Electronic Engineering (ElConRus), pp. 1641–1644. https://doi.org/10.1109/ElConRus51938.2021.9396301.
Njogu, P.K., 2016. Enhancement of X-Ray Images for Industrial Applications. Doctor thesis, University of Nairobi.
Oh, S.J., Jung, M.J., Lim, C.O., Shin, S.C., 2020. Automatic detection of welding defects using faster R-CNN. Appl. Sci. 10 (23), 8689. https://doi.org/10.3390/app10238629.
Palma-Ramírez, D., Ross-Veitía, B.D., Font-Ariosa, P., et al., 2024. Deep convolutional neural network for weld defect classification in radiographic images. Heliyon 10 (9), e30590. https://doi.org/10.1016/j.heliyon.2024.e30590.
Pan, H.H., Li, S.T., Chen, L., et al., 2023. Weld defect recognition method based on improved DG-MobileNet Model. Automatic Manuf Technique 2023 (8), 127–130. https://doi.org/10.13462/j.cnki.mmtamt.2023.08.027 (in Chinese).
Pan, H.H., Pang, Z.J., Wang, Y.W., et al., 2020. A new image recognition and classification method combining transfer learning Algorithm and MobileNet model for welding defects. IEEE Access 8, 119951–119960. https://doi.org/10.1109/ACCESS.2020.3005450.
Perona, P., Malik, J., 1990. Scale-space and edge detection using anisotropic diffusion. IEEE Trans. Pattern Anal. Mach. Intell. 12 (7), 629–639. https://doi.org/10.1109/34.56205.
Perri, S., Spagnolo, F., Frustaci, F., Corsonello, P., 2023. Welding defects classification through a Convolutional Neural Network. Manuf. Letters 35, 29–32. https://doi.org/10.1016/j.mfglet.2022.11.006.
Pisano, E.D., Zong, S.Q., Hemminger, B.M., et al., 1998. Contrast limited adaptive histogram equalization image processing to improve the detection of simulated spiculations in dense mammograms. J. Digit. Imag. 11 (4), 193. https://doi.org/10.1007/BF03178082.
Poudel, R.P.K., Liwicki, S., Cipolla, R., 2019. Fast-SCNN: Fast semantic segmentation network. arXiv. https://doi.org/10.48550/arXiv.1902.04502.
Purnomo, T.W., Ramadhany, H.A.R., Jati, H.H.C., Handoko, D., 2024. A comparison of CNN-based image feature extractors for weld defects classification. Indonesian J. Applied Physics 14, 190. https://doi.org/10.13057/ijap.v14i1.72509.
Qian, W.C., Dong, S.H., Chen, L., Ren, Q.Y., 2024. Image enhancement method for low-light pipeline weld X-ray radiographs based on weakly supervised deep learning. NDT E Int. 143, 103049. https://doi.org/10.1016/j.ndteint.2024.103049.
Qiao, R.H., Dong, J.G., Zhang, Y.H., 2016. Research on recognition and diagnosis technology of weld Defect image based on RBF network. Hot Work. Technol. 45 (1), 217–220. https://doi.org/10.14158/j.cnki.1001-3814.2016.01.062 (in Chinese).
Qiu, R., Zhang, B., Zhao, W., et al., 2024. An integrated MINLP model for multi-party coordination in downstream oil supply chain. Pet. Sci. 21 (3), 2066–2079. https://doi.org/10.1016/j.petsci.2023.12.008.
Radi, D., Abo-Elsoud, M.E.A., Khalifa, F., 2021. Segmenting welding flaws of non-horizontal shape. Alex. Eng. J. 60 (4), 4057–4065. https://doi.org/10.1016/j.aej.2021.02.052.
Radi, D., Abo-Elsoud, M.E.A., Khalifa, F., 2022. Accurate segmentation of weld defects with horizontal shapes. NDT E Int. 126, 102599. https://doi.org/10.1016/j.ndteint.2021.102599.
Rajab, M.I., El-Benawy, T.A., Al-Hazmi, M.W., 2007. Application of frequency domain processing to X-ray radiographic images of welding defects. J. X Ray Sci. Technol. 15 (3), 147–156. https://doi.org/10.3233/XST-2007-00178.
Rale, A.P., Gharpure, D.C., Ravindran, V.R., 2009. Comparison of different ANN techniques for automatic defect detection in X-Ray images. In: 2009 International Conference on Emerging Trends in Electronic and Photonic Devices & Systems, pp. 193–197. https://doi.org/10.1109/ELECTRO.2009.5441138.
Redmon, J., Farhadi, A., 2018. YOLOv3: An incremental improvement. arXiv. https://doi.org/10.48550/arXiv.1804.02767.
Ren, P.Z., Xiao, Y., Chang, X.J., et al., 2021. A Survey of deep active learning. ACM Comput. Surv. 54 (9), 1–40. https://doi.org/10.1145/3472291.
Ronneberger, O., Fischer, P., Brox, T., 2015. U-Net: Convolutional networks for biomedical image segmentation. In: Medical Image Computing and Computer-Assisted Intervention – MICCAI 2015. Springer International Publishing, pp. 234–241. https://doi.org/10.1007/978-3-319-24574-4_28.
Rudin, L.I., Osher, S., Fatemi, E., 1992. Nonlinear total variation based noise removal algorithms. Phys. Nonlinear Phenom. 60 (1), 259–268. https://doi.org/10.1016/0167-2789(92)90242-F.
Rumelhart, D.E., Hinton, G.E., Williams, R.J., 1986. Learning representations by back-propagating errors. Nature 323 (6088), 533–536. https://doi.org/10.1038/323533a0.
Sadah, Y.A., Al-Najdawi, N.A., Tedmori, S., 2013. Exploiting hybrid methods for enhancing digital x-ray images. Int. Arab J. Inf. Technol. 10 (1), 28–35.
Saravanan, T., Bagavathiappan, S., Philip, J., et al., 2007. Segmentation of defects from radiography images by the histogram concavity threshold method.

Insight - Non-Destr. Test. Cond. Monit. 49 (10), 578–584. https://doi.org/10.1784/insi.2007.49.10.578.
Sato, M., Lakare, S., Wan, M., et al., 2000. A gradient magnitude based region growing algorithm for accurate segmentation. In: Proceedings 2000 International Conference on Image Processing (Cat No00CH37101), pp. 448–451. https://doi.org/10.1109/ICIP.2000.899432.
Say, D., Zidi, S., Qaisar, S.M., Krichen, M., 2023. Automated categorization of multiclass welding defects using the X-ray image augmentation and convolutional neural network. Sensors 23 (14), 6422. https://doi.org/10.3390/s23146422.
Schwartz, C., 2003. Automatic evaluation of welded joints using image processing on radiographs. In: AIP Conference Proceedings, pp. 689–694. https://doi.org/10.1063/1.1570203.
Shafeek, H.I., Gadelmawla, E.S., Abdel-Shafy, A.A., Elewa, I.M., 2004a. Assessment of welding defects for gas pipeline radiographs using computer vision. NDT E Int. 37 (4), 291–299. https://doi.org/10.1016/j.ndteint.2003.10.003.
Shafeek, H.I., Gadelmawla, E.S., Abdel-Shafy, A.A., Elewa, I.M., 2004b. Automatic inspection of gas pipeline welding defects using an expert vision system. NDT E Int. 37 (4), 301–307. https://doi.org/10.1016/j.ndteint.2003.10.004.
Shang, G., Chen, J., 2024. Automatic detection of subsurface defects of concrete slabs by domain adaptation algorithm. Case Stud. Constr. Mater. 21, e03987. https://doi.org/10.1016/j.cscm.2024.e03987.
Shang, J.Z., An, W.P., Liu, Y., et al., 2020. Oil pipeline weld defect identification system based on convolutional neural network. KSII Trans. Internet Inform. Syst. 14 (3), 1086–1103. https://doi.org/10.3837/tiis.2020.03.010.
Shao, J.X., Shi, H., Du, D., et al., 2011. Automatic weld defect detection in real-time X-ray images based on support vector machine. In: 2011 4th International Congress on Image and Signal Processing, pp. 1842–1846. https://doi.org/10.1109/CISP.2011.6100637.
Shen, F., 2020. X-ray Image Denoising Using Blind Source Separation in Anscombe Domain. Master thesis (in Chinese), Nanjing University of Posts and Telecommunications. https://doi.org/10.27251/d.cnki.gnjdc.2020.001111.
Shen, F., Li, H.L., Sun, B., Yu, C.Y., 2020. X-ray image denoising using blind source separation in anscombe domain. Opt Precis. Eng. 28 (1), 244–250. https://doi.org/10.3788/OPE.20202801.0244 (in Chinese).
Shen, Q.M., Wang, G.B., Zhao, J.Z., Xu, G.L., 2014. Multi-noise model-based denoising method for radiographic image. Acta Armamentarii 35 (12), 2087–2091. https://doi.org/10.3969/j.issn.1000-1093.2014.12.022 (in Chinese).
Shen, X.K., Li, L., Ma, Y.S., et al., 2025a. VLCIM: A vision-language cyclic interaction model for industrial defect detection. IEEE Trans. Instrum. Meas. 74, 1–13. https://doi.org/10.1109/TIM.2025.3583364.
Shen, X.K., Liu, J.H., Jiang, L., et al., 2024. A novel weld defect detection method for intelligent magnetic flux leakage detection system via contextual relation network. IEEE Trans. Ind. Electron. 71 (6), 6304–6314. https://doi.org/10.1109/TIE.2023.3294578.
Shen, X.K., Liu, J.H., Ren, Y.F., et al., 2025b. A task-oriented physical collaborative network for pipeline defect diagnosis in a magnetic flux leakage detection system. Comput. Ind. 169, 104290. https://doi.org/10.1016/j.compind.2025.104290.
Shen, X.K., Liu, J.H., Zhang, H.G., et al., 2025c. A novel incremental defect detection method via elastic heterogeneous distillation network. IEEE Trans. Autom. Sci. Eng. 22, 10149–10161. https://doi.org/10.1109/TASE.2024.3519164.
Shi, B., 2021. Research on weld defect detection method of small diameter pipe based on full feature fusion and multi-level detection head.. Master thesis, Hebei University of Technology. https://doi.org/10.27105/d.cnki.ghbgu.2021.000830 (in Chinese).
Shi, H., Du, D., Zou, Y.R., et al., 2013. X-ray image noise reduction in thr defect detection of straight-weld steel. China Sci. paper 8 (8), 717–720. https://doi.org/10.3969/j.issn.2095-2783.2013.08.001 (in Chinese).
Shi, H., Shao, J.X., Du, D., et al., 2011. Noise reduction of the real-time X-ray image based on modified adaptive local noise reduction filter. In: 2011 4th International Congress on Image and Signal Processing, pp. 1945–1949. https://doi.org/10.1109/CISP.2011.6100647.
Shi, L.K., Shi, B., Bai, J.P., et al., 2023a. Welding defect detection method based on full feature fusion for small diameter pipes. Transducer Microsys. Technol. 42 (9), 116–120. https://doi.org/10.13873/j.1000-9787(2023)09-0116-05 (in Chinese).
Shi, X.W., Zhang, S.B., Cheng, M., et al., 2023b. Few-shot semantic segmentation for industrial defect recognition. Comput. Ind. 148, 103901. https://doi.org/10.1016/j.compind.2023.103901.
Shin, H.K., Ahn, Y.H., Song, M.H., et al., 2023. Visualization for explanation of deep learning-based defect detection model using class activation map. Comput. Mater. Continua (CMC) 75 (3), 4753–4766. https://doi.org/10.32604/cmc.2023.038362.
Silva, R.R.d., Calôba, L.P., Siqueira, M.H.S., Rebello, J.M.A., 2003. Patterns nonlinear classifiers of weld defects in industrial radiographies. In: American Conferences for Nondestructive Testing, pp. 1–12.
Silva, R.R.d., Calôba, L.P., Siqueira, M.H.S., Rebello, J.M.A., 2004. Pattern recognition of weld defects detected by radiographic test. NDT E Int. 37 (6), 461–470. https://doi.org/10.1016/j.ndteint.2003.12.004.
Silva, R.R.d., Siqueira, M., Calôba, L.P., Rebello, J.M.A., 2001. Radiographics pattern recognition of welding defects using linear classifiers. Insight - Non-Destr. Test. Cond. Monit. 43, 669–674+682.
Song, K.Y., Kittler, J., Petrou, M., 1996. Defect detection in random colour textures. Image Vis Comput. 14 (9), 667–683. https://doi.org/10.1016/0262-8856(96)84491-X.
Sonwane, S., Chiddarwar, S., 2024. Enhancing weld defect detection and classification with MDCBNet: A multi-scale Dense Cross Block Network for improved explainability. NDT E Int. 142, 103029. https://doi.org/10.1016/j.ndteint.2023.103029.
Srikanth, T., 2012. A novel approach for automatic detection of defects in radiographic weld images by morphological and statistical operations. IOSR J. Eng. 2 (6), 1–5. https://doi.org/10.9790/3021-02620105.
Stephen, D., Lalu, P.P., 2021. Development of radiographic image classification System for weld defect identification using deep learning technique. Int. J. Sci. Eng. Res. 12 (5), 390–394. https://doi.org/10.14299/ijser.2021.05.01.
Stephen, D., Lalu, P.P., Sudheesh, R.S., 2021. X-Ray weld defect recognition using deep learning technique. Intern. Res. J. Eng. Technol. 8 (6), 818–823.
Sun, H.H., Xia, L.Q., Zhou, Y.H., et al., 2024. Online detection and evaluation of weld surface defects based on lightweight network VGG16-UNet and laser scanning. J. Manuf. Process. 129, 292–306. https://doi.org/10.1016/j.jmapro.2024.08.037.
Sun, S.B., Yin, L.H., Yan, X.L., et al., 2018a. Defect recognition of welding image based on texture feature. Comput. Appl. Softw. 35 (5), 242–246+312. https://doi.org/10.3969/j.issn.1000-386x.2018.05.043 (in Chinese).
Sun, X., 2019. Research on image model identification of pipeline weld defects. Master thesis, Chian University of Petroleum (Beijing). https://doi.org/10.27643/d.cnki.gsybu.2019.001149 (in Chinese).
Sun, Y., Yuan, P.X., 2006. Application of image processing to identify the flaw of the radiograph. Mechan. Eng. Automation 2006 (5), 61–63. https://doi.org/10.3969/j.issn.1672-6413.2006.05.024 (in Chinese).
Sun, Y.W., Liu, X.M., Cong, P., et al., 2018b. Digital radiography image denoising using a generative adversarial network. J. X Ray Sci. Technol. 26 (4), 523–534. https://doi.org/10.3233/XST-17356.
Sundaram, M., Jose, J.P., Jaffino, G., 2014. Welding defects extraction for radiographic images using C-means segmentation method. In: 2014 International Conference on Communication and Network Technologies, pp. 79–83. https://doi.org/10.1109/CNT.2014.7062729.
Tan, K.P., Tang, J.F., Zhao, Z.B., et al., 2024. Efficient and lightweight layer-wise in-situ defect detection in laser powder bed fusion via knowledge distillation and structural re-parameterization. Expert Syst. Appl. 255, 124628. https://doi.org/10.1016/j.eswa.2024.124628.
Tang, B., Chen, Q.R., Duan, C.H., 2024. Image dehazing and brightness enhancement algorithm based on atmospheric scattering model. J. Optoelectron. Laser 35 (3), 303–310. https://doi.org/10.16136/j.joel.2024.03.0628 (in Chinese).
Tang, G.W., Gong, M., Zhang, F.Z., et al., 2014. Research on weld defects distinguishing based on fuzzy neural networks. Comp. Technol. Develop. 24 (5), 243–247. https://doi.org/10.3969/j.issn.1673-629X.2014.05.060 (in Chinese).
Thien, N.D., Chi, C.L., Ngoc, H.N., 2017. An approach to the automatic detection of weld defects in radiography films using digital image processing. In: 2017 International Conference on System Science and Engineering (ICSSE), pp. 371–374. https://doi.org/10.1109/ICSSE.2017.8030899.
Thiruganam, M., Anouncia, S.M., Kantipudi, S., 2010. Automatic defect detection and counting in radiographic weldment images. Int. J. Comput. Appl. 10 (2), 1–5. https://doi.org/10.5120/1457-1971.
Tian, Y.X., Zhang, Y., Jiang, H.Q., et al., 2025. The comprehensive evaluation method for radiographic film Image quality with multi-region quality feature fusion. Aero. Mat. Technol. 55 (1), 44–50. https://doi.org/10.12044/j.issn.1007-2330.2025.01.006 (in Chinese).
Ting, T.C., Rahman, H., Lim, T.H., et al., 2024. Deep learning in manufacturing: a focus on welding defect classification with CNNs. In: Proceedings of International Conference on Artificial Life and Robotics, pp. 877–882. https://doi.org/10.5954/ICAROB.2024.OS26-9.
Tokime, R.B., Maldague, X.P.V., Perron, L., 2019. Automatic defect Detection for X-Ray inspection: identifying defects with deep convolutional network. In: Proceedings of the Canadian Institute for Non-destructive Evaluation (CINDE), pp. 18–20.
Tomasi, C., Manduchi, R., 1998. Bilateral filtering for gray and color images. In: Sixth International Conference on Computer Vision. IEEE Cat No98CH36271), pp. 839–846. https://doi.org/10.1109/ICCV.1998.710815.
Totino, B., Spagnolo, F., Perri, S., 2023. RIAWELC: a novel dataset of radiographic images for automatic weld defects classification. Intern. J. Electric. Comput. Eng. Res. 3, 13–17. https://doi.org/10.53375/ijecer.2023.320.
Tridi, M., Belaïfa, S.S., Nacereddine, N., 2005. Weld defect classification using EM algorithm for Gaussian mixture model. Comput. Sci. Eng. https://api.semanticscholar.org/CorpusID:14947909.
Tyystjärvi, T., Virkkunen, I., Fridolf, P., et al., 2022. Automated defect detection in digital radiography of aerospace welds using deep learning. Weld. World 66 (4), 643–671. https://doi.org/10.1007/s40194-022-01257-w.
Vaithiyanathan, V., Raj, M.M.A., Balasubramaniam, V., 2013. PCA and clustering based weld Flaw detection from radiographic Weld images. Int. J. Eng. Technol. 5 (3), 2879–2883.
Valavanis, I., Kosmopoulos, D., 2010. Multiclass defect detection and classification in weld radiographic images using geometric and texture features. Expert Syst. Appl. 37 (12), 7606–7614. https://doi.org/10.1016/j.eswa.2010.04.082.
Vilar, R., Zapata, J., Ruiz, R., 2008. Weld defects recognition and classification based on ANN. In: Proceedings of the Fifth IASTED International Conference on Signal Processing, Pattern Recognition and Applications. ACTA Press, pp. 181–186. https://doi.org/10.5555/1722683.1722720.

Vilar, R., Zapata, J., Ruiz, R., 2009a. An automatic system of classification of weld defects in radiographic images. NDT E Int. 42 (5), 467–476. https://doi.org/10.1016/j.ndteint.2009.02.004.
Vilar, R., Zapata, J., Ruiz, R., 2009b. Classification of welding defects in radiographic images using an ANN with modified performance function. In: Bioinspired Applications in Artificial and Natural Computation. Springer Berlin Heidelberg, pp. 284–293. https://doi.org/10.1007/978-3-642-02267-8_31.
Vilnrotter, F.M., Nevatia, R., Price, K.E., 1986. Structural analysis of natural textures. IEEE Trans. Pattern Anal. Mach. Intell. PAMI-8 (1), 76–89. https://doi.org/10.1109/TPAMI.1986.4767754.
Wang, G., Liao, T.W., 2002. Automatic identification of different types of welding defects in radiographic images. NDT E Int. 35 (8), 519–528. https://doi.org/10.1016/S0963-8695(02)00025-7.
Wang, L., 2015. X-ray image enhancement method based on histogram equalization. Laser J. 36 (12), 39–41+46. https://doi.org/10.14016/j.cnki.jgzz.2015.12.039 (in Chinese).
Wang, L., Zhang, H.G., Liu, J.H., Zuo, F.Y., 2025a. Knowledge transfer and reinforcement based on biunbiased neural network: a novel solution for open-set fault transfer diagnosis. IEEE Transact. Neural Networks Learn. Syst. 36 (9), 1–13. https://doi.org/10.1109/TNNLS.2025.3569582.
Wang, L.Y., Gao, W.X., Wang, X., 2017. Research of X-ray weld defect classification algorithm Basedon SVM and LE dimensionality reduction. J. Xi'an Shiyou University(Nat. Sci. Ed.) 32 (5), 96–101+106. https://doi.org/10.3969/j.issn.1673-064X.2017.05.016 (in Chinese).
Wang, M.Q., Han, Y., 2002. Application of nonlinear filtering to reducing noise and enhancing radiographic image. Nondestr. Test. Eval. 24 (7), 281–285. https://doi.org/10.3969/j.issn.1000-6656.2002.07.002 (in Chinese).
Wang, P., Du, W.D., Wang, L.X., et al., 2012. Film Weld flaw location and identification technology in ray detection. J. Xi'an Technol. Univer. 32 (4), 321–324. https://doi.org/10.16185/j.jxatu.edu.cn.2012.04.017 (in Chinese).
Wang, P., Li, L.L., Li, X.Y., et al., 2025b. An automatic welding defect detection method based on deep learning for super 8-bit high grayscale X-ray films of solid rocket motor shells. NDT E Int. 151, 103306. https://doi.org/10.1016/j.ndteint.2024.103306.
Wang, X., Gao, W.X., Wu, X.M., et al., 2016a. Image detecting of weld defect based on fuzzy pattern recognition. J. Xi'an Shiyou University(Nat. Sci. Ed.) 31 (4), 115–121. https://doi.org/10.3969/j.issn.1673-064X.2016.04.020 (in Chinese).
Wang, X., He, F., Huang, X., 2024a. A new method for deep learning detection of defects in X-ray images of pressure vessel welds. Sci. Rep. 14 (1), 6312. https://doi.org/10.1038/s41598-024-56794-9.
Wang, X., Shuai, J., Zhang, S.Z., et al., 2022a. Numerical study on the strain capacity of girth-welded X80 grade pipes. Pet. Sci. 19 (5), 2399–2412. https://doi.org/10.1016/j.petsci.2022.04.009.
Wang, X., Wong, B.S., 2005. Radiographic image segmentation for weld inspection using a robust algorithm. Res. Nondestr. Eval. 16 (3), 131–142. https://doi.org/10.1080/09349840591008235.
Wang, X.F., Zhang, Y.N., Liu, J., et al., 2022b. Online detection of weld surface defects based on improved incremental learning approach. Expert Syst. Appl. 195, 116407. https://doi.org/10.1016/j.eswa.2021.116407.
Wang, X.P., D'Avella, S., Liang, Z.M., et al., 2025c. On the effect of the attention mechanism for automatic welding defects detection based on deep learning. Expert Syst. Appl. 268, 126386. https://doi.org/10.1016/j.eswa.2025.126386.
Wang, X.P., Yu, X.H., 2023. Understanding the effect of transfer learning on the automatic welding defect detection. NDT E Int. 134, 102784. https://doi.org/10.1016/j.ndteint.2022.102784.
Wang, X.p., Zhang, B.X., Yu, X.H., 2024b. Zoom in on the target network for the prediction of defective images and welding defects' location. NDT E Int. 143, 103059. https://doi.org/10.1016/j.ndteint.2024.103059.
Wang, Y.T., Shi, F.H., Tong, X.F., 2019. A welding defect identification approach in X-ray images based on deep convolutional neural networks. In: Intelligent Computing Methodologies. Springer International Publishing, pp. 53–64. https://doi.org/10.1007/978-3-030-26766-7_6.
Wang, Y.Y., Sun, H.B., Yang, J., et al., 2023. A reliability-oriented genetic algorithm-levenberg marquardt model for leak risk assessment based on time-frequency features. Pet. Sci. 20 (5), 3194–3209. https://doi.org/10.1016/j.petsci.2023.04.016.
Wang, Z., Wang, X., Gao, W.X., Wang, Y.K., 2016b. Automatic recognition algorithm of SAW defects with image dimension reduction. Welding & Joining 2016 (9), 12–16+72. https://doi.org/10.3969/j.issn.1001-1382.2016.09.004 (in Chinese).
Wang, Z.N., Gao, W.X., Tang, N., 2018. A X-ray weld seam detection method based on sparse description. J. Xi'an Shiyou University(Nat. Sci. Ed.) 33 (5), 113–119. https://doi.org/10.3969/j.issn.1673-064X.2018.05.017 (in Chinese).
Wang, Z.N., Liu, Y.T., Li, Y., 2021. Research on defect detection algorithm of oil pipeline weld images based on sparse solution. Inner Mongolia. Petrochem. Ind. 47 (7), 4–5+110. https://doi.org/10.3969/j.issn.1006-7981.2021.07.002 (in Chinese).
Wang, Z.Q., 2022. Based on deep learning research on the technology of digitized weld film defect recognition. Master thesis, China University of Petroleum(Beijing). https://doi.org/10.27643/d.cnki.gsybu.2022.001467 (in Chinese).
Wang, Z.R., Li, W.F., Wang, M., et al., 2024c. Semi-supervised adaptive network for commutator defect detection with limited labels. J. Manuf. Syst. 77, 639–651. https://doi.org/10.1016/j.jmsy.2024.09.016.
Wei, C., Wang, W.J., Yang, W.H., Liu, J.Y., 2018. Deep retinex decomposition for low-light enhancement. arXiv. https://doi.org/10.48550/arXiv.1808.04560.
Wei, M.H., Wu, H.L., He, S.M., 2019. Intelligent detection of weld defects based on wavelet transform and RBF neural networks. Technol. Innov. Appli. 28, 35–36, 2019 10.CNKI:SUN:CXYY.0.2019-28-011 (in Chinese).
Weickert, J., 1998. Anisotropic diffusion in image processing. Bgteubner Stuttgart 16 (1), 272. https://doi.org/10.1109/34.588012.
Wu, H.X., Yue, X.F., Qin, W.Y., Zhang, P.F., 2019. A texture defect feature extraction algorithm. Comput. Digi. Eng. 47 (5), 1055–1059+1077. https://doi.org/10.3969/j.issn.1672-9722.2019.05.008 (in Chinese).
Wu, T.T., Zhao, H., Gao, B.X., Meng, F.B., 2021. Structural optimization strategy of pipe isolation tool by dynamic plugging process analysis. Pet. Sci. 18 (6), 1829–1839. https://doi.org/10.1016/j.petsci.2021.09.010.
Xiao, Y., Gao, W.X., Deng, G.H., 2024. Recognition algorithm of small-diameter tube X-ray welding defect image. Trans. China Weld. Inst. 45 (2), 82–88–134. https://doi.org/10.12073/j.hjxb.20230228001 (in Chinese).
Xu, C., Yu, B., Zhang, Z.W., et al., 2010. Numerical simulation of a buried hot crude oil pipeline during shutdown. Pet. Sci. 7 (1), 73–82. https://doi.org/10.1007/s12182-010-0008-x.
Xu, G.Y., Chen, Y., Zhang, X.G., Liu, Y.K., 2011. Study of welding defect recognition algorithm based on selective ensemble learning. J. China Inst. Min. Technol. 40 (6), 949–953. https://doi.org/CNKI:SUN:ZGKD.0.2011-06-020 (in Chinese).
Xu, H., Yan, Z.H., Ji, B.W., et al., 2022. Defect detection in welding radiographic images based on semantic segmentation methods. Measurement 188, 110569. https://doi.org/10.1016/j.measurement.2021.110569.
Xu, J.W., Yang, L., Hao, S.J., 2023a. Deep learning-based model for identifying defects in X-ray images of weld seams. Sci. Technol Innov. (18), 59–62. https://doi.org/10.3969/j.issn.1673-1328.2023.18.016, 2023. (in Chinese).
Xu, L.S., Dong, S.H., Wei, H.T., et al., 2023b. Defect signal intelligent recognition of weld radiographs based on YOLO V5-IMPROVEMENT. J. Manuf. Process. 99, 373–381. https://doi.org/10.1016/j.jmapro.2023.05.058.
Xu, M.F., Han, Y., Dong, J.L., 2005a. Linear filter methods for image denoising in digital radiography. Nondestruct. Test. 2005 (4), 198–201. https://doi.org/10.3969/j.issn.1000-6656.2005.04.010 (in Chinese).
Xu, M.F., Han, Y., Dong, J.L., 2005b. Nonlinear filter methods for image denoising in digital radiography. Nondestruct. Test. 2005 (5), 259–263. https://doi.org/10.3969/j.issn.1000-6656.2005.05.011 (in Chinese).
Yahaghi, E., Mirzapour, M., Movafeghi, A., 2021. Comparison of traditional and adaptive multi-scale products thresholding for enhancing the radiographs of welded object. Eur Phys. J. Plus 136 (7), 744. https://doi.org/10.1140/epjp/s13360-021-01733-0.
Yahia, N.B., Belhadj, T., Brag, S., Zghal, A., 2011. Automatic detection of welding defects using radiography with a neural approach. Procedia Eng. 2011 (10), 671–679. https://doi.org/10.1016/j.proeng.2011.04.112.
Yan, H.X., 2024. Research on Industrial X-ray Image Enhancement Algorithm Based on Neural Netrworks. Master thesis, North University of China. https://doi.org/10.27470/d.cnki.ghbgc.2024.000896 (in Chinese).
Yan, Z.H., Xu, H., Huang, P.F., 2020. Multi-scale multi-intensity defect detection in ray image of weld bead. NDT E Int. 116, 102342. https://doi.org/10.1016/j.ndteint.2020.102342.
Yang, B., Shuai, L., Xuan, W., Shi, L.K., 2025. A welding defect detection network based on multi-dimensional collaborative enhancement of spatial-frequency features. Nondestr. Test. Eval. 1–21. https://doi.org/10.1080/10589759.2025.2495799.
Yang, D.H., Song, X.Z., Zhu, Z.P., et al., 2024a. An automatic workflow for the quantitative evaluation of bit wear based on computer vision. Pet. Sci. 21 (6), 4376–4390. https://doi.org/10.1016/j.petsci.2024.10.005.
Yang, D.M., Cui, Y.R., Yu, Z.Y., Yuan, H.Q., 2021a. Deep learning based steel pipe weld defect detection. Appl. Artif. Intell. 35 (15), 1237–1249. https://doi.org/10.1080/08839514.2021.1975391.
Yang, D.Y., Jiang, H.Q., Liu, Z., et al., 2022a. Radiographic image enhancement based on a triple constraint U-Net network. Insight - Non-Destr. Test. Cond. Monit. 64 (9), 511–519. https://doi.org/10.1784/insi.2022.64.9.511.
Yang, H., Wang, M.Q., 2009. Technology research on shell beam image intensification based on the wavelet transformation. J. Projectiles Rockets Missiles Guid. 29 (6), 294–296. https://doi.org/10.3969/j.issn.1673-9728.2009.06.082 (in Chinese).
Yang, J., Fu, B., Zeng, J.Q., Wu, S.X., 2022b. YOLO-Xweld: efficiently detecting pipeline welding defects in X-Ray images for constrained environments. In: 2022 International Joint Conference on Neural Networks (IJCNN), pp. 1–7. https://doi.org/10.1109/IJCNN55064.2022.9892765.
Yang, L., Jiang, H.Q., 2021. Weld defect classification in radiographic images using unified deep neural network with multi-level features. J. Intell. Manuf. 32 (2), 459–469. https://doi.org/10.1007/s10845-020-01581-2.
Yang, L., Liu, Y.H., Peng, J.Z., 2019a. An automatic detection and identification method of welded joints based on deep neural network. IEEE Access 7, 164952–164961. https://doi.org/10.1109/ACCESS.2019.2953313.
Yang, L., Song, S.A., Fan, J.F., et al., 2022c. An automatic deep segmentation network for pixel-level welding defect detection. IEEE Trans. Instrum. Meas. 71, 1–10. https://doi.org/10.1109/TIM.2021.3127645.
Yang, L., Wang, H.X., Huo, B.Y., et al., 2021b. An automatic welding defect location algorithm based on deep learning. NDT E Int. 120, 102435. https://doi.org/10.1016/j.ndteint.2021.102435.
Yang, L., Xu, S., Fan, J.F., et al., 2023a. A pixel-level deep segmentation network for automatic defect detection. Expert Syst. Appl. 215, 119388. https://doi.org/10.1016/j.eswa.2022.119388.

Yang, L.J., Shi, M., Geng, H., 2024b. Internal detection technology of long-distance oil and gas pipeline. J. Shenyang Univers. Technol. 46 (5), 676–684. https://doi.org/10.7688/j.issn.1000-1646.2024.05.16 (in Chinese).
Yang, W., Xiao, Y.C., Shen, H.K., Wang, Z.P., 2023b. An effective data enhancement method of deep learning for small weld data defect identification. Measurement 206, 112245. https://doi.org/10.1016/j.measurement.2022.112245.
Yang, Z.C., Zhou, Q., Hu, K., Zhao, Y., 2019b. Welding defect recognition technology based on convolutional neural network and application. J. Wuhan Univ. Technol. 41 (1), 17–21. https://doi.org/10.3963/j.issn.2095-3852.2019.01.004 (in Chinese).
Yazid, H., Arof, H., Yazid, H., 2012. Automated thresholding in radiographic image for welded joints. Nondestr. Test. Eval. 27 (1), 69–80. https://doi.org/10.1080/10589759.2011.591795.
Yazid, H., Arof, H., Yazid, H., et al., 2011. Discontinuities detection in welded joints based on inverse surface thresholding. NDT E Int. 44 (7), 563–570. https://doi.org/10.1016/j.ndteint.2011.06.002.
Yin, Y., Tian, G.Y., Yin, G.F., Luo, A.M., 2008. Defect identification and classification for digital X-Ray images. Appl. Mech. Mater. 10, 543–547. https://doi.org/10.4028/0-87849-470-7.543.
Zahran, O., Kasban, H., El-Kordy, M., El-Samie, F.E.A., 2013. Automatic weld defect identification from radiographic images. NDT E Int. 57, 26–35. https://doi.org/10.1016/j.ndteint.2012.11.005.
Zapata, J., Vilar, R., Ruiz, R., 2011. Performance evaluation of an automatic inspection system of weld defects in radiographic images based on neuro-classifiers. Expert Syst. Appl. 38 (7), 8812–8824. https://doi.org/10.1016/j.eswa.2011.01.092.
Zhan, X.H., Zhang, D., Yu, H.S., et al., 2018. Research on X-ray image processing technology for laser welded joints of aluminum alloy. Int. J. Adv. Manuf. Technol. 99 (1), 683–694. https://doi.org/10.1007/s00170-018-2249-6.
Zhang, A.Y., Cai, M., Wei, N., et al., 2024. Analysis of sensitivity to hydrate blockage risk in natural gas gathering pipeline. Pet. Sci. 21 (4), 2723–2733. https://doi.org/10.1016/j.petsci.2024.01.016.
Zhang, B.X., Wang, X.P., Cui, J.H., et al., 2023a. Welding defects classification by weakly supervised semantic segmentation. NDT E Int. 138, 102899. https://doi.org/10.1016/j.ndteint.2023.102899.
Zhang, C.S., Bi, J.P., Lv, Y.X., et al., 2023b. Numerical analysis and experimental research on detection of welding defects in pipelines based on magnetic flux leakage. Pet. Res. 8 (4), 550–560. https://doi.org/10.1016/j.ptlrs.2023.05.013.
Zhang, H., Gao, M.Q., Tang, B., et al., 2022a. Dynamic characteristics of the pipeline inspection gauge under girth weld excitation in submarine pipeline. Pet. Sci. 19 (2), 774–788. https://doi.org/10.1016/j.petsci.2021.09.044.
Zhang, J., 2017a. Weld defect recognition Algorithm based on principal component analysis. Ind. Cont. Comput. 30 (1), 108–109. https://doi.org/10.3969/j.issn.1001-182X.2017.01.047 (in Chinese).
Zhang, J., 2017b. Welding Defects Recognition Algorithm Reasearching Based on Principal Component Analysis. Master. Xi'an Shiyou University (in Chinese).
Zhang, L., Wang, W.H., Wang, J.R., Yang, Y.X., 2021a. Oil pipeline weld defect classification based on improved ResNet50. Modern Comput. 20, 98–102. https://doi.org/10.3969/j.issn.1007-1423.2021.20.019, 2021. (in Chinese).
Zhang, L., Zhang, Y.J., Dai, B.C., et al., 2019. Welding defect detection based on local image enhancement. IET Image Process. 13 (13), 2647–2658. https://doi.org/10.1049/iet-ipr.2018.5840.
Zhang, L.F., Gao, W.X., Feng, X.X., 2022b. X-ray circumferential weld defect detection based on convolutional neural network. Welding & Joining 2022 (3), 26–34. https://doi.org/10.12073/j.hj.20211110003 (in Chinese).
Zhang, L.F., Gao, W.X., Wang, Z., Wu, X.M., 2021b. Research on weld defect identification with X-ray based on convolutional neural network. J. Phys. Conf. 1894 (1), 012071. https://doi.org/10.1088/1742-6596/1894/1/012071.
Zhang, M., Guo, Y.B., Zhang, Z., et al., 2023c. Extraction of pipeline defect feature based on variational mode and optimal singular value decomposition. Pet. Sci. 20 (2), 1200–1216. https://doi.org/10.1016/j.petsci.2022.11.007.
Zhang, M., Hu, Y.Z., Xu, B.B., et al., 2025. DSF-YOLO for weld defect detection in X-ray images with dynamic staged fusion. Sci. Rep. 15 (1), 23305. https://doi.org/10.1038/s41598-025-06811-2.
Zhang, S., Shi, F., 2022. Study on weld defect recognition method based on machine vision. Henan Chem. Ind. 39 (6), 15–19. https://doi.org/10.14173/j.cnki.hnhg.2022.06.007 (in Chinese).
Zhang, T., Wang, D.W., 2024. X-ray weld defect identification based on dilated hierarchical attention capsule network. J. Astronautic Metrol. Meas. 44 (2), 45–51. https://doi.org/10.12060/j.issn.1000-7202.2024.02.08 (in Chinese).
Zhang, W.L., 2022. Research of Industrial X-ray Image Enhancement Algorithm. Master. North University of China. https://doi.org/10.27470/d.cnki.ghbgc.2022.000885 (in Chinese).
Zhang, W.L., Liu, Y., Zhang, P.C., Gui, Z.G., 2021c. A X-Ray image enhancement Algorithm based on simple radiographic scattering model. J. North Univ. China (Natural Sci. Ed.) 42 (5), 441–448. https://doi.org/10.3969/j.issn.1673-3193.2021.05.009 (in Chinese).
Zhang, X.G., Li, Y., Xu, J.J., 2003a. Weld seam defects distinguishing expert System based on neural network. Comput. Eng. 2003 (17), 22–23+28. https://doi.org/10.3969/j.issn.1000-3428.2003.17.010 (in Chinese).
Zhang, X.G., Lin, J.J., 2023a. Fuzzy neural network recognition of real time radiation detection on defects of weld lines. Process Autom. Instrum. 2003 (2), 24–26. https://doi.org/10.3969/j.issn.1000-0380.2003.02.008 (in Chinese).
Zhang, X.G., Lin, J.J., 2023b. Weld defects distinguishing method based on fuzzy neural networks. J. China Inst. Min. Technol. 2003 (1), 95–98. https://doi.org/10.3321/j.issn:1000-1964.2003.01.022 (in Chinese).
Zhang, X.G., Lin, J.J., 2004. Research of image processing and defect recognition for industrial radiographic weld inspection. J. East China Univ. Sci. Technol. 2004 (2), 199–202. https://doi.org/10.14135/j.cnki.1006-3080.2004.02.017 (in Chinese).
Zhang, X.G., Sun, Z., Ruan, D.X., et al., 2009. Research and application of integration of RS and FNN in defect recognition of welding. J. Harbin Inst. Technol. 41 (1), 141–144. https://doi.org/10.3321/j.issn:0367-6234.2009.01.032 (in Chinese).
Zhang, X.S., Gao, W.X., Mu, X.Y., et al., 2021d. Research on the Noise reduction and enhancement of X-ray girth weld image. Laser J. 42 (3), 79–85. https://doi.org/10.14016/j.cnki.jgzz.2021.03.079 (in Chinese).
Zhao, A.L., Zhang, P.C., Yang, Y.M., et al., 2020. Improved histogram equalization and bilateral filtering X-Ray image contrast enhancement Algorithm. J. North Univ. China (Natural Sci. Ed.) 41 (6), 564–570. https://doi.org/10.3969/j.issn.1673-3193.2020.06.014 (in Chinese).
Zhao, A.L., 2021. Research of Industrial X-ray Image Enhancement Algorithm. Master. North University of China. https://doi.org/10.27470/d.cnki.ghbgc.2021.000980 (in Chinese).
Zhao, H., Liu, J.H., Wang, Q.N., et al., 2025. A novel anomaly detection method for magnetic flux leakage signals via a feature-based unsupervised detection network. Comput. Ind. 164, 104190. https://doi.org/10.1016/j.compind.2024.104190.
Zhao, M., 2018. Research and Implementation of Industrial X-ray Image Enhancement Algorithms Based on CUDA.. Master thesis, North University of China (in Chinese).
Zhao, Y., Liu, S.Y., Li, X.H., 2021. Radiographic inspection of Submerged Arc Welding using semantic segmentation. In: 2021 IEEE Sensors, pp. 1–4. https://doi.org/10.1109/SENSORS47087.2021.9639555.
Zhong, H., Xiao, L., Wang, H.F., et al., 2024. LiFSO-Net: A lightweight feature screening optimization network for complex-scale flat metal defect detection. Knowl. Base Syst. 304, 112520. https://doi.org/10.1016/j.knosys.2024.112520.
Zhou, C., Liu, H., Zhao, A.L., et al., 2019. Industrial X-ray image enhancement algorithm based on gradient field. J. Comput. Appl. 39 (10), 3088–3092. https://doi.org/10.11772/j.issn.1001-9081.2019040694 (in Chinese).
Zhou, H.M., Lu, J.F., Lu, J.S., Zhou, W.Q., 2018. Research on weld defect type recognition method based on multiscale texture feature. Mech. Electric. Technol. 2018 (3), 14–16. https://doi.org/10.19508/j.cnki.1672-4801.2018.03.004 (in Chinese).
Zhou, W.J., Wu, Y., Qiu, W.W., et al., 2024. Effective Bi-decoding networks for rail-surface defect detection by knowledge distillation. Appl. Soft Comput. 167, 112422. https://doi.org/10.1016/j.asoc.2024.112422.
Zhou, X., 2020. Research on industrial ray image enhancement algorithm.. Master thesis, South China University of Technology. https://doi.org/10.27151/d.cnki.ghnlu.2020.002091 (in Chinese).
Zhu, X.K., Lyu, S.C., Wang, X., Zhao, Q., 2021. TPH-YOLOv5: improved YOLOv5 based on transformer prediction head for object detection on drone-captured scenarios. In: 2021 IEEE/CVF International Conference on Computer Vision Workshops (ICCVW), pp. 2778–2788. https://doi.org/10.1109/ICCVW54120.2021.00312.
Zhu, X.X., Fu, C.M., Wang, Y.T., Zhang, S.M., 2023. Experimental research on the contact force of the bi-directional pig in oil and gas pipeline. Pet. Sci. 20 (1), 474–481. https://doi.org/10.1016/j.petsci.2022.08.021.
Zou, Y.R., Du, D., Chang, B.H., et al., 2015. Automatic weld defect detection method based on Kalman filtering for real-time radiographic inspection of spiral pipe. NDT E Int. 72, 1–9. https://doi.org/10.1016/j.ndteint.2015.01.002.
Zuo, F.Y., Liu, J.H., Fu, M.R., et al., 2023. An effective detection method for complex weld defects based on adaptive feature Pyramid. In: 2023 CAA Symposium on Fault Detection, Supervision and Safety for Technical Processes (SAFEPROCESS), pp. 1–5. https://doi.org/10.1109/SAFEPROCESS58597.2023.10295953.
Zuo, F.Y., Liu, J.H., Fu, M.R., et al., 2024a. An efficient anchor-free defect detector with dynamic receptive field and task alignment. IEEE Trans. Ind. Inf. 20 (6), 8536–8547. https://doi.org/10.1109/TII.2024.3371982.
Zuo, F.Y., Liu, J.H., Fu, M.R., et al., 2024b. STMA-Net: A spatial transformation-based multi-scale attention network for complex defect detection with X-ray images. IEEE Trans. Instrum. Meas. 73, 1–11. https://doi.org/10.1109/TIM.2024.3376014.
Zuo, F.Y., Liu, J.H., Fu, M.R., et al., 2024c. An X-Ray-Based multiexpert inspection method for automatic welding defect assessment in intelligent pipeline systems. IEEE ASME Trans. Mechatron. 30 (3), 1–12. https://doi.org/10.1109/TMECH.2024.3408337.
Zuo, F.Y., Liu, J.H., Fu, M.R., Wen, Z.T., 2025a. An end-to-end intelligent welding defect detection system for low-quality X-ray images with adaptive progressive learning. Expert Syst. Appl. 279, 127428. https://doi.org/10.1016/j.eswa.2025.127428.
Zuo, F.Y., Liu, J.H., Zhang, H.Q., et al., 2025b. A complex welding defect detection method based on active learning in pipeline transportation system. IEEE Trans. Instrum. Meas. 74, 1–12. https://doi.org/10.1109/TIM.2025.3551482.
Zuo, F.Y., Liu, J.H., Zhao, X., et al., 2024d. An X-Ray-Based automatic welding defect detection method for special equipment system. IEEE ASME Trans. Mechatron. 29 (3), 2241–2252. https://doi.org/10.1109/TMECH.2023.3327713.